1   Heat stored in the Earth system 1960-2020: Where does the energy go?

3   **Authors:** Karina von Schuckmann[1], Audrey Minère[1], Flora Gues[1,2], Francisco José Cuesta
4   Valero[3,36], Gottfried Kirchengast[4], Susheel Adusumilli[5], Fiamma Straneo[5], Richard P. Allan[6], Paul
5   M. Barker[7], Hugo Beltrami[8,51], Tim Boyer[9], Lijing Cheng[10,11], John A. Church[7], Damien
6   Desbruyeres[12], Han Dolman[13], Catia M. Domingues[14], Almudena García-García[3,36], Donata
7   Giglio[15], John E. Gilson[5], Maximilian Gorfer[16,4], Leopold Haimberger[17], Stefan Hendricks[18],
8   Shigeki Hosoda[19], Gregory C. Johnson[20], Rachel Killick[21], Brian King[14], Nicolas Kolodziejczyk[22],
9   Anton Korosov[23], Gerhard Krinner[24], Mikael Kuusela[25], Moritz Langer[26,27], Thomas Lavergne[28],
10   Isobel Lawrence[29], Yuehua Li[30], John Lyman[20], Ben Marzeion[21], Michael Mayer[17,31], Andrew H.
11   MacDougall[32], Trevor McDougall[7], Didier Paolo Monselesan[33], Jan Nitzbon[26,34], Inès Otosaka[35],
12   Jian Peng[3,36], Sarah Purkey[5], Dean Roemmich[5], Kanako Sato[19], Katsunari Sato[37], Abhishek
13   Savita[38], Axel Schweiger[39], Andrew Shepherd[35], Sonia I. Seneviratne[40], Leon Simons[41], Donald
14   A. Slater[42], Thomas Slater[35], Noah Smith[43], Andrea Steiner[4], Toshio Suga[44,19], Tanguy Szekely[45],
15   Wim Thiery[46], Mary-Louise Timmermans[47], Inne Vanderkelen[46], Susan E. Wjiffels[33,48], Tonghua
16   Wu[49], Michael Zemp[50]

18   Corresponding author: Karina von Schuckmann, karina.von.schuckmann@mercator-ocean.fr

20   1 Mercator Ocean International, Toulouse, France
21   2 CELAD, Toulouse, France
22   3 Department of Remote Sensing, Helmholtz Centre for Environmental Research, Leipzig, 04318, Germany
23   4 Wegener Center for Climate and Global Change and Institute of Physics, University of Graz, Graz, Austria
24   5 Scripps Institution of Oceanography, University of California San Diego, San Diego, California, USA
25   6 University of Reading, UK
26   7 University of New South Wales, Sydney, Australia
27   8 Climate & Atmospheric Sciences Institute and Department of Earth Sciences, St. Francis Xavier University,
28   Antigonish, B2G 2W5, Canada
29   9 NOAA's National Centers for Environmental Information, Silver Spring, Maryland, USA
30   10 Institute of Atmospheric Physics, Chinese Academy of Sciences, Beijing, China
31   11 Center for Ocean Mega-Science, Chinese Academy of Sciences, Qingdao, 266071, China
32   12 Ifremer, University of Brest, CNRS, IRD, Laboratoire d'Océanographie Physique et Spatiale, Brest, France
33   13 Netherlands Institute for Sea Research, Den Burg, Texel, Netherlands
34   14 National Oceanographic Centre, Southampton, UK
35   15 University of Colorado, Boulder, USA
36   16 Center for Climate Systems Modeling, ETH Zurich, Zurich, Switzerland
37   17 Department of Meteorology and Geophysics, University of Vienna, Vienna, Austria
38   18 Alfred Wegener Institute Helmholtz Centre for Polar and Marine Research, Germany
39   19 Japan Marine-Earth Science and Technology (JAMSTEC), Japan
40   20 NOAA, Pacific Marine Environmental Laboratory, Seattle, USA
41   21 Met Office Hadley Centre, Exeter, UK
42   22 University of Brest, CNRS, IRD, Ifremer, Laboratoire d'Océanographie Physique et Spatiale, IUEM, Brest,
43   France
44   23 Nansen Environmental and Remote Sensing Center, Norway
45   24 Institut des Géosciences de l'Environnement, CNRS, Université Grenoble Alpes, Grenoble, France
46   25 Carnegie Mellon University, Pittsburg, USA
47   26 Alfred Wegener Institute Helmholtz Centre for Polar and Marine Research, Permafrost Research Section,
48   Potsdam, Germany
49   27 Humboldt-Universität zu Berlin, Geography Department, Berlin, Germany
50   28 Norwegian Meteorological Institute, Norway
51   29 European Space Agency, ESRIN, Via Galileo Galilei, 1, 00044 Frascati RM, Italy
52   30 University of Bremen, Germany

53   31 European Centre for Medium-Range Weather Forecasts (ECMWF), Reading, UK
54   32 Climate & Environment Program, St. Francis Xavier University Antigonish, Nova Scotia, Canada B2G 2W5
55   33 CSIRO Oceans and Atmosphere, Hobart, Tasmania, Australia
56   34 Alfred Wegener Institute Helmholtz Centre for Polar and Marine Research, Paleoclimate Dynamics Section,
57   Bremerhaven, Germany.
58   35 Centre for Polar Observation and Modelling, University of Leeds, UK
59   36 Remote Sensing Centre for Earth System Research, Leipzig University, 04103, Leipzig, Germany
60   37 Japan Meteorological Agency, Japan
61   38 GEOMAR, Kiel, Germany
62   39 Polar Science Center, Applied Physics Laboratory, University of Washington, Seattle, WA, USA
63   40 Institute for Atmospheric and Climate Science, ETH Zurich, Zurich, 8092, Switzerland
64   41 The Club of Rome, The Netherlands Association, 's-Hertogenbosch, The Netherlands
65   42 Glaciology and Oceanography, Univ. of Edinburgh, UK
66   43 Department of Mathematics, University of Exeter, Exeter, United Kingdom
67   44 Tohoku University, Japan
68   45 Ocean Scope, Brest, France
69   46 Department of Hydrology and Hydraulic Engineering, Vrije Universiteit Brussel, Brussels, 1050, Belgium
70   47 Department of Earth and Planetary Sciences, Yale University, New Haven, Connecticut, USA
71   48 Woods Hole Oceanographic Institution, Massachusetts, USA
72   49 Cryosphere Research Station on Qinghai–Xizang Plateau, State Key Laboratory of Cryospheric Science,
73   Northwest Institute of Eco–Environment and Resources (NIEER), Chinese Academy of Sciences (CAS), Lanzhou,
74   730000, China
75   50 Department of Geography, University of Zurich, Switzerland
76   51 Département des sciences de la Terre et de l'atmosphère, Université du Québec à Montréal, Montréal, Québec,
77   Canada.
78
79

80   **Abstract.** The Earth climate system is out of energy balance and heat has accumulated
81   continuously over the past decades, warming the ocean, the land, the cryosphere and the
82   atmosphere. According to the 6th Assessment Report of the Intergovernmental Panel on Climate
83   Change, this planetary warming over multiple decades is human-driven and results in
84   unprecedented and committed changes to the Earth system, with adverse impacts for ecosystems
85   and human systems. The Earth heat inventory provides a measure of the Earth energy imbalance,
86   and allows for quantifying how much heat has accumulated in the Earth system, and where the
87   heat is stored. Here we show that 380 ± 62 ZJ of heat has accumulated in the Earth system from
88   1971 to 2020, at a rate of 0.48 ± 0.1 W m^{-2}, with 89 ± 17 % of this heat stored in the ocean, $6 \pm$
89   0.1 % on land, 4 ± 1% in the cryosphere and 1 ± 0.2 % in the atmosphere. Over the most recent
90   decade (2006-2020), the Earth heat inventory shows increased warming at rate of $0.48 \pm$
91   0.3 W m^{-2}/decade, and the Earth climate system is out of energy balance by 0.76 ± 0.2 Wm^{-2}. The
92   Earth heat inventory is the most fundamental global climate indicator that the scientific community
93   and the public can use as the measure of how well the world is doing in the task of bringing
94   anthropogenic climate change under control. We call for an implementation of the Earth heat
95   inventory into the Paris agreement's global stocktake based on best available science. The Earth
96   heat inventory in this study, updated from von Schuckmann et al, 2020, is underpinned by
97   worldwide multidisciplinary collaboration and demonstrates the critical importance of concerted
98   international efforts for climate change monitoring and community-based recommendations as
99   coordinated by the Global Climate Observing System (GCOS). We also call for urgently needed
100   actions for enabling continuity, archiving, rescuing and calibrating efforts to assure improved and
101   long-term monitoring capacity of the relevant GCOS Essential Climate Variables (ECV) for the
102   Earth heat inventory.
103

104
Introduction
106

107   Since a recent international quantification of the Earth heat inventory (von Schuckmann et al.,
108   2020), three main reports of the 6th assessment cycle of the Intergovernmental Panel for Climate
109   Change (IPCC)[1] have been published. The IPCC report of Working Group III (WGIII) 'Climate
110   Change 2022: Mitigation of Climate Change' (IPCC, 2022b) states that '*options available now in*
111   *every sector that can at least halve emissions by 2030*' and that '*accelerated climate action is*
112   *critical to sustainable development*'[2]. The IPCC report of Working Group II (WGII) 'Climate
113   Change 2022: Impacts, Adaptation and Vulnerability' (IPCC, 2022a) offers solutions, while
114   pointing out that '*every small increase in warming will result in increased risks*', and that *'it is*
115   *essential to make rapid, deep cuts in greenhouse gas emissions to keep the maximum number of*
116   *adaptation options open[3]*. The IPCC report of Working Group I (WGI) 'Climate Change 2022:
117   The Physical Science Basis' (IPCC, 2021) concluded that '*recent human-induced changes in the*
118   *climate are widespread, rapid, and intensifying, and unprecedented in thousands of years*', and
119   '*that there is no going back from some changes in the climate system, from which some changes*
120   *could be slowed and others could be stopped by limiting warming*'[4].
121

122   These assessment outcomes further emphasize the need to extend the Global Climate Observing
123   System (GCOS) beyond the strict scientific observation of the climate state to also supporting
124   policy and planning (GCOS, 2021). The GCOS was established in 1992 to aid in developing and
125   coordinating a GCOS that supported scientific understanding of climate change. More recently it
126   has broadened its focus to include policy development, public information and planning for
127   adaptation and mitigation (GCOS, 2016). GCOS started assessments of the Earth's heat inventory
128   in 2018, and the carbon and the water cycles, to identify potential gaps and inconsistencies in
129   existing observation systems (Crisp et al., 2022; Dorigo et al., 2021; von Schuckmann et al., 2020).
130   The first call for concerted international collaboration on the Earth's energy imbalance and the
131   associated Earth heat inventory had been established in a perspective paper in 2016 (von
132   Schuckmann et al., 2016), initiating a research focus activity under WCRP/CLIVAR[5]. One of the
133   outcomes was the development of an internationally and multidisciplinary driven publication on
134   the Earth heat inventory, now under the auspices of GCOS (von Schuckmann et al., 2020), which
135   further continues with this study. With this second study we aim to contribute to a more frequent
136   and regular update of the state of the Earth heat inventory as an important indicator of climate
137   change.
138

139   The Earth heat inventory provides a quantitative measure of the heat accumulated in the Earth
140   system, which results from the anthropogenically perturbed planetary radiation budget – i.e., a
141   positive Earth Energy Imbalance (EEI) forced by increasing atmospheric concentrations of
142   radiatively active greenhouse gasses from human-induced emissions (Forster et al., 2022; Hansen
143   et al., 2011) (Fig. 1). Estimates of the Earth heat inventory can be obtained by analyzing several

---

1   https://www.ipcc.ch/
2   https://report.ipcc.ch/ar6wg3/pdf/IPCC_AR6_WGIII_PressConferenceSlides.pdf
3   https://report.ipcc.ch/ar6wg2/pdf/IPCC_AR6_WGII_PressConferenceSlides.pdf
4   https://www.ipcc.ch/report/ar6/wg1/resources/presentations-and-multimedia
5   https://www.clivar.org/research-foci/heat-budget

144 Essential Climate Variables (ECVs) of GCOS, complemented by model and reanalysis outputs to
145 fill the gaps, through the quantification of increases in heat content of the ocean, the land, the
146 atmosphere, and the heat used to melt ice (Forster et al., 2022; von Schuckmann et al., 2020). This
147 assessment allows for evaluating the total heat accumulated in the Earth system and where and
148 how much heat is stored in the different Earth system components (Fig. 1). The derivative of the
149 Earth heat inventory over time provides then an estimate of the global heating rate, and hence, the
150 absolute value of the EEI (Loeb et al., 2012; Trenberth et al., 2016). A recent quantification of the
151 Earth heat inventory (von Schuckmann et al., 2020) revealed a consistent long-term Earth system
152 heat gain over the period 1971–2018, with a total heat gain of 358±37 ZJ, which is equivalent to a
153 global heating rate of 0.47±0.1 W m^{-2}. Over the period 1971–2018, the majority of heat gain is
154 reported for the global ocean, with 89 % of the excess heat in the climate system stored there, and
155 for 2010–2018 that was 90%. 52 % of the excess heat was stored in the upper 700 m of the ocean
156 for both time periods, with 28 % stored in the 700–2000 m depth layer and 9 % below 2000 m
157 depth for 1971–2018 (30% in the 700–2000 m layer and 8% below 2000 m for 2010–2018). For
158 1971–2018, heat gain by the land amounts to 6 % of the total, 4 % is used for the melting of
159 grounded and floating ice, and 1 % goes to atmospheric warming. Those fractions are 5%, 3%, and
160 2% respectively for 2010–2018. The results are consistent within uncertainty ranges with the
161 assessment outcomes as obtained in the recent IPCC report (Forster et al., 2022).

162

163 The rate of change in the Earth heat inventory, and hence, the EEI, is the portion of the forcing
164 that the Earth has not yet realized as warming (Hansen et al., 2005). The Earth system responds to
165 an imposed radiative forcing through a number of feedbacks, which operate on various different
166 timescales. Earth's radiative response is complex, comprising a variety of climate feedbacks (e.g.,
167 water vapor feedback, cloud feedbacks, ice-albedo feedback) (Forster et al., 2022). Conceptually,
168 the relationships between EEI, radiative forcing and surface temperature change can be expressed
169 as (Gregory & Andrews, 2016):

170

171 $\Delta N_{TOA} = \Delta F_{ERF} - |\alpha_{FP}| \Delta T_S$, (1)

172

173 where ΔN_{TOA} is the Earth's net energy imbalance at the Top Of the Atmosphere (TOA) (in W m^{-2}),
174 ΔF_{ERF} is the effective radiative forcing (W m^{-2}), ΔT_S is the global surface temperature anomaly
175 (K) relative to the equilibrium state and α_{FP} is the net total feedback parameter (W m^{-2} K^{-1}), which
176 represents the combined effect of the various climate feedbacks. Essentially, α_{FP} in Eq. (1) can be
177 viewed as a measure of how efficient the system is at restoring radiative equilibrium for a unit
178 surface temperature rise. Thus, ΔN_{TOA} represents the difference between the applied radiative
179 forcing and Earth's radiative response through climate feedbacks associated with surface
180 temperature increase (e.g., Hansen et al., 2011). Observation-based estimates of ΔN_{TOA} are
181 therefore crucial both to our understanding of past climate change and for refining projections of
182 future climate change (Gregory & Andrews, 2016; Kuhlbrodt & Gregory, 2012). The long
183 atmospheric lifetime of carbon dioxide means that ΔN_{TOA}, ΔF_{ERF} and ΔT_S will remain positive for
184 centuries, even with substantial reductions in greenhouse gas emissions, and lead to substantial
185 sea-level rise, ocean warming and ice shelf loss (Cheng et al., 2019; Forster et al., 2022; Hansen
186 et al., 2017; IPCC, 2021; Nauels et al., 2017). In other words, warming will continue even if
187 atmospheric greenhouse gas (GHG) amounts are stabilized at today's level, and the EEI defines
188 additional global warming that will occur without further change in forcing (Hansen et al., 2017).
189 The EEI is less subject to decadal variations associated with internal climate variability than global

190 surface temperature and therefore represents a robust measure of the rate of climate change, and
191 its future commitment (Cheng et al., 2017; Forster et al., 2022; Palmer & McNeall, 2014; von
192 Schuckmann et al., 2016).
193
194

195
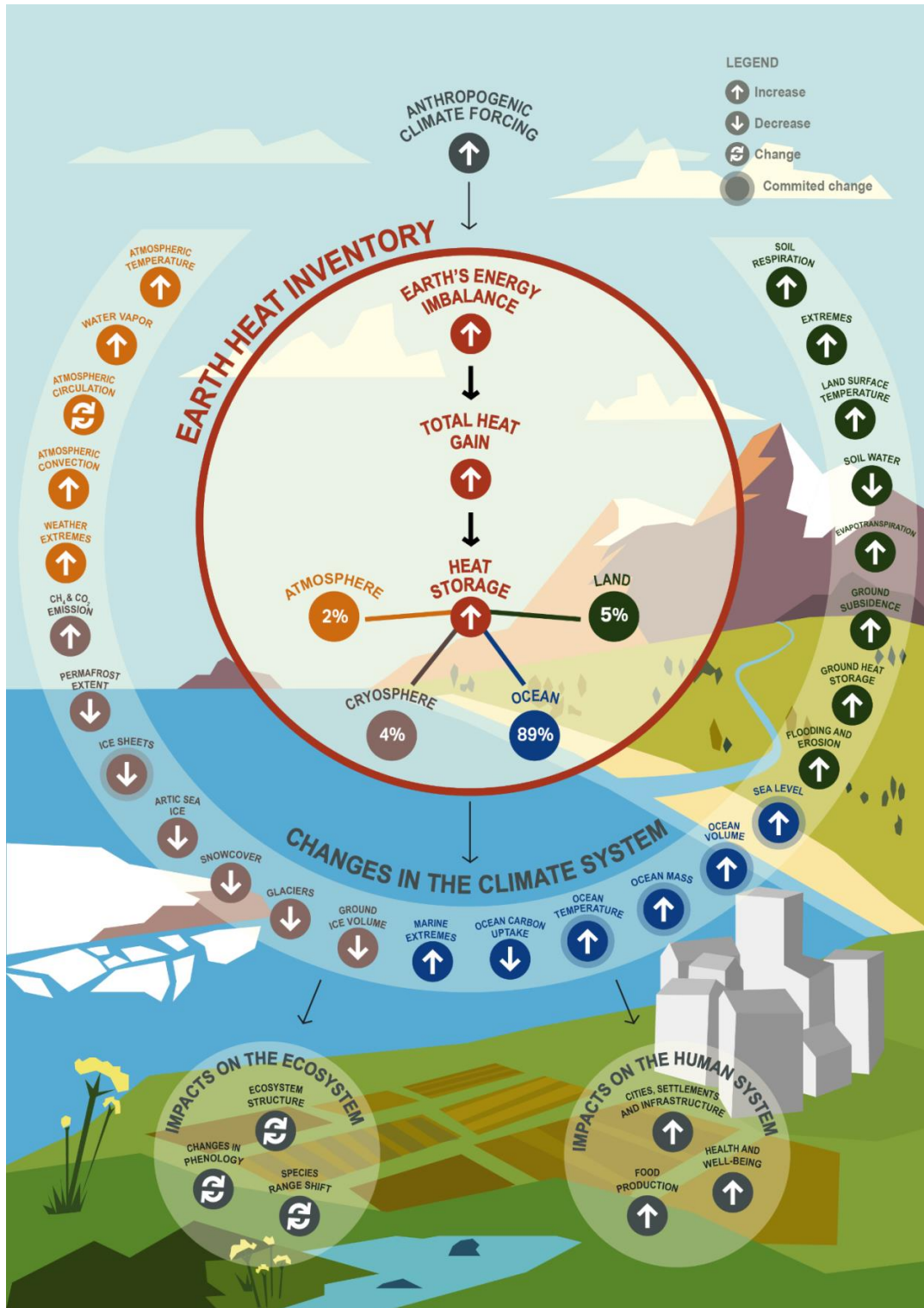
196 **Fig. 1:** *Schematic overview on the central role of the Earth heat inventory and its linkage to*
197 *anthropogenic emissions, the Earth energy imbalance, change in the Earth system and*
198 *implications for ecosystems and human systems. The Earth heat inventory plays a central role for*
199 *climate change monitoring as it provides information on the absolute value of the Earth energy*
200 *imbalance, the total Earth system heat gain, and how much and where heat is stored in the different*
201 *Earth system components. Examples of associated global-scale changes in the Earth system as*
202 *assessed in (Gulev et al., 2021) are drawn, together with major implications for the ecosystem and*
203 *human systems (IPCC, 2022c). Upward arrows indicate increasing change, downward arrows*
204 *indicate decreasing change, and turning arrows indicate change in both directions. The % for heat*
205 *stored in the Earth system are provided over the period 2006-2020 (see section 6).*
206
207 The heat gain in the Earth system from a positive EEI results in directly and indirectly triggered
208 changes in the climate system, with a variety of implications for the environment and human
209 systems (Fig. 1). One of the most direct implications from a positive EEI is the rise of Global Mean
210 Surface Temperature (GMST). The accumulation and storage of surplus anthropogenic heat leads
211 to ocean warming and thermal expansion of the water column, which together with terrestrial ice
212 melt leads to sea level rise (WCRP Global Sea Level Budget Group, 2018). Moreover, there are
213 various facets of impacts from ocean warming such as on climate extremes, which are provided in
214 more detail in a recent review (Cheng et al., 2022). The heat accumulation in the Earth system also
215 leads to warming of the atmosphere, particularly to a temperature increase in the troposphere,
216 leading to water vapor increase and changes in atmospheric circulation (Gulev et al., 2021).
217
218 On land, the heat accumulation leads to an increase in ground heat storage, which in turn triggers
219 an increase in ground surface temperature that may increase soil respiration, and evaporation, and
220 may lead to a decrease in soil water, depending on the climatic and meteorological conditions and
221 factors such as land cover and soil characteristics (Cuesta-Valero et al., 2022; Gulev et al., 2021).
222 Moreover, inland water heat storage increases, which in turn leads to increases in lake water
223 temperature that may result in algal blooms and lake stratification, and typically leads to a decrease
224 in ice cover. Heat gain in the Earth system also induces an increase in permafrost heat content,
225 which in turn increases ground subsidence, CH_4 and CO_2 emissions, and a decrease in permafrost
226 extent and ground ice volume. More details are synthesized in (Cuesta-Valero et al., 2022). In the
227 cryosphere associated changes include a loss of glaciers, ice sheets and Arctic sea ice (IPCC,
228 2019). These human-induced changes have already impacted terrestrial, freshwater and ocean
229 ecosystems, and have adverse impacts on human systems (Fig.1). Particularly, they have emerged
230 for ecosystem structure, species ranges and phenology (timing of life cycles), and include adverse
231 impacts such as for water security and food production, health and wellbeing, cities, settlements
232 and infrastructures as assessed in detail in the recent IPCC Working Group II report (IPCC, 2022c,
233 see their Fig. SPM.2).
234
235 In summary, the Earth heat inventory is a global climate indicator integrating fundamental aspects
236 of the Earth system under global warming. Particularly, the global climate indicator of the Earth
237 heat inventory
238
239 • provides the best available current estimate of the absolute value of the Earth Energy
240   Imbalance (Cheng et al., 2017; Cheng et al., 2019; Hakuba et al., 2021; Hansen et al., 2011;
241   Loeb et al., 2012, 2022; Trenberth et al., 2016; von Schuckmann et al., 2020),

242

243 • enables an integrated view of the effective radiative climate forcing, Earth's surface
244   temperature response and the climate sensitivity (Forster et al., 2022; Hansen et al., 2011;
245   Hansen et al., 2005; Palmer & McNeall, 2014; Smith et al., 2015),

246

247 • informs about the status of global warming in the Earth system as it integrates the heat 'in
248   the pipeline' that will ultimately warm the deep ocean and melt ice sheets in the long term
249   (Hansen et al., 2011; Hansen et al., 2005; IPCC, 2021),

250

251 • reveals how much and where surplus anthropogenic heat is available for melting the
252   cryosphere and warming the ocean, land and atmosphere, which in turn allows for an
253   evaluation of associated changes in the climate system and is essential to improve seasonal-
254   to-decadal climate predictions and projections on century timescales to enable improved
255   planning for and adaptation to climate change (Hansen et al., 2011; von Schuckmann et al.,
256   2016, 2020),

257

258 • provides a tool for assessing the status of the GCOS, the identification of its strength and
259   gaps, and the development of crucial recommendations of its future evolution (GCOS,
260   2021; von Schuckmann et al., 2020),

261

262 • creates an opportunity for a safe climate pathway while evaluating an atmospheric CO_2
263   reduction amount to bring Earth back towards energy balance (Hansen et al., 2000; von
264   Schuckmann et al., 2020).

265

266 • Enables concerted international and multidisciplinary collaboration and advancements in
267   climate science.

268

269 Hence, regularly assessing, quantifying and evaluating the Earth heat inventory creates a unique
270 opportunity to support the call of action and solution pathways as assessed during the 6th
271 assessment cycle of the IPCC. Moreover, the Earth heat inventory allows for a regular stock taking
272 of the implementation of the Paris Agreement[6] while monitoring progress towards achieving the
273 purpose of the agreement and its long-term goals based on best available science.

274

275 Based on the quantification of the Earth heat inventory published in 2020 (von Schuckmann et al.,
276 2020), we will present the updated results of the Earth heat inventory over the period 1960-2020,
277 along with the long-term Earth's system heat gain over this period, and the partitions of where the
278 heat goes for the ocean, atmosphere, land and cryosphere. Section 2 provides the updates for ocean
279 heat content, which is based on improved evaluations and the addition of further international data
280 products of subsurface temperature. Updated estimates and refinements for atmospheric heat
281 content are discussed in Section 3. For the land component in section 4, an improved uncertainty
282 framework is proposed for the ground heat storage estimate, and new evaluations for inland
283 freshwater heat storage and thawing of permafrost have been included (Cuesta-Valero et al., 2022).
284 Heat available to melt the cryosphere is described in section 5. In section 6, the updated Earth heat
285 inventory is established and discussed based on the results of sections 2-5. In the final section,

6   https://unfccc.int/process-and-meetings/the-paris-agreement/the-paris-agreement

286   challenges and recommendations for future improved estimates are discussed for each Earth
287   system component, with associated recommendations for future evolutions of the GCOS.
288
289   **2. Heat stored in the ocean**
290
291   Estimating global Ocean Heat Content (OHC) directly depends on the variables of the in situ
292   component of the Global Ocean Observing System (GOOS), which has continued to evolve during
293   the past century (Abraham et al., 2013; Gould et al., 2013; Moltmann et al., 2019). Many global
294   OHC estimates for the historical period start from about the 1950s and 1960s, i.e., when shipboard
295   Nansen bottle and mechanical bathythermograph (MBT) instruments, conductivity–temperature–
296   depth (CTD) instruments and the expendable bathythermograph (XBT) became available
297   (Abraham et al., 2013; Goni et al., 2019). In the 1980s and 1990s, the GOOS (GOOS, 2019) started
298   to further evolve, including programs for moored arrays in the tropical ocean basins, and the
299   international World Ocean Circulation Experiment (WOCE) (Gould et al., 2013; King et al., 2001).
300   Estimates of global OHC are, however, challenged by various factors, such as limited global
301   coverage and data quality. The international community, especially under the auspices of the
302   International qualiy-controlled Ocean Database project (IQuOD[7]), works together to face these
303   obstacles through data and meta-data recovery and improved observational uncertainty
304   specification, bias correction methods, and data processing techniques (Boyer et al., 2016;
305   Castelao, 2020; Castelão, 2021; Cheng et al., 2018; Cowley et al., 2021; Goni et al., 2019;
306   Gouretski & Cheng, 2020; Leahy et al., 2018; Mieruch et al., 2021; Palmer et al., 2018; Savita et
307   al., 2022). Satellite altimeter measurements of sea surface height began in 1993 and are used to
308   complement in situ-derived OHC estimates, either for validation purposes (Cabanes et al., 2013)
309   or for establishing global gridded ocean temperature fields (Guinehut et al., 2012; Willis et al.,
310   2004). Indirect estimates of OHC from remote sensing through the global sea-level budget became
311   possible with satellite-derived ocean mass information in 2002 (Dieng et al., 2017; Hakuba et al.,
312   2021; Llovel et al., 2014; Marti et al., 2022; Meyssignac et al., 2019), and should be considered in
313   future establishments of the Earth heat inventory.
314
315   From the year 2000 onwards, the in situ component of the GOOS was revolutionized with the
316   implementation of an international program of profiling floats targeting global hydrographic
317   measurements of the upper 2000m depth (Riser et al., 2016; Roemmich et al., 2019) – a target
318   which was largely reached in 2005 for the ocean area between 60°S-60°N and fully realized in
319   2006 (Riser et al. 2016). The opportunity for improved OHC estimates provided by Argo is
320   tremendous and has led to major advancements in climate science, particularly on the discussion
321   of the EEI (Cheng et al., 2019; Forster et al., 2022; Hansen et al., 2011; Johnson et al., 2016; Loeb
322   et al., 2012, 2021; Trenberth & Fasullo, 2010). The near global coverage of the Argo network also
323   provides an excellent test bed for the long-term OHC reconstruction extending back well before
324   the Argo period (Allison et al., 2019; Cheng, Trenberth, Fasullo, Boyer, et al., 2017). Moreover,
325   these evaluations inform further observing system recommendations for global climate studies,
326   i.e., gaps in the deep ocean layers below 2000m depth, in marginal seas, in shelf areas and in the
327   polar regions (von Schuckmann et al., 2016; 2020). Gap implementations are underway, for
328   example, for the deep Argo array (Johnson et al., 2019). Different research groups have developed
329   gridded products of subsurface temperature fields using different processing methodologies, and

---

7   www.iquod.org

Earth System
Science
Data

330   an exhaustive list can be found in (Abraham et al., 2013; Boyer et al., 2016; Savita et al., 2022;
331   Cheng et al., 2022; Gulev et al., 2021). Additionally, specific Argo-based products are listed on
332   the Argo web page (http://www.argo.ucsd.edu/, last access: 12 July 2022). Albeit the tremendous
333   improvement of in situ subsurface temperature measurements over time, estimates of global OHC
334   remain an area of active research to minimize effects from different data processing techniques of
335   the irregular in situ database, the choice of the climatology used in the mapping process, and data
336   bias corrections, which today induce discrepancies between the different estimates (Boyer et al.,
337   2016; Cheng et al., 2019; Good, 2017; Gouretski & Cheng, 2020; Savita et al., 2022). Ocean
338   reanalysis systems have also been used to deliver estimates of near-global OHC (Trenberth et al.,
339   2016; von Schuckmann et al., 2018), and their international assessments show increased agreement
340   with increasing in situ data availability for the assimilation, particularly after 2005, i.e. when Argo
341   had achieved nearly global scale data sampling (Palmer et al., 2017; Storto et al., 2018, 2019).
342
343   This initiative relies on the availability of regular updates of data products, their temporal
344   extensions and direct interactions with the different research groups. A complete view of all
345   subsurface ocean temperature products can be only achieved through a concerted international
346   effort and over time, particularly accounting for the continued development of new or improved
347   OHC products. In this study, we do not achieve a holistic view of all available products but present
348   a starting point for future international regular assessments of global OHC. A first established
349   international ensemble mean and standard deviation of near global OHC up to 2018 was
350   established in von Schuckmann et al. (2020), which has now been updated up to 2020, and further
351   extended with the addition of 4 new products (Fig. 3). The ensemble spread gives an indication of
352   the agreement among products and can be used as a proxy for uncertainty. Compared to the results
353   in von Schuckmann et al. (2020), the spread has increased by about 0.1 W m^{-2} the recent period
354   2006-2020 for the 0-2000m and 700-2000m integration depth layers. Concerns about common
355   errors in the products remain. Accurate understanding of the uncertainties of the product is an
356   essential element in their use. So far, a basic assumption is that the error distribution for the
357   observations is Gaussian with a mean of zero, which has been approximated by an ensemble of
358   various products. However, a more complete understanding of any apparent trends requires
359   determination of systematic errors (e.g., systematic calibration errors), or the impacts of changing
360   observation densities, and of instrument technologies (Wong et al., 2020). These elements can
361   result in biases across the ensemble, or produce artificial changes in the energetics of the system
362   (Wunsch, 2020). The uncertainty can also be estimated in other ways including some purely
363   statistical methods (Cheng et al., 2019; Levitus et al., 2012; MacIntosh et al., 2017) or methods
364   explicitly accounting for the error sources (Gaillard et al., 2016; Lyman & Johnson, 2014; von
365   Schuckmann & Le Traon, 2011). Each method has its caveats; for example, the error covariances
366   are mostly unknown, and must be estimated a priori. For this study, adopting a straightforward
367   method with a "data democracy" strategy (i.e., all OHC estimates have been given equal weights)
368   has been chosen as a starting point, differently from the ensemble approach adopted in AR6
369   (Forster et al., 2022).
370
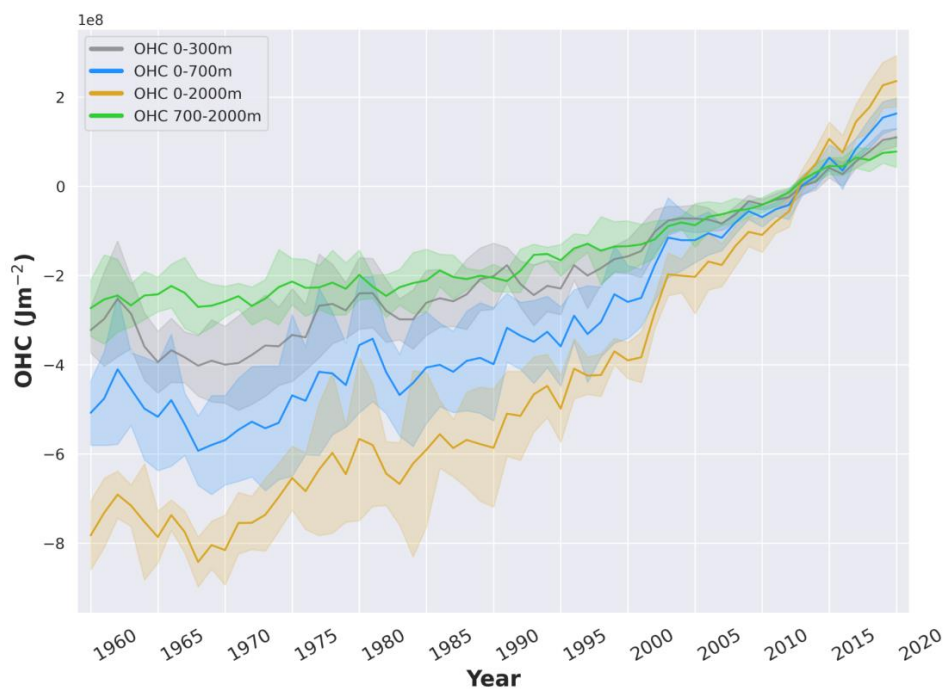
371
372 *Figure 2. Ensemble mean time series and ensemble standard deviation (2-σ, shaded) of global*
373 *ocean heat content (OHC) anomalies relative to the 2005–2020 climatology for the 0–300m*
374 *(gray), 0–700m (blue), 0–2000m (yellow) and 700–2000m depth layer (green). The ensemble mean*
375 *is an outcome of an international assessment initiative, and all products used are referenced in*
376 *the legend of Fig. 3. The trends derived from the time series are given in Table 1. Note that values*
377 *are given for the ocean surface area between 60°S and 60°N and are limited to the 300m*
378 *bathymetry of each product.*
379
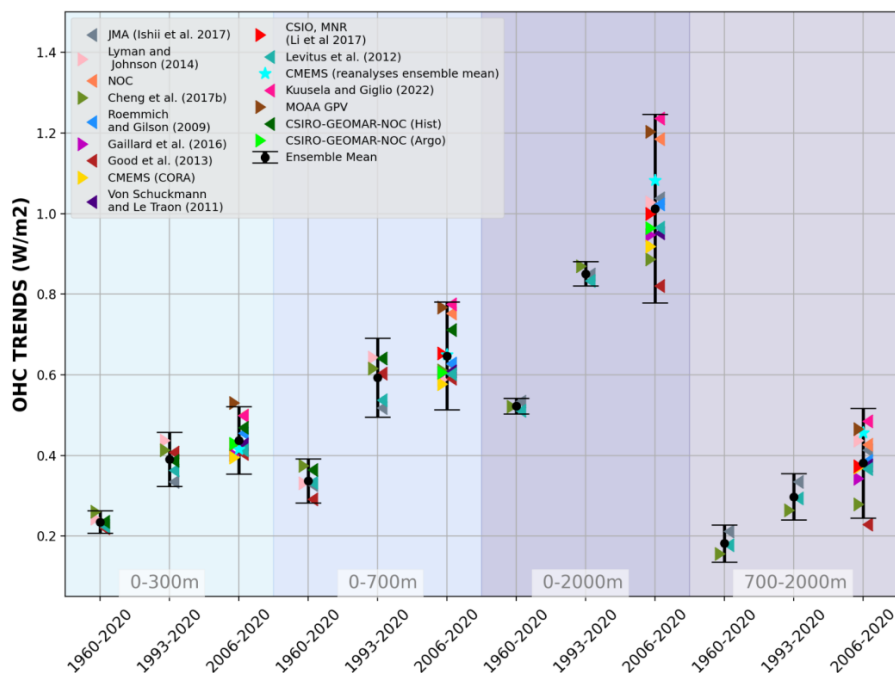
380
381 *Figure 3. Trends of global ocean heat content (OHC) as derived from different products (colors),*
382 *and using LOWESS (see text for more details). References are given in the figure legend, except,*
383 *CMEMS (CORA and ARMOR-3D, http://marine.copernicus.eu/science-learning/ocean-*
384 *monitoring-indicators, last access: 28 June 2022), CSIRO-GEOMAR-NOC (Argo) (Domingues et*
385 *al., 2008; Roemmich et al., 2015; Wijffels et al., 2016), CSIRO-GEOMAR-NOC (hist) (Church et*
386 *al., 2011; Domingues et al., 2008), NOC (National Oceanographic Institution) (Desbruyères et*
387 *al., 2017) and the Argo dataset MOAA GPV (Hosoda et al., 2008). The ensemble mean and*
388 *standard deviation (2 σ) are indicated in black. The shaded areas show trends from different depth*
389 *layer integrations, i.e., 0–300m (light turquoise), 0–700m (light blue), 0–2000m (purple) and 700–*
390 *2000m (light purple). For each integration depth layer, trends are evaluated over the three study*
391 *periods, i.e., historical (1960–2020), altimeter era (1993–2020) and golden Argo era (2006–*
392 *2020). See text for more details on the international assessment criteria. Note that values are given*
393 *for the ocean surface area (see text for more details). References as indicated in the legend include*
394 *(Cheng, Trenberth, Fasullo, Boyer, et al., 2017; Gaillard et al., 2016; Good et al., 2013; Ishii et*
395 *al., 2017; Kuusela & Giglio, 2022; Levitus et al., 2012; Li et al., 2017; Lyman & Johnson, 2014;*
396 *Roemmich & Gilson, 2009; von Schuckmann & Le Traon, 2011).*

397
398 The continuity of this activity will help to further expand international collaboration and to unravel
399 uncertainties due to the community's collective efforts on data quality as well as on detecting and
400 reducing processing errors (e.g., IQuOD). It also provides up-to-date scientific knowledge of ocean
401 warming. Products used for this assessment are referenced in the caption of Fig. 3. Estimates of
402 OHC have been provided by the different research groups under largely homogeneous criteria. All

403 estimates use a coherent ocean volume limited by the 300m isobath of each product and are limited
404 to 60°S–60°N since most observational products exclude high latitude ocean areas because of the
405 low observational coverage, and only annual averages have been used. The ocean areas within
406 60°S–60°N includes 91% of the global ocean surface area, and limiting to the 300m isobath
407 neglects the contributions from coastal and shallow waters, so the resultant OHC trends will be
408 underestimated if these ocean regions are warming. For example, neglecting shallow waters is
409 discussed to account for more than 10% for 0–2000m OHC trends (Savita et al., 2022; von
410 Schuckmann et al., 2014), and about 4% for the Arctic area (Mayer et al., 2021). The assessment
411 is based on three distinct periods to account for the evolution of the observing system, i.e., 1960–
412 2020 (i.e., "historical"), 1993–2020 (i.e., "altimeter era") and 2006–2020 (i.e., "golden Argo era").
413 All time series go up to 2020 – which was one of the principal limitations for the inclusion of some
414 products. Our final estimates of OHC for the 0-300m, 0-700m, 700-2000m and 0-2000 m depth
415 layers are the ensemble average of all products, with the uncertainty range defined by the standard
416 deviation (2σ) of the corresponding estimates used (Fig. 2).

418 For the trend evaluation we have followed the most recent study of (Cheng et al., 2022), and used
419 a Locally Weighted Scatterplot Smoothing (LOWESS) approach to reduce the effect of high-
420 frequency variability (e.g., year-to-year variability), data noise or changes in the GCOS as it relies
421 on a weighted regression (Cleveland, 1979) within a prescribed span width of 25 years for the
422 historical and altimeter era, and 15 years for the recent period 2006-2020. The change in OHC(t)
423 over a specific period, ΔOHC, is then calculated by subtracting the first value to the last value of
424 the fitted time series, $OHC_{LOWESS(t)}$, to obtain the trend while dividing by the considered period.
425 To obtain an uncertainty range on the trend estimate, and take into account the sensitivity of the
426 calculation to interannual variability, we implement a Monte-Carlo simulation to generate 1000
427 surrogate series $OHC_{random}(t)$, under the assumption of a given mean (our "true" time series
428 OHC(t)) (Cheng et al., 2022). Each surrogate $OHC_{random}(t)$ consists of the "true" time serie OHC(t)
429 plus a randomly generated residual which follows a normal (Gaussian) distribution, and which is
430 included in an envelope equal to 2 times the uncertainty associated to the time series. Then, a
431 LOWESS fitted line is estimated for each of the 1000 surrogates. The 95% confidence interval for
432 the trend is then calculated based on $\pm$ 2 times the standard deviation ($\pm$ 2-σ) of all 1000 trends of
433 the surrogates. However, the use of either trend estimates following a linear, or LOWESS
434 approach, or the approach discussed in (Palmer et al., 2021) lead to consistent results within
435 uncertainties (not shown).

437 In agreement with (Cheng et al., 2019; Gulev et al., 2021), our results reveal a continuous increase
438 of ocean warming over the entire study period (Fig. 2). Moreover, rates of global ocean warming
439 have increased over the 3 different study periods, i.e., historical up to the recent decadal change.
440 The trend values are all given in Table 1. The major fraction of heat is stored in the upper ocean
441 (0–300 m and 0–700 m depth). However, heat storage at intermediate depth (700–2000 m)
442 increases at a nearly comparable rate as reported for the 0–300 m depth layer (Table 1, Fig. 3).
443 There is a general agreement among the 16 international OHC estimates (Fig. 3). However, for
444 some periods and depth layers the standard deviation reaches maxima to about 0.3 W m^{-2}. All
445 products agree on the fact that global ocean warming rates have increased in the past decades and
446 doubled since the beginning of the altimeter era (1993–2020 compared with 1960–2020) (Fig. 3).
447 Moreover, there is a clear indication that heat sequestration into the deeper ocean layers below
448 700 m depth took place over the past 6 decades linked to an increase in OHC trends over time (Fig.

449 3). Ocean warming rates for the 0–2000 m depth layer reached record rates of 1.0 (0.7) $\pm$0.3 W m^{-2}
450 over the period 2006-2020 for the ocean (global) area.
451
452

	Ocean Heat Content linear trends (W/m²)			
	0-300m	**0-700m**	**0-2000m**	**700-2000m**
1960-2020	0.24 ± 0.1	0.34 ± 0.1	0.53 ± 0.1	0.18 ± 0.04
1971-2020	0.30 ± 0.1	0.44 ± 0.1	0.62 ± 0.1	0.21 ± 0.03
1993-2020	0.39 ± 0.1	0.60 ± 0.1	0.86 ± 0.2	0.30 ± 0.04
2006-2020	0.44 ± 0.1	0.64 ± 0.1	1.00 ± 0.3	0.38 ± 0.1

453
454 *Table 1: OHC trends using LOWESS (Locally Weighted Scatterplot Smoothing, see text for more*
455 *details) as derived from the ensemble mean (Fig. 2) for different time intervals, as well as different*
456 *integration depths. The regression was done for each time period (1960 - 2020, 1971 - 2020, 1993*
457 *- 2020, 2006 -2020). A time window of 25 years was used for the periods that allowed it (1960 -*
458 *2020, 1971 - 2020, 1993 - 2020). For the period 2006 - 2020, a time window of 15 years was used.*
459 *Note that values are given in Wm^{-2} relative to the ocean surface area between 60°S and 60°N and*
460 *are limited to the 300 m bathymetry of each product. See also text and Fig. 2-3 for more details.*
461
462
463 For the deep OHC changes below 2000 m, we adapted an updated estimate from (Purkey &
464 Johnson, 2010) (PG10 hereinafter) from 1991 to 2020, which is a constant linear trend estimate
465 (0.97 ± 0.48 ZJ yr^{-1}, 0.06 ±0.03 W m^{-2}) derived from a global integration of OHC below 2000 m
466 using basin scale deep ocean temperature trends from repeated hydrographic sections. Some recent
467 studies strengthened the results in PG10 (Desbruyères et al., 2016; Zanna et al., 2019). Desbruyères
468 et al. (2016) examined the decadal change of the deep and abyssal OHC trends below 2000 m in
469 the 1990s and 2000s, suggesting that there has not been a significant change in the rate of decadal
470 global deep/abyssal warming from the 1990s to the 2000s and the overall deep ocean warming rate
471 is consistent with PG10. Using a Green's function method and ECCO reanalysis data, Zanna et al.
472 (2019) reported a deep ocean warming rate of ~0.06 W m^{-2} during the 2000s, consistent with PG10
473 used in this study. Zanna et al. (2019) shows a fairly weak global trend during the 1990s, different
474 from observation-based estimates. This mismatch might come from how surface-deep connections
475 are represented in ECCO reanalysis data and the use of time-mean Green's functions in Zanna et
476 al. (2019), as well as from the sparse coverage of the observational network for relatively short
477 time spans. Furthermore, combining hydrographic and deep-Argo floats, a recent study (Johnson
478 et al., 2019) reported an accelerated warming in the South Pacific Ocean in recent years, but a
479 global estimate of the OHC rate of change over time is not available yet, and the rates of warming
480 may vary by ocean basin.
481
482 Before 1990, we assume zero OHC trend below 2000 m due to insufficient global observations
483 below 2000m, following the methodology in some studies (Cheng et al. 2017; 2022), IPCC-AR5
484 (Rhein et al., 2013) and IPCC-AR6 (Forster et al., 2022; Gulev et al. 2021). The deep warming is
485 likely driven by decadal variability in deep water formation rates, which could have been in a non-
486 steady state mode prior to 1990, introducing additional uncertainty to the pre-1990 OHC estimates.
487 Using surface temperature observations and assuming the heat is advected by mean circulation,

488   Zanna et al. (2019) shows a near-zero (small cooling trend) OHC trend below 2000 m from the
489   1960s to 1980s, suggesting the assumption of zero-trend before 1990 might be small. The derived
490   time following PG10 series after 1991 and zero-trend before 1990 is used for the Earth energy
491   inventory in Sect. 5. A centralized (around the year 2006) uncertainty approach has been applied
492   for the deep (>2000 m depth) OHC estimate following the method of Cheng et al. (2017), which
493   allows us to extract an uncertainty range over the period 1993–2018 within the given [lower (0.96–
494   0.48 ZJ yr^{-1}), upper (0.96+0.48 ZJ yr^{-1})] range of the deep OHC trend estimate. We then extend
495   the obtained uncertainty estimate back from 1993 to 1960, with 0 OHC anomaly.

3. Heat available to warm the atmosphere

501   The heat content of the atmosphere is small in absolute terms, since its heat capacity as a gas is
502   small compared to the one of the other Earth subsystems discussed in this paper. Yet it is by no
503   means negligible, since in relative terms, the atmospheric heat gain is rapid over the recent decades
504   and has a high impact on human life (Fig. 1). As for Earth's surface, widespread and rapid changes
505   are ongoing in the atmosphere due to human-induced climate change (IPCC, 2021).

506   Atmospheric observations show a warming of the troposphere and a cooling and contraction of the
507   stratosphere since at least 1979 (Pisoft et al., 2021; Steiner et al., 2020). In the tropics, the upper
508   troposphere has warmed faster than the near-surface atmosphere since at least 2001, as seen with
509   the new observation technique of GPS radio occultation (Gulev et al., 2021; Steiner et al., 2020a;
510   2020b), while observations based on microwave soundings have likely underestimated
511   tropospheric temperature trends in the past (Santer et al., 2021; Zou et al., 2021).

512   Recently, a continuous rise of the tropopause has been observed for 1980 to 2020 over the northern
513   hemisphere (Meng et al., 2022). The increase is equally due to tropospheric warming and
514   stratospheric cooling in the period 1980 to 2000 while the rise after 2000 resulted primarily from
515   enhanced tropospheric heat gain. Moreover, indications exist on a widening of the tropical belt (Fu
516   et al., 2019; Grise et al., 2019; Staten et al., 2020) as well as on changes in the seasonal cycle
517   (Santer et al., 2022). However, changes in atmospheric circulation and conditions for extreme
518   weather are still subject to uncertainty (Cohen et al., 2020) while the occurrence of heat-related
519   extreme weather events has clearly increased over the recent decades (Cohen et al., 2020; IPCC,
520   2021), with high risks for society, economy, and the environment (Fischer et al., 2021).

521   A regular assessment of atmospheric heat content changes is hence critical for a complete overview
522   of energy and mass exchanges with other climate components and for a complete energy budgeting
523   of Earth's climate system.

3.1 Atmospheric heat content

525   In a globally averaged and vertically integrated sense, heat accumulation in the atmosphere arises
526   from a small imbalance between net energy fluxes at the top-of-atmosphere (TOA) and the surface
527   (denoted s). The heat energy budget of the vertically integrated and globally averaged atmosphere
528   (indicated by the global averaging operator <.>) reads as follows (Mayer et al., 2017):

529
$$\frac{\partial AE}{\partial t} > N_{TOA} > -F_s > -F_{snow} > -F_{PE} >, (1)$$

530   where the vertically integrated atmospheric energy content AE per unit surface area [Jm^{-2}] reads

531
$$AE = \int_{z_s}^{z_{TOA}} \rho \left(c_v T + g(z - z_s) + L_e q + \frac{1}{2}V^2 \right) dz. (2)$$

532   In Equation (1), formulated in mean-sea-level altitude (z) coordinates used here for integrating
533   over observational data, N_{TOA} is the net radiation at top of the atmosphere, F_s is the net surface
534   energy flux defined as the sum of net surface radiation and latent and sensible heat fluxes, F_{snow}
535   denotes the latent heat flux associated with snowfall, and F_{PE} additionally accounts for sensible
536   heat of precipitation. See Mayer et al. (2017) or von Schuckmann et al. (2020) for a discussion of
537   the latter two terms, which are small on a global scale and hence often neglected.

538   Equation (2) provides a decomposition of AE into sensible heat energy (sum of the first two terms,
539   internal heat energy and gravity potential energy), latent heat energy (third term), and kinetic
540   energy (fourth term), where ρ is the air density, c_v the specific heat for moist air at constant volume,
541   T the air temperature, g the acceleration of gravity, L_e the temperature-dependent effective latent
542   heat of condensation L_v or sublimation L_s (the latter relevant below 0 °C), q the specific humidity
543   of the moist air, and V the wind speed. We neglect atmospheric liquid water droplets and ice
544   particles as separate species, as their amounts and especially their trends are small.

545   In computing AE for the purpose of this update to the von Schuckmann et al. (2020) heat storage
546   assessment, we continued to use the formulations described therein, including that we refer to the
547   (geographically aggregated) AE as atmospheric heat content (AHC) in this context, acknowledging
548   the dominance of the heat-related terms in Eq. (2). Briefly, in deriving the AHC from observational
549   datasets, we accounted for the intrinsic temperature-dependence of the latent heat of water vapor
550   in formulating L_e (for details see Gorfer, 2022) while the reanalysis derivations approximated L_e
551   by constant values of L_v, as this simplification is typically also made in the assimilating models
552   (e.g., ECMWF-IFS, 2015). As another small difference, the observational estimations neglected
553   the kinetic energy term in Eq. (2) while the reanalysis estimations accounted for it. The resulting
554   differences in AHC anomalies from any of these differences are negligibly small, however,
555   especially when considering trends over time.

556   **3.2 Datasets and heat content estimation**

557   Turning to the actual datasets used, the AHC and its changes and trends over time can be quantified
558   using various data sources, observation-based and reanalyses. Reassessing possible data sources,
559   we extended the high-quality datasets that we used in the initial von Schuckmann et al. (2020)
560   assessment. In particular, we updated the time period from 2018 to 2020 and improved the back-
561   extension from 1980 to 1960. Specifically, the adopted datasets and the related AHC data record
562   preparations can be summarized as follows.

563   Atmospheric reanalyses combine observational information from various sources (radiosondes,
564   satellites, weather stations, etc.) and a dynamical model in a statistically optimal way. These data
565   have reached a high level of maturity, thanks to continuous improvement work since the early
566   1990s (Hersbach et al., 2018). Especially reanalyzed thermodynamic state variables, like

567 temperature and water vapor that are most relevant for AHC computation, are of high quality and
568 suitable for climate studies, although temporal discontinuities introduced from changing observing
569 systems continue to deserve due attention (Berrisford et al., 2011; Chiodo & Haimberger, 2010;
570 Hersbach et al., 2020; Mayer et al., 2021).

571 We use the latest generation of reanalyses, including ECMWF's Fifth generation reanalysis ERA5
572 (Bell et al., 2021; Hersbach et al., 2020), JMA's reanalysis JRA55 (Kobayashi et al., 2015), and
573 NASA's Modern-Era Retrospective analysis for Research and Applications version 2 (MERRA2)
574 (Gelaro et al., 2017). ERA5 and JRA55 are both available over the full joint timeframe of this heat
575 storage assessment from 1960 to 2020, while MERRA2 complements these from 1980 to 2020.
576 The additional JRA55C reanalysis variant of JRA55, included for initial inter-comparison in von
577 Schuckmann et al. (2020), is no longer used since it is available to 2012 only and due to its
578 similarity to JRA55 is not adding appreciable complementary value.

579 In addition to these three reanalyses, the datasets from two climate-quality observation techniques
580 are used, for complementary observational AHC estimates. These include the Wegener Center
581 (WEGC) multi-satellite radio occultation (RO) data record, WEGC OPSv5.6 (Angerer et al., 2017;
582 Steiner et al., 2020b), over 2002-2020 and its radiosonde (RS) data record derived from the high-
583 quality Vaisala sondes RS80/RS92/VS41, WEGC Vaisala (Ladstädter et al., 2015), covering 1996-
584 2020. These RO and RS data sets provide atmospheric profiles of temperature, specific humidity,
585 and density that are vertically completed by collocated ERA5 profiles in domains not fully covered
586 by the data (e.g., in the lower troposphere for RO or at polar latitudes for RS). Similar to dropping
587 the JRA55C reanalysis variant for no longer adding value, the microwave sounding unit (MSU)
588 observational data, inter-compared in von Schuckmann et al. (2020), are no longer used.

589 From the observational data, the AHC is estimated by first evaluating Eq. (2) (using all terms for
590 total and the third term only for latent AHC) at each available profile location and subsequently
591 deriving it as volumetric heat content, for up to global scale, from vertical integration, temporal
592 averaging, and geographic aggregation according to the approach summarized in von Schuckmann
593 et al. (2020) and described in detail by (Gorfer, 2022). For the reanalyses, the estimation is based
594 on the full gridded fields. Applying the approach for crosscheck to reanalysis profiles sub-sampled
595 at observation locations only, confirms its validity as it accurately leads to the same AHC results
596 as from the full gridded fields.

597 **3.3 Atmospheric heat content change since 1960 and its amplification**

598 Figure 4 shows the resulting global AHC change inventory over 1960 to 2020 (61 years record),
599 in terms of total AHC anomalies for each data type (Fig. 4a), and for the ensemble mean with
600 trends for selected periods and uncertainty estimates (Fig. 4c). The selected trend periods align
601 with those for ocean data and with availability of atmospheric data sets (see subsection 3.2 above)
602 and represent a reference trend 1961-2000 plus recent trends of the last about 30, 20, and 15 years,
603 respectively. Latent AHC anomalies, a key component of the AHC (Matthews et al., 2022), are
604 also shown (Fig. 4b and 4d). Compared to von Schuckmann et al. (2020), the AHC data have the
605 ENSO signal removed (with ENSO regressed out via the Nino 3.4 Index; and cross-check with
606 non-ENSO-corrected data showing that trend differences are reasonably small). Variability due to

607 volcanic eruptions is still included, however, and may somewhat influence the trends over 1993-
608 2020, which start in the cold anomaly after the Pinatubo eruption (Santer et al., 2001).

609 The latent AHC (Fig. 4b and 4d), which accounts for about one-quarter of the total AHC, exhibits
610 a qualitatively similar temporal evolution as total AHC, however with larger relative uncertainty
611 compared to the total AHC. The RO and RS data sets in Fig. 3b show some differences, particularly
612 the low latent AHC values in the 1990s and early 2000s from the RS WEGC Vaisala data set likely
613 stem from known dry biases of the RS80/RS90/RS92 humidity sensors (Verver et al., 2006; Vömel
614 et al., 2007). Estimated trends based on these RS data are thus likely too high, although the overall
615 increase in latent AHC is substantial also in the other datasets.

616
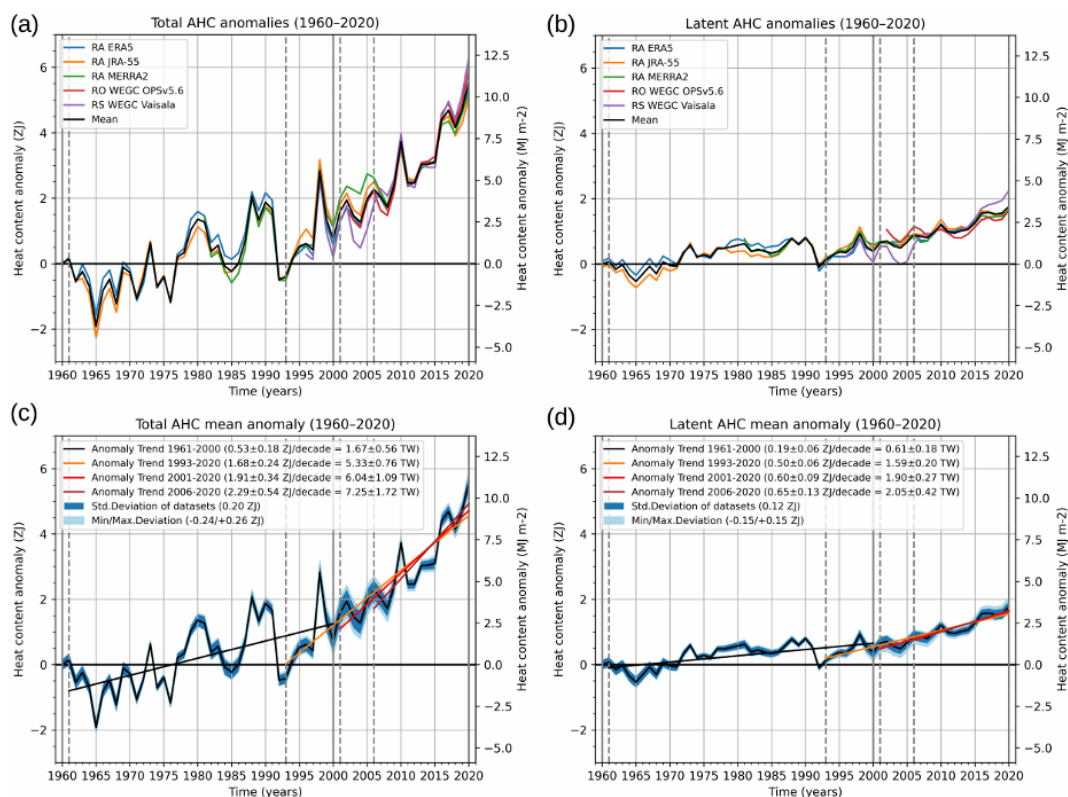
618 *Figure 4. Annual-mean global AHC anomalies from 1960 to 2020 of total AHC (left) and latent-*
619 *only AHC (right), respectively, of three different reanalyses and two different observational*
620 *datasets shown together with their mean (top), and the mean AHC anomaly shown together with*
621 *four representative AHC trends and ensemble spread measures of its underlying datasets (bottom).*
622 *The in-panel legends identify the individual datasets (top) and the selected trend periods together*
623 *with the associated trend values (plus 90 % confidence range) and ensemble spread measures*
624 *(bottom), the latter including the time-average standard deviation and minimum/maximum*
625 *deviations of the individual datasets from the mean.*

626

627   The results clearly show that the AHC trends have increased from the earlier decades represented
628   by the 1961-2000 trend of near 1.7 TW. We find the mean trend about 2.5 times higher over 1993-
629   2020 (about 5.3 TW) and about four times higher in the most recent two decades (about 6-7 TW),
630   a period that is already covered also by the RO and RS records. Latent AHC trends in the most
631   recent periods are 3 times larger than the 1961-2000 reference period. Since 1971, the heat gain in
632   the atmosphere amounts to 5 ± 1 ZJ (see also Fig. 8).

633   The remarkable amplification of total AHC and latent AHC trends is highlighted in Figure 4 and
634   summarized in Table 2 for the representative recent periods vs. the 1961-2000 reference period.
635   The 1961-2000 and 1993-2020 periods were covered by reanalysis only, while the WEGC Vaisalä
636   RS dataset additionally covers the 2001-2020 and 2006-2020 periods and the RO dataset the most
637   recent period (see dataset descriptions in subsection 3.2). The larger diversity of recent datasets
638   induces more spread; for example, the RS dataset shows an amplification factor of near 4.5 in the
639   global total AHC gain for 2001-2020, while the amplification factors from the reanalyses range
640   from 2.6 to 3.8. Amplifications are generally largest in the southern hemisphere extratropics and
641   weakest in the tropics. In the most recent period 2006-2020, the amplification factors are strongest,
642   with the RS and RO data sets on the high end of the spread (near factor 5 in global total AHC) and
643   somewhat smaller but still high from the reanalyses (around factor 4).
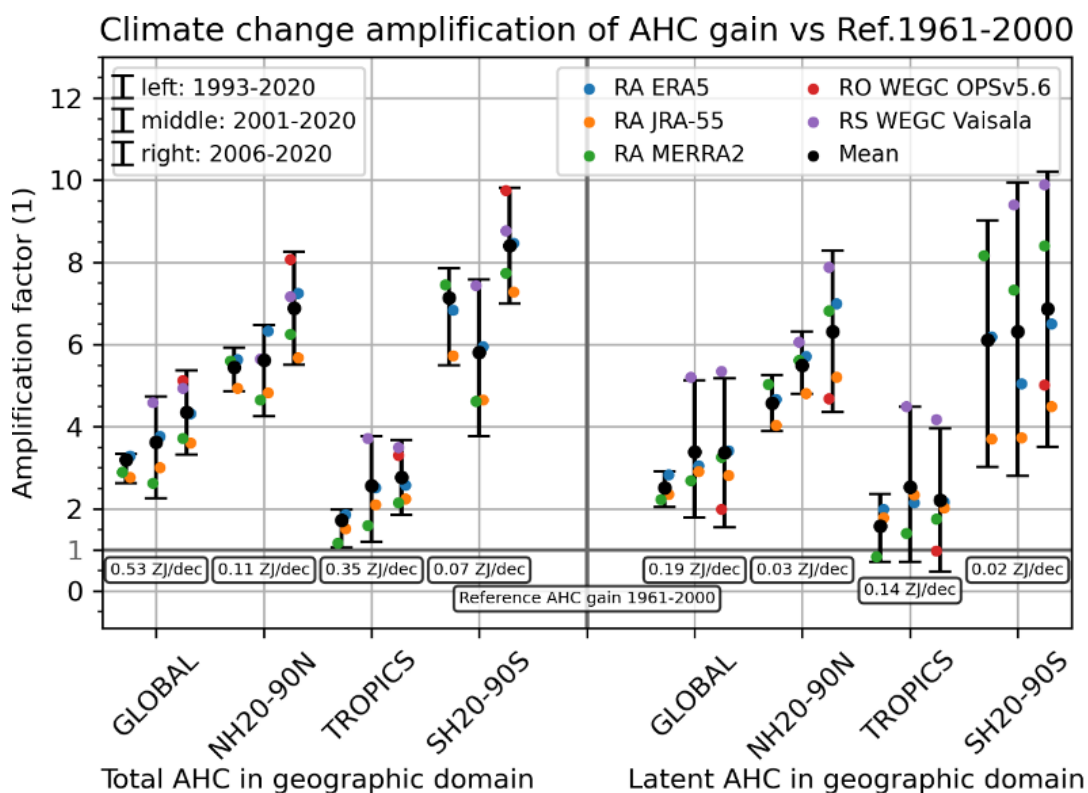
644

645 ***Figure 5.** Amplification of long-term trends in AHC anomalies ("AHC gain") for total AHC (left)*
646 *and latent-only AHC (right) in four geographic domains (global, northern-hemisphere*
647 *extratropics, tropics, southern-hemisphere extratropics) for three recent time periods (legend*
648 *upper-left) expressed as a ratio of the trend of each period relative to the trend in the previous-*
649 *century reference period 1961-2000 (noted below the "amplification factor = 1" reference line).*
650 *The amplification factor for each recent-trend case (for the four domains of both total and latent*
651 *AHC) is depicted for the mean anomaly serving as best estimate (larger black circles), the related*
652 *recent trends in the individual-dataset anomalies (colored circles as per upper-right legend). The*
653 *related 90 % uncertainty range (black "error bar") is estimated from the spread (standard*
654 *deviation) of the individual-dataset amplification factors. The trend in the mean anomaly over*
655 *1961-2000 is used as the reference AHC gain.*

656 For the latent AHC amplification factors, we see moderate values in the 1993-2020 period in the
657 global mean and tropics. In the tropics, the lower uncertainty bound for amplification is slightly
658 below 1 during all three recent trend periods. The spread of the amplification factors increases for
659 the most recent periods, which is on the one hand due to the shorter period duration. The range
660 increase is also related to the introduction of the RS and RO data sets after 1993-2020 which
661 contribute the largest and smallest latent AHC gain amplification factors. For 2006-2020, the
662 global mean amplification factor from RO is about 2, whereas from the RS data set it is near 5.
663 Regarding latitudinal bands, the amplification factors are again strongest in the extratropics,
664 exhibiting a large spread especially in the southern extratropics. The relatively large amplification
665 factors of the RS WEGC Vaisala data set are likely exaggerated due to the well documented dry
666 bias of the early RS humidity sensors as noted above (Vömel, 2007; Verver et al., 2006).

667 Despite the uncertainties and spread described, the overall message from Figure 5 and Table 2 is
668 very clear and substantially reinforcing the evidence from the initial von Schuckmann et al. (2020)
669 assessment: the trends in the AHC, including in its latent heat component, show that atmospheric
670 heat gain has accelerated over the recent decades at an unprecedented rate.

Domain	Time range	Total AHC Gain		Latent AHC Gain	
		Gain ZJ/decade (TW)	Amplification vs Ref.	Gain ZJ/decade (TW)	Amplification vs Ref.
GLOBAL	1993-2020	1.68±0.24 (5.33±0.76)	3.19 [2.63 to 3.34]	0.50±0.06 (1.59±0.20)	2.51 [2.05 to 2.91]
	2001-2020	1.91±0.34 (6.04±1.09)	3.62 [2.27 to 4.73]	0.60±0.09 (1.90±0.27)	3.39 [1.79 to 5.13]
	2006-2020	2.29±0.54 (7.25±1.72)	4.35 [3.33 to 5.36]	0.65±0.13 (2.05±0.42)	3.37 [1.55 to 5.18]
	Ref. 1961-2000	0.53±0.18 (1.67±0.56)	1.0	0.19±0.06 (0.61±0.18)	1.0
NH20-90N	1993-2020	0.62±0.11 (1.97±0.35)	5.44 [4.86 to 5.92]	0.16±0.02 (0.50±0.08)	4.57 [3.90 to 5.26]
	2001-2020	0.64±0.15 (2.03±0.47)	5.62 [4.26 to 6.48]	0.18±0.03 (0.58±0.11)	5.50 [4.79 to 6.31]
	2006-2020	0.79±0.25 (2.49±0.80)	6.89 [5.51 to 8.26]	0.22±0.05 (0.70±0.17)	6.32 [4.36 to 8.28]
	Ref. 1961-2000	0.11±0.08 (0.36±0.24)	1.0	0.03±0.02 (0.11±0.05)	1.0
TROPICS	1993-2020	0.60±0.13 (1.90±0.41)	1.72 [1.05 to 1.98]	0.24±0.04 (0.75±0.12)	1.58 [0.71 to 2.36]
	2001-2020	0.89±0.15 (2.82±0.47)	2.56 [1.20 to 3.77]	0.31±0.05 (1.00±0.16)	2.52 [0.70 to 4.49]
	2006-2020	0.96±0.24 (3.04±0.77)	2.76 [1.86 to 3.67]	0.31±0.07 (0.99±0.22)	2.22 [0.48 to 3.96]
	Ref. 1961-2000	0.35±0.08 (1.10±0.25)	1.0	0.14±0.03 (0.45±0.11)	1.0
SH20-90S	1993-2020	0.46±0.09 (1.46±0.29)	7.14 [5.49 to 7.86]	0.11±0.02 (0.33±0.05)	6.11 [3.02 to 9.02]
	2001-2020	0.37±0.17 (1.18±0.52)	5.80 [3.76 to 7.58]	0.10±0.03 (0.32±0.08)	6.31 [2.81 to 9.95]
	2006-2020	0.54±0.25 (1.71±0.79)	8.40 [6.99 to 9.81]	0.11±0.04 (0.36±0.12)	6.87 [3.52 to 10.22]
	Ref. 1961-2000	0.06±0.06 (0.20±0.18)	1.0	0.02±0.01 (0.05±0.05)	1.0

671

672   ***Table 2.*** *Long-term trend values in mean AHC anomalies (AHC gains; in units ZJ/decade and TW)*
673   *and amplification factors vs. the 1961-2000 reference gain (grey "Ref." lines), for total AHC (left*
674   *block) and latent-only AHC (right block) for the three recent time periods in four geographic*
675   *domains as illustrated in Figure 4. The AHC gain and amplification values are listed together with*
676   *their 90% confidence ranges.*

677

678

679   **4. Heat available to warm land**

680

681   In previous studies the land term of the Earth heat inventory was considered as the heat used to
682   warm the continental subsurface (Hansen et al. 2011; Rhein et al. 2013; von Schuckmann et al.
683   2020). Temperature changes within the continental subsurface are typically retrieved by analyzing
684   the global network of temperature-depth profiles, measured mostly in the northern hemisphere,
685   southern Africa, and Australia. Each temperature profile records changes in subsurface
686   temperatures caused by the heat propagated through the ground due to alterations in the surface
687   energy balance (Cuesta-Valero et al., 2022a). Such perturbations in the subsurface temperature
688   profiles can be analyzed to recover the changes in past surface conditions that generated the
689   measured profile, allowing a reconstruction of the evolution of ground surface temperatures and
690   ground heat fluxes at decadal to centennial time scales (Beltrami et al., 2002; Beltrami &
691   Mareschal, 1992; Demezhko & Gornostaeva, 2015; Hartmann & Rath, 2005; Hopcroft et al., 2007;
692   Jaume-Santero et al., 2016; Lane, 1923; Pickler et al., 2016; Shen et al., 1992). Although previous
693   estimates only considered changes in ground temperatures for representing the heat storage by
694   exposed land, ground heat storage has been found to be the second largest term of the Earth heat
695   inventory accounting for 4 % to 6 % of the total heat in the Earth System (von Schuckmann et al.
696   2020, section 6).

697

698   The ground heat is, nevertheless, not the only energy component of the continental landmasses.
699   Other processes with large thermodynamic coefficients, such as permafrost thawing and the
700   warming of inland water bodies, occur across large areas, leading to the exchange of large amounts
701   of heat with their surroundings over time. To account for those heat exchanges, a recent study
702   (Cuesta-Valero et al., 2022a) has estimated the heat uptake by permafrost thawing and the warming
703   of inland water bodies, as well as ground heat storage from subsurface temperature profiles,
704   resulting in a comprehensive estimate of continental heat storage. The authors used the same global
705   network of subsurface temperature profiles as in von Schuckmann et al. (2020) to estimate ground
706   heat storage but applied an improved inversion technique to analyze the profiles. This new
707   technique is based on combining bootstrapping sampling with a widely-used Singular Value
708   Decomposition (SVD) algorithm (e.g., Beltrami et al., 1992) to retrieve past changes in surface
709   temperatures and ground heat fluxes, which also resulted in smaller uncertainty estimates for
710   global results (Cuesta-Valero et al., 2022b). Heat uptake from permafrost thawing was estimated
711   using a large ensemble of simulations performed with the CryoGridLite permafrost model
712   (Nitzbon et al., 2022). Ground stratigraphies required for this purpose, including ground ice
713   distributions, were generated using various global ground datasets. Latent heat storage due to
714   melting of ground ice is evaluated to a depth of 550 m over the Arctic region. Uncertainty ranges
715   are evaluated using 100 parameter ensemble simulations with strongly varied soil properties and
716   soil ice distributions. The climate forcing at the surface is based on a paleoclimate simulation

Earth System
Open Access Science
Data
Discussions

717 performed by the Commonwealth Scientific and Industrial Research Organization (CSIRO)
718 providing the initialization of the permafrost model, and data from the ERA-Interim reanalysis
719 since 1979 onwards. Heat storage by inland water bodies was estimated by integrating water
720 temperature anomalies in natural lakes and reservoirs from a set of Earth System Model (ESM)
721 simulations participating in the Inter-Sectoral Impact Model Intercomparison Project phase 2b
722 (ISIMP2b) (Frieler et al., 2017; Golub et al., 2022; Grant et al., 2021). Heat storage is then
723 computed using simulations with four global lake models following the methodology presented in
724 (Vanderkelen et al., 2020), but replacing the cylindrical lake assumption in that study for a more
725 detailed lake morphometry, which leads to a more realistic representation of lake volume.
726
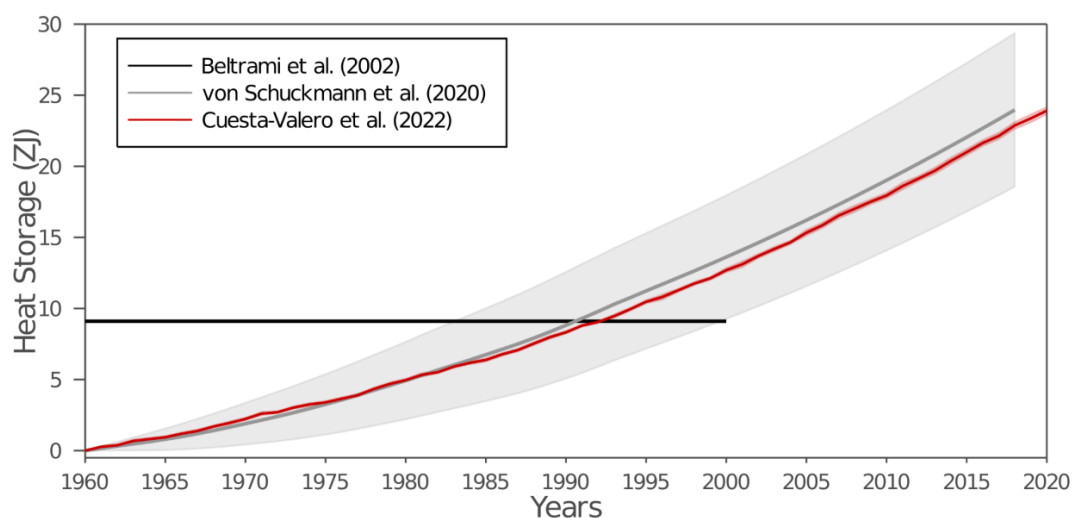
727
728 **Figure 6:** *Continental heat storage from Beltrami et al. (2002) (black), von Schuckmann et al.*
729 *(2020) (gray), and Cuesta-Valero et al. (2022a) (red). Gray and red shadows show the uncertainty*
730 *range of the heat storage from von Schuckmann et al. (2020) and Cuesta-Valero et al. (2022a),*
731 *respectively.*
732
733 Figure 6 shows the three main estimates of heat gain by the continental landmasses since 1960.
734 The first global estimate of continental heat storage was provided by Beltrami et al. (2002),
735 consisting of changes in ground heat content for the period 1500-2000 as time steps of 50 years
736 (black line in Figure 6). These estimates were retrieved by inverting 616 subsurface temperature
737 profiles constituting the global network of subsurface temperature profiles in 2002, yielding a heat
738 gain of 9.1 ZJ during the second half of the 20th century. A comprehensive update was included
739 in von Schuckmann et al. (2020) using the results of (Cuesta-Valero et al., 2021) (gray line in
740 Figure 6), with the main difference consisting in the use of a larger dataset with 1079 subsurface
741 temperature profiles. Since many of these new profiles were measured at a later year than those in
742 Beltrami et al. (2002), the inversions from this new data set were able to include the recent
743 warming of the continental subsurface, yielding higher ground heat content than those from
744 Beltrami et al. (2002). Concretely, the estimates in von Schuckmann et al. (2020) showed a heat
745 gain of 24 ± 5 ZJ from 1960 to 2018.
746

747 Recently, a new estimate of continental heat gain including the heat used in permafrost thawing
748 and in warming inland water bodies was presented in Cuesta-Valero et al. (2022a) (red line in
749 Figure 6), achieving a heat gain of 24 ± 1 ZJ since 1960, and 22 ± 1 ZJ since 1971 (see also Fig.
750 8). Although this estimate uses the same 1079 measurement sites as in von Schuckmann et al.
751 (2020) and includes inland water bodies and permafrost thawing, it yields similar values of heat
752 content to those in von Schuckmann et al. (2020). These similar results are caused by the different
753 aggregation techniques used to derive the change in global ground heat storage in von Schuckmann
754 et al. (2020) and in Cuesta-Valero et al. (2022a). There is a difference of ~ 3 ZJ between the
755 average ground heat storage in Cuesta-Valero et al. (2022a) (21.6 ± 0.2 ZJ) and in von Schuckmann
756 et al. (2020) (24 ± 5 ZJ), which is similar to the heat storage in inland water bodies and the heat
757 storage due to permafrost thawing together (see below). Another important result is the narrower
758 confidence interval in estimates from Cuesta-Valero et al. (2022a), which is directly related to the
759 new bootstrap technique used to invert the subsurface temperature profiles (Cuesta-Valero et al.,
760 2022b). Heat storage within inland water bodies has reached 0.2 ± 0.4 ZJ since 1960, with
761 permafrost thawing accounting for 2 ± 2 ZJ. Therefore, ground heat storage is the main contributor
762 to continental heat storage (90 %), with inland water bodies accounting for 0.7 % of the total heat,
763 and permafrost thawing accounting for 9 %. Despite the smaller proportion of heat stored in inland
764 water bodies and permafrost thawing, several important processes affecting both society and
765 ecosystems depend on the warming of lakes and reservoirs, and on the thawing of ground ice
766 (Gädeke et al., 2021). Therefore, it is important to continue quantifying and monitoring the
767 evolution of heat storage in all three components of the continental landmasses.
768
769 **5. Heat utilized to melt ice**
770
771 Changes in Earth's cryosphere affect almost all other elements of the environment including the
772 global sea level, ocean currents, marine ecosystems, atmospheric circulation, weather patterns,
773 freshwater resources and the planetary albedo (Abram et al., 2019). The cryosphere includes frozen
774 components of the Earth system that are at or below the land and ocean surface: snow, glaciers,
775 ice sheets, ice shelves, icebergs, sea ice, lake ice, river ice, permafrost and seasonally frozen
776 ground (IPCC, 2019). In this study, we estimate the heat uptake by the melting of ice sheets
777 (including both floating and grounded ice), glaciers and sea ice at global scale (Fig. 7).
778 Notwithstanding the important role snow cover plays in the Earth's energy surface budget as a
779 result of changes in the albedo (de Vrese et al., 2021; Qu & Hall, 2007; Weihs et al., 2021), or its
780 influence on the temperature of underlying permafrost (Jan & Painter, 2020; Park et al., 2015), or
781 on sea ice in the Arctic (Perovich et al., 2017; Webster et al., 2021) and Antarctica (Eicken et al.,
782 1995; Nicolaus et al., 2021; Shen et al., 2022), estimates of changes in global snow cover are still
783 highly uncertain and not included in this inventory. However, they should be considered in future
784 estimates. Similarly, changes in lake ice cover (Grant et al., 2021) are not taken into account here
785 and warrant more attention in the future. Permafrost is accounted for in the land component (see
786 section 4).
787
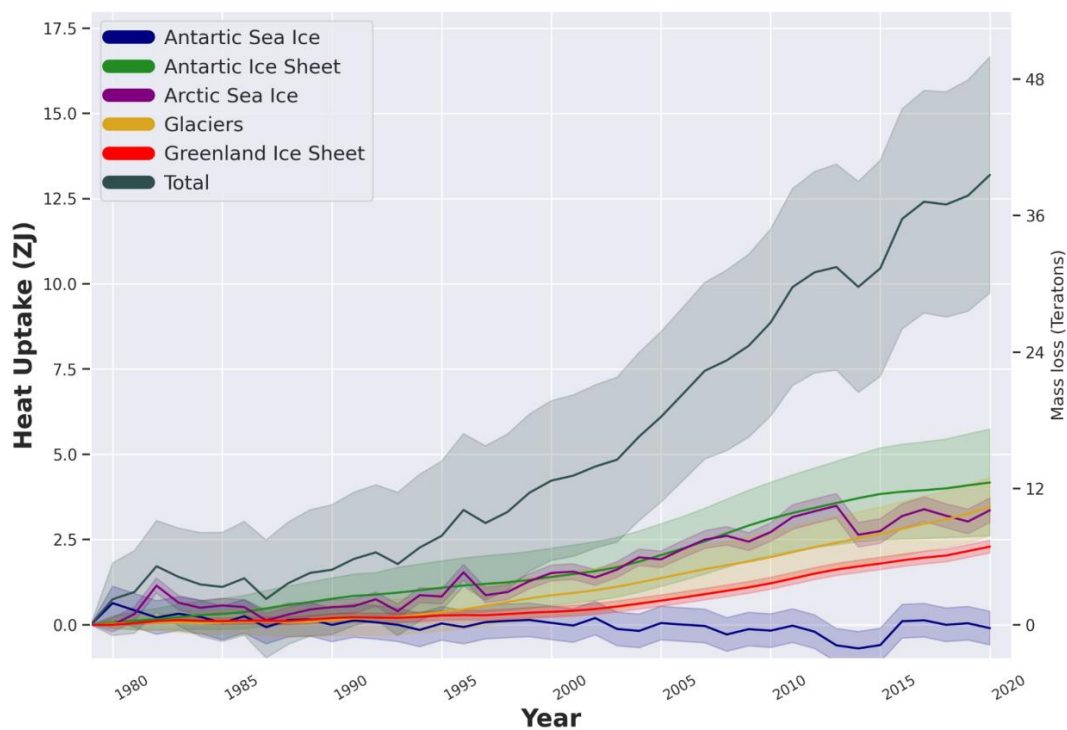
788
789
790 **Figure 7:** *Heat uptake (in ZJ) and Mass Loss (Trillions of tons) for the Antarctic Ice Sheet*
791 *(grounded and floating ice, green), Glaciers (orange), Arctic sea ice (purple), Greenland Ice Sheet*
792 *(grounded and floating ice, red) and Antarctic sea ice (blue), together with the sum of the energy*
793 *uptake within each one of its components (total, black). Uncertainties are 95% confidence*
794 *intervals provided as shaded areas, respectively. See text for more details.*
795
796 We equate the energy uptake by the cryosphere (glaciers, grounded and floating ice of the Antarctic
797 and Greenland Ice Sheets, and sea-ice) with the energy needed to drive the estimated mass loss. In
798 doing so we assume that the energy change associated with the temperature change of the
799 remaining ice is negligible. As a result, the energy uptake by the cryosphere is directly proportional
800 to the mass of melted ice:
801
802 $E = \Delta M * (L + c * \Delta T)$,
803
804 where, for any given component, ΔM is the mass of ice loss, L is the latent heat of fusion, c is the
805 specific heat capacity of the ice and ΔT is the rise in temperature needed to bring the ice to the
806 melting point. For consistency with previous estimates (Ciais et al., 2014; Slater et al., 2021; von
807 Schuckmann et al., 2020), we use a constant latent heat of fusion of 3.34×10^5 J kg^{-1}, a specific
808 heat capacity of 2.01×10^3 J/(kg °C) and, a density of ice of 917 kg/m^3. Estimating the energy used
809 to warm the ice to its melting point requires knowledge of the mean ice temperature for each
810 component. Here we assume a temperature of -15 °C for floating ice in Greenland, -2 °C for the
811 floating ice in Antarctica, -20 ± 10 °C for grounded ice in Antarctica and Greenland and 0 °C for

24

812 sea-ice and glaciers. Although this assumption is poorly constrained, the energy required to melt
813 ice is primarily associated with its phase transition and the fractional energy required for warming
814 is a small percentage (< 1% °C^{-1}) of the total energy uptake (Slater et al., 2021). Nevertheless, we
815 include an additional uncertainty of ±10 °C on the assumed initial ice temperature within our
816 estimate of the energy uptake.

818 Grounded ice losses from the Greenland and Antarctic Ice Sheets from 1992 to 2020 are estimated
819 from a combination of 50 satellite-based estimates of ice sheet mass balance produced from
820 observations of changes in ice sheet volume, flow and gravitational attraction, compiled by the Ice
821 Sheet Mass Balance Intercomparison Exercise (IMBIE[8]) (Shepherd et al., 2018, 2019). To extend
822 those time-series further back in time, we use ice sheet mass balance estimates produced using the
823 input-output method, which combines estimates of solid ice discharge with surface mass balance
824 estimates. Satellite estimates of ice velocity are available from the Landsat historical archive from
825 1972 allowing the calculation of ice discharge before the 1990s while surface mass balance is
826 estimated from regional climate models. We extend the IMBIE mass balance time-series
827 backwards to 1979 for Greenland using (Mouginot et al., 2019) and (Mankoff et al., 2019) and for
828 Antarctica from 1972 to 1991 using (Rignot et al., 2019).

830 Changes in Antarctic floating ice shelves due to thinning between 1994 and 2017 are derived from
831 satellite altimetry reconstructions (Adusumilli et al., 2020). There were no estimates of ice shelf
832 thinning between 1979 and 1993, therefore we assume zero mass loss from ice shelf thinning
833 during that period. Changes in Antarctic ice shelves due to increased calving in the Antarctic
834 Peninsula and the Amundsen Sea sector are derived from ERS-1 radar altimetry (Adusumilli et al.
835 2020) for 1994-2017. For the 1979-1994 period, we only have data for changes in the extent of the
836 Antarctic Peninsula ice shelves from (Cook & Vaughan, 2010). These are converted to changes in
837 mass using an ice shelf thickness of 140 +/- 110 m ice equivalent which represents the range of
838 ice thickness values for the portions of Antarctic Peninsula ice shelves that have collapsed since
839 1994 (Adusumilli et al. 2020). Once icebergs calve off large Antarctic floating ice shelves, the
840 timescales of dissolution of the icebergs are largely unknown; therefore, we assumed a linear rate
841 of energy uptake between 1979–2018. For icebergs, we use an initial temperature of -16°C, which
842 was the mean ice temperature in the Ross Ice Shelf J-9 ice core (Clough & Hansen, 1979). There
843 are no large-scale observations or manifestations of significant firn layer temperature change for
844 the Antarctic ice shelf; for example, there is no significant trend in the observationally-constrained
845 model outputs of surface melt described in (Smith et al., 2020). Therefore, the change in
846 temperature of any ice that does not melt is assumed to be negligible.

848 Changes in the floating portions of the Greenland Ice Sheet include ice shelf collapse, ice shelf
849 thinning and tidewater glacier retreat. As in von Schuckmann et al. 2020, we assume no ice shelf
850 mass loss pre-1997 and estimate a loss of 13 Gt/yr post-1997 based on studies of Zacharie Isstrom,
851 C. H. Ostenfeld, Petermann, Jakobshavn, 79N and Ryder Glaciers (Moon & Joughin, 2008;
852 Motyka et al., 2011; Mouginot et al., 2015; Münchow et al., 2014; Wilson et al., 2017). We assign
853 a generous uncertainty of 50% to this value. For tidewater glacier retreat we note a mean retreat
854 rate of 37.6 m/yr during 1992-2000 and 141.7 m/yr during 2000-2010. We assume the former
855 estimate is also valid for 1979-1991 and the latter estimate is valid for 2011-2020. Assuming a

---

8   https://imbie.org

856 mean glacier width of 4 km and thickness of 400 m we estimate mass loss from glacier retreat to
857 be 9.3 Gt/yr during 1979-2000 and 35.1 Gt/yr during 2000-2020. Based on firn modeling we
858 assessed that warming of Greenland's firn has not yet contributed significantly to its energy uptake
859 (Ligtenberg et al., 2018).
860
861 The contributions from both the Antarctic and Greenland Ice Sheets to the EEI are obtained by
862 summing the mass loss from the individual components (ice shelf mass, grounded ice mass, and
863 ice shelf extent) for each ice sheet separately and, given that the datasets used for each component
864 are independent, the uncertainties were summed in quadrature. This is then converted to an energy
865 uptake according to the equation above.
866
867 Glaciers are another part of the land-based ice, and we here include glaciers found in the periphery
868 of Greenland and Antarctica, but distinct from the ice sheets, in our estimate. We build our estimate
869 on the international efforts to compile and reconcile measurements of glacier mass balance, under
870 the lead of the World Glacier Monitoring Service (WGMS[9]). Up to 2016, the results are based on
871 (Zemp et al., 2019), who combine geodetic mass balance observations from DEM differencing on
872 long temporal and large spatial scales with in-situ glaciological observations, which are spatially
873 less representative, but provide information of higher temporal resolution. Through this
874 combination, they achieve coverage that is globally complete yet retains the interannual variability
875 well. For 2017 to 2021, the numbers are based on the ad-hoc method of (Zemp et al., 2020), which
876 corrects for the spatial bias of the limited number of recent in-situ glaciological observations that
877 are available with short delay (WGMS, 2021), to derive globally representative estimates. Error
878 bars include uncertainties related to the in-situ and spaceborne observations, extrapolation to
879 unmeasured glaciers, density conversion, as well as to glacier area and its changes. For the
880 conversion from mass loss to energy uptake, only the latent heat uptake is considered, which is
881 based on the assumption of ice at the melting point, due to lack of glacier temperature data at the
882 global scale. Moreover, since the absolute mass change estimates are based on geodetic mass
883 balances, mass loss of ice below floatation is neglected. While this is a reasonable approximation
884 concerning the glacier contribution to sea-level rise, it implies a systematic underestimation of the
885 glacier heat uptake. While to our knowledge there are no quantitative estimates available of glacier
886 mass loss below sea level on the global scale, it is reasonable to assume that this effect is minor,
887 based on the volume-altitude distribution of glacier mass (Farinotti et al., 2019; Millan et al., 2022).
888 Further efforts are under way within the Glacier Mass Balance Intercomparison Exercise
889 (GlaMBIE[10]), particularly to reconcile global glacier mass changes including also estimates from
890 gravimetry and altimetry, and to further assess related sources of uncertainties (Zemp et al., 2019).
891
892 Sea ice, formed from freezing ocean water, and further thickened by snow accumulation is not
893 only another important aspect of the albedo effect (Kashiwase et al., 2017; R. Zhang et al., 2019)
894 and water formation processes (Moore et al., 2022), but also provides essential services for polar
895 ecosystems and human systems in the Arctic (Abram et al., 2019). Observations of sea-ice extent
896 are available over the satellite era, i.e. since the 1970s, but ice thickness data - required to obtain
897 changes in volume - have only recently become available through the launch of CryoSat-2 and
898 ICESat-2. For the Arctic, we use a combination of sea ice thickness estimates from from the Pan-

---

9   https://wgms.ch
10   https://glambie.org

899 Arctic Ice Ocean Modeling and Assimilation System (PIOMAS) between 1980 and 2011
900 (Schweiger et al., 2019; Zhang & Rothrock, 2003) and CryoSat-2 satellite radar altimeter
901 measurements between 2011 and 2020 when they are available (Slater et al., 2021; Tilling et al.,
902 2018). PIOMAS assimilates ice concentration and sea surface temperature data and is validated
903 with most available thickness data (from submarines, oceanographic moorings, and remote
904 sensing) and against multidecadal records constructed from satellite (Labe et al., 2018; Laxon et
905 al., 2013; Wang et al., 2016). We note that the PIOMAS domain does not extend sufficiently far
906 south to include all regions covered by sea ice in winter (Perovich et al., 2017). Given that the
907 entirety of the regions that are unaccounted for (e.g., the Sea of Okhotsk and the Gulf of St.
908 Lawrence) are only seasonally ice covered since the start of the record, this should not influence
909 the results. We convert monthly estimates of sea ice volume from CryoSat-2 satellite altimetry to
910 mass using densities of 882 and 916.7 kg/m^3 in regions of multi- and first-year ice respectively
911 (Tilling et al., 2018). During the summer months (May to September) the presence of melt ponds
912 on Arctic sea ice makes it difficult to discriminate between radar returns from leads and sea ice
913 floes, preventing the retrieval of summer sea ice thickness from radar altimetry (Tilling et al.,
914 2018). As a result, we use the winter-mean (October to April) mass trend across the Arctic for both
915 CryoSat-2 and PIOMAS estimates for consistency. According to PIOMAS, winter Arctic sea ice
916 mass estimates are 19 Gt/yr (6 %) smaller than the annual mass trend between 1980 and 2011 (-
917 324 Gt/yr) and so are a conservative estimate of Arctic sea ice mass change (Slater et al., 2021).
918 The uncertainty on monthly Arctic sea ice volume measurements from CryoSat-2 ranges from 14.5
919 % in October to 13 % in April (Slater et al., 2021; Tilling et al., 2018), and is estimated as $\pm 1.8 \times 10^3$
920 km^3 for PIOMAS (Schweiger et al., 2011).

922 Satellite radar altimeter retrievals of sea ice thickness in the Southern Ocean are complicated by
923 the presence of thick snow layers with unknown radar backscatter properties on Antarctic sea ice
924 floes. As a result, no remote sensing estimates are available for Antarctic sea ice and we use sea
925 ice volume anomalies from the Global Ice-Ocean Modeling and Assimilation System (GIOMAS,
926 Zhang & Rothrock, 2003), the global equivalent to PIOMAS. GIOMAS output has been recently
927 validated against in-situ and satellite data by (Liao et al., 2022). We compute Antarctic sea ice
928 trends as annual averages between January and December. In the absence of a detailed
929 characterization of uncertainties for these estimates, we attribute the same uncertainty to GIOMAS
930 estimates as for PIOMAS ($\pm 1.8 \times 10^3$ km^3). For future updates of the GCOS Earth heat inventory,
931 we also aim to include observation-based (remote sensing) estimates in the Southern Ocean
932 (Lavergne et al., 2019).

934 Our estimate of the total heat gain in the cryosphere amounts to 14 ± 4 ZJ over the period 1971-
935 2020 (see also Fig. 8 and section 6), (assuming negligible contribution before 1979 according to
936 the data availability limitation), which is consistent with the estimate obtained in (von Schuckmann
937 et al., 2020) within uncertainties. Approximately half of the cryosphere's energy uptake is
938 associated with the melting of grounded ice, while the remaining half is associated with the melting
939 of floating ice (ice shelves in Antarctica and Greenland, Arctic sea ice). Compared to earlier
940 estimates, and in particular the 8.83 ZJ estimate from Ciais et al. (2013), this larger estimate is a
941 result both of the longer period of time considered and, also, the improved estimates of ice loss
942 across all components, especially the ice shelves in Antarctica. Contributions to the total
943 cryosphere heat gain are dominated by the Antarctic Ice Sheet (including the floating and grounded
944 ice, 33 ± 11%) and Arctic Sea ice (26 ± 3%), directly followed by the heat utilized to melt glaciers

945   (25 ± 7%). The Greenland Ice Sheet amounts to 17 ± 2%, whereas Antarctic sea ice is accounted
946   for with a non-significant contribution of 0.2 ± 4%.
947
948
949   **6. The Earth heat inventory: where does the energy go?**
950
951   Evaluations of the heat storage in the different Earth system components as performed in section
952   2-5 allow now for the establishment of the Earth heat inventory. Our results reconfirm a continuous
953   accumulation of heat in the Earth system since our estimate begins (Fig. 8). The total Earth system
954   heat gain in this study amounts to 380±62 ZJ over the period 1971–2020. For comparison, the heat
955   gain obtained in IPCC AR6 obtained a total heat gain of 434.9 [324.5 to 545.5] ZJ for the period
956   1971-2018, and is hence consistent with our estimate within uncertainties (Forster et al., 2021).
957   However, it is important to note that our estimate still excludes some aspects of Earth heat
958   accumulation, such as for example the shallow areas of the ocean. Although some estimates and
959   discussions have been provided to account for the relative contributions of these areas, these results
960   are still hampered by a number of assumptions and are challenging to be quantified with respect
961   to gaps in the observing system.
962
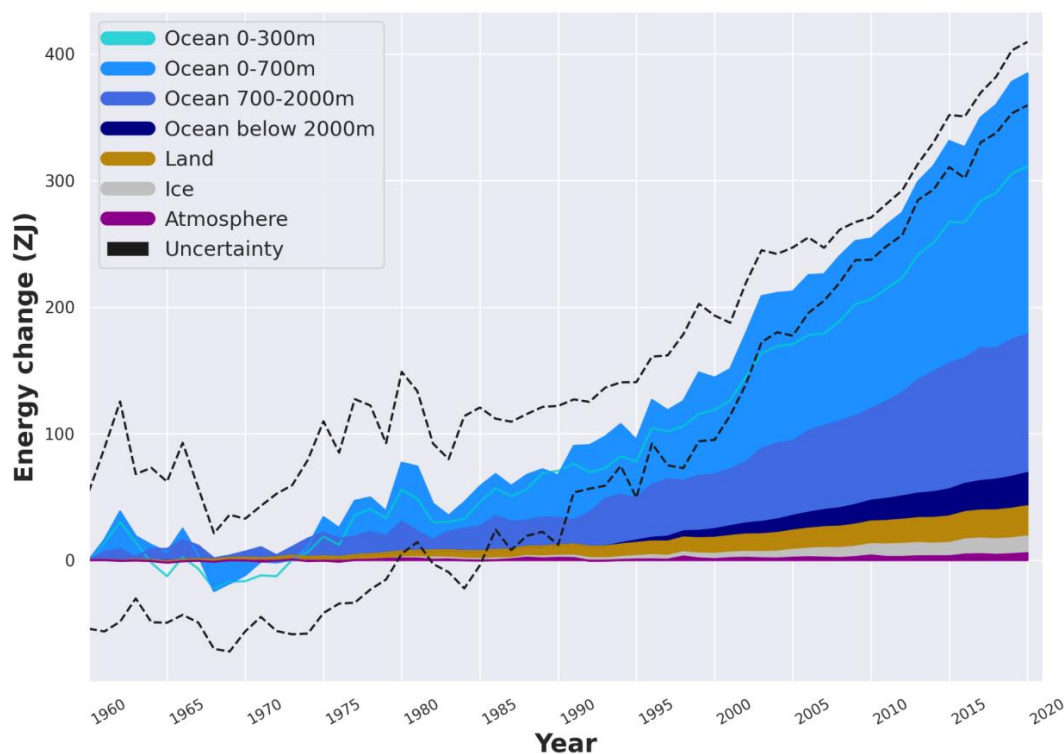
963
964   **Figure 8:** *Total Earth system heat gain in ZJ (1 ZJ =10²¹ J) relative to 1960 and from 1960 to*
965   *2020. The upper ocean (0–300 m, light blue line, and 0–700 m, light blue shading) accounts for*
966   *the largest amount of heat gain, together with the intermediate ocean (700–2000 m, blue shading)*
967   *and the deep ocean below 2000 m depth (dark blue shading). The second largest contributor is the*

968 *storage of heat on land (orange shading), followed by the gain of heat to melt grounded and*
969 *floating ice in the cryosphere (gray shading), and heating of the atmosphere (magenta shading).*
970 *Uncertainty in the ocean estimate also dominates the total uncertainty (dot-dashed lines derived*
971 *from the standard deviations (2σ) for the ocean, cryosphere, land and atmosphere). See sections*
972 *2-5 for more details of the different estimates. The dataset for the Earth heat inventory is published*
973 *at the German Climate Computing Centre (DKRZ, https://www.dkrz.de/) (see section 7).*
974 *Consistent with von Schuckmann et al. (2020), we obtain a total heat gain of 380±62 ZJ over the*
975 *period 1971–2020, which is equivalent to a heating rate (i.e., the EEI) of 0.48±0.1 W m^{-2} applied*
976 *continuously over the surface area of the Earth (5.10×10^{14} m^2). The corresponding EEI over the*
977 *period 2006–2020 amounts to 0.76±0.2 W m^{-2}. The LOWESS method and associated uncertainty*
978 *evaluations have been used as described in section 2.*
979
980 The estimate of heat storage in all Earth system components not only allows for obtaining a
981 measure of how much and where heat is available for inducing changes in the Earth system (Fig.
982 1), but also to improve the accuracy of the Earth's system total heat gain. In 1971-2020 and for the
983 total heat gain, the ocean accounts for the largest contributor with a $89 \pm 17\%$ fraction of the global
984 inventory. The second largest component in the Earth heat inventory relies on heat stored in land
985 with a $6 \pm 0.1\%$ contribution. The cryosphere component accounts for $4 \pm 1\%$, and the atmosphere
986 $1 \pm 0.2\%$. For the most recent era of best available GCOS data for the Earth heat inventory since
987 the year 2006, the fractions amount to $89 \pm 20\%$ for the ocean, $5 \pm 1\%$ for land, $4 \pm 3\%$ for the
988 cryosphere, and $2 \pm 0.4\%$ for the atmosphere.
989
990 The change of the Earth heat inventory over time allows for an estimate of the absolute value of
991 the Earth energy imbalance. Our results of the total heat gain in the Earth system over the period
992 1971-2020 is equivalent to a heating rate of 0.48±0.1 W m^{-2}, and is applied continuously over the
993 surface area of the Earth (5.10×10^{14} m^2). For comparison, the heat gain obtained in IPCC AR5
994 amounts to 274 ± 78 ZJ and 0.4 W m^{-2} over the period 1971–2010 (Rhein et al., 2013). In IPCC
995 AR6, the total heat rate has been assessed by 0.57 [0.43 to 0.72] W m^{-2} for the period 1971-2018
996 (Forster et al., 2021). We further infer a total heating rate of 0.76 ± 0.2 W m^{-2} for the most recent
997 era 2006-2020.
998
999 Thus, the number of how fast heat has been accumulated in the Earth system has increased during
1000 the most recent era as compared to the long-term estimate – an outcome which reconfirms the
1001 earlier finding in von Schuckmann et al. (2020), and which had then been concurrently and
1002 independently confirmed in Foster et al. (2021), Hakuba et al. (2021), Loeb et al. (2021) and
1003 Kramer et al. (2021). The drivers of a larger EEI in the 2000s than in the long-term period since
1004 1971 are still unclear, and several mechanisms are discussed in literature. For example, Loeb et al.
1005 (2021) argue for a decreased reflection of energy back into space by clouds and sea-ice, and
1006 increases in well-mixed greenhouse gases (GHG) and water vapor to account for this increase in
1007 EEI. (Kramer et al., 2021) refers to a combination of rising concentrations of well-mixed GHG
1008 and recent reductions in aerosol emissions accounting for the increase, and (Liu et al., 2020)
1009 addresses changes in surface heat flux together with planetary heat re-distribution and changes in
1010 ocean heat storage. Future studies are needed to further explain the drivers of this change, together
1011 with its implications for changes in the Earth system.
1012

Earth System
Science
Data

Open Access

Discussions
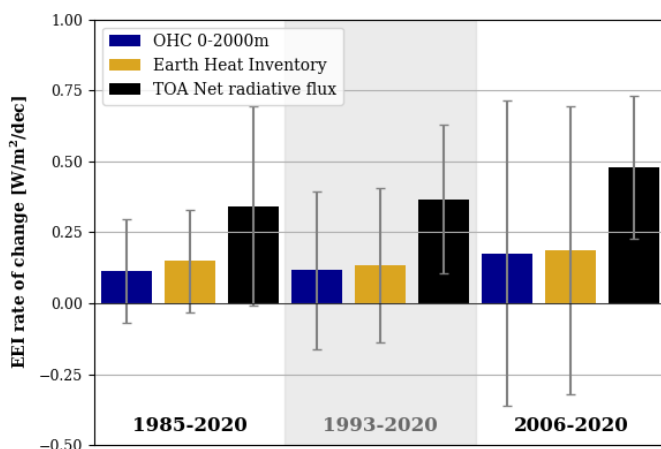
1013
1014 *Figure 9: Decadal scale rate of change for the Earth Energy Imbalance (EEI) in Wm⁻²/decade as*
1015 *derived from the Earth heat inventory in Fig. 8 (yellow), OHC of the 0-2000m depth layer (blue,*
1016 *see section 2) and net flux at the top of the atmosphere (TOA, black) based on the estimates of Liu*
1017 *et al. (2020) and Loeb et al. (2021) for three different periods, 1985-2020 (i.e., the full available*
1018 *net flux at TOA estimate), 1993-2020 (i.e., the altimeter era) and 2006-2020 (i.e., the GCOS golden*
1019 *period for the Earth heat inventory). See Liu et al. (2020) and Loeb et al. (2021) on more details*
1020 *of the uncertainty estimate, and note that satellite instrument drift error is not considered. A linear*
1021 *regression has been applied to obtain the rate of change.*
1022
1023 With respect to the current status of the GCOS, we further want to emphasize the fact that today
1024 the Earth heat inventory is the best estimate for the absolute value of the Earth energy imbalance.
1025 This is explained by the fact that satellite derived measurements for the net flux at the top of the
1026 atmosphere (TOA) have to be anchored by an absolute value, which is done through the use of the
1027 Earth heat inventory, and for which mostly global OHC is used (Loeb et al., 2012; 2021; Liu et
1028 al., 2020). However, the temporal change of the EEI can be best estimated from the net flux at
1029 TOA from remote sensing data as these are superior in terms of temporal stability. To further
1030 discuss the temporal change of the EEI, we compare our results of the Earth heat inventory with
1031 the satellite derived net flux at TOA. Consistent with the results of Loeb et al. (2021), the net flux
1032 estimates at TOA show a change in the EEI at a significant rate of 0.48 ± 0.3 Wm⁻²/decade during
1033 the period 2006-2020. In 1985-2020 (1993-2020), the value amounts to 0.3 ± 0.4 Wm⁻²/decade
1034 (0.4 ± 0.3 Wm⁻²/decade) (Fig. 9).
1035
1036 For the Earth heat inventory, the results show that uncertainties for estimating temporal changes
1037 of the EEI are still too large to obtain significant results, even during the GCOS 'golden period'
1038 for the Earth heat inventory in 2006-2020 (Loeb et al., 2022). In other words, this comparison
1039 highlights the strength of the complementary use of different independent GCOS components. But
1040 the results also show that the current status of the GCOS does not allow for unraveling the rate of
1041 change of heat stored in the Earth system components, which is critical information to further
1042 understand associated changes in the Earth system (Fig. 1), and to validate climate models for

1043 improving projections of these changes into the future. Hence, these results further underpin the
1044 need for sustaining and further extending the GCOS for improving our knowledge and monitoring
1045 capacity of estimates for how much and where heat is stored in the Earth system.
1046
1047 Besides heat, which is the focus of this study, Earth also stores energy chemically through
1048 photosynthesis in living and dead biomass with plant growth. Recent studies (Crisp et al., 2022;
1049 Denning, 2022; Friedlingstein et al., 2022) on the Global Carbon Budget and cycle show that
1050 approximately 25% of the added anthropogenic CO2 is removed from the atmosphere by increased
1051 plant growth, which is a result of fertilization by rising atmospheric CO2 and Nitrogen inputs and
1052 of higher temperatures and longer growing seasons in northern temperate and boreal areas
1053 (Friedlingstein et al., 2022). This significant increase in carbon uptake by the biosphere indicates
1054 that more energy is stored inside biomass, together with the stored carbon. The quantification of
1055 the additional amount of energy stored inside the biosphere is outside the scope of this study.
1056
1057 ## 7. Data availability
1058
1059 The time series of the Earth heat inventory are published at DKRZ (https://www.dkrz.de/, last
1060 access: 20 July 2020) under https://www.wdc-climate.de/ui/entry?acronym=GCOS_EHI_1960-
1061 2020, more precisely for:
1062
1063 • (von Schuckmann et al., 2022); data for ocean heat content (section 2), and the total heat
1064   inventory as presented in section 6 are integrated.
1065 • (Kirchengast et al., 2022) ; data for the atmospheric heat content are distributed (section
1066   3).
1067 • (Cuesta Valero et al., 2022c); data for the ground heat storage, together with the total
1068   continental heat gain are provided (section 4)
1069 • (Vanderkelen et al., 2022); data for inland freshwater heat storage is included (section 4)
1070 • (Nitzbon et al., 2022b); data for permafrost are delivered (section 4).
1071 • (Adusumilli et al., 2022); data for the cryosphere heat inventory are provided.
1072
1073 Persistent identifiers (PIDs) for the specific data access are provided in Table 2.
1074

Earth heat inventory component	PID	Reference
Ocean heat content; Total Earth heat inventory	https://hdl.handle.net/21.14106/9b2fddbe4637e3bb9fbf2414c55e6aad0e3923b0	von Schuckmann et al., 2022
Atmospheric heat content	https://hdl.handle.net/21.14106/2c4e7216177fcb742f324eae2792c43faf8361f1	Kirchengast et al., 2022
Continental heat content	https://hdl.handle.net/21.14106/302a4aedadcabf09d5f432003361275e9102a48a	Cuesta Valero et al., 2022c
Inland water heat content	https://hdl.handle.net/21.14106/e095f83398baa6e5b355ba88ae97cd7dedd008de	Vanderkelen et al., 2022
Heat available to melt permafrost	https://hdl.handle.net/21.14106/a9654c3d10c0002da4dde3ef080f6503e2deebf5	Nitzbon et al., 2022b
Heat available to melt the cryosphere	https://hdl.handle.net/21.14106/b9829ba3230f0631d3545a66a88e1c89803510ee	Adusumilli et al., 2022

1075

1076 ***Table 2:*** *Overview on persistent identifiers (PIDs) for data access for each component of the Earth heat*
1077 *inventory. The results are presented in Fig. 8.*
1078

8. Conclusion

1080

1081 This study builds on the first internationally and multidisciplinary driven Earth heat inventory in
1082 2020 (von Schuckmann et al., 2020) and provides an update on total Earth system heat
1083 accumulation, heat storage in all Earth system components (ocean, land, cryosphere, atmosphere)
1084 and the Earth energy imbalance up to the year 2020. Moreover, this study succeeded to improve
1085 estimates, to further extent and foster international collaboration, and to continue to move towards
1086 a more complete view on where and how much heat is stored in the Earth system through the
1087 addition of new estimates such as for permafrost thawing, inland freshwater (section 4) and
1088 Antarctic sea ice (section 5). Results obtained reveal a total Earth system heat gain of 380±62 ZJ
1089 over the period 1971–2020, with an associated total heating rate of 0.48 ± 0.1 W m^{-2}. 89 ± 17 % of
1090 this heat stored in the ocean, 6 ± 0.1 % on land, 4 ± 1% in the cryosphere and 1 ± 0.2 % in the
1091 atmosphere (Fig. 8, 11). The analysis additionally reconfirms an increased heating rate which
1092 amounts to 0.76 ± 0.2 W/m^{-2} for the most recent era 2006-2020. These results are consistent with
1093 previous estimates, which is again demonstrated through a comprehensive assessment of estimates
1094 for the EEI published in peer-reviewed literature (Fig. 10). Albeit the drivers for this change still
1095 need to be elucidated and most likely reflect the interplay between natural variability and
1096 anthropogenic change (Loeb et al., 2021; Kramer et al., 2021; Liu et al., 2020), their implications
1097 for changes in the Earth system are reflected in the many record levels of change in the 2000s
1098 reported elsewhere, e.g., (Cheng et al., 2022; Forster et al., 2022; Gulev et al., 2021; WMO, 2022).
1099

1100 The recent Glasgow Climate Pact (UNFCCC, 2021) is '*Acknowledging that climate change is a*
1101 *common concern of humankind* …' and '*Recognizing … the importance of international*
1102 *cooperation in addressing climate change and its impacts…*', and '*Recognizes the importance of*
1103 *the best available science for effective climate action and policy making*'. The UN 2030 Agenda
1104 for Sustainable Development[11] states that climate change is "*one of the greatest challenges of our*
1105 *time ...*" and warns *"... the survival of many societies, and of the biological support systems of the*
1106 *planet, is at risk*". The outcome document of the Rio+20 Conference, The Future We Want[12],
1107 defines climate change as "*an inevitable and urgent global challenge with long-term implications*
1108 *for the sustainable development of all countries*". The Paris Agreement builds upon the United
1109 Nations Framework Convention on Climate Change and for the first time all nations agreed to
1110 undertake ambitious efforts to combat climate change, with the central aim to keep global
1111 temperature rise this century well below 2 °C above pre industrial levels and to limit the
1112 temperature increase even further to 1.5 °C. Article 14 of the Paris Agreement requires the
1113 Conference of the Parties serving as the meeting of the Parties to the Paris Agreement (CMA) to
1114 periodically take stock of the implementation of the Paris Agreement and to assess collective

---

[11]
https://sustainabledevelopment.un.org/content/documents/21252030%20Agenda%20for%20Sustainable%20Development%20web.pdf
[12]   https://sustainabledevelopment.un.org/content/documents/733FutureWeWant.pdf

1115   progress towards achieving the purpose of the agreement and its long-term goals through the so-
1116   called Global Stocktake of the Paris Agreement (GST)[13] based on best available science.
1117
1118   The Earth heat inventory provides information on how much and where heat is accumulated and
1119   stored in the Earth system. Moreover, it provides a measure of how much the Earth is out of energy
1120   balance, and when combined with directly measured net flux at the top of the atmosphere, enables
1121   also to understand the change of the EEI over time. This in turn allows for assessing the portion of
1122   the anthropogenic forcing that the Earth's climate system has not yet responded to (Hansen et al.,
1123   2005) and defines additional global warming that will occur without further change in human-
1124   induced forcing (Hansen et al., 2017). The Earth heat inventory is thus one of the key critical global
1125   climate change indicators defining the prospects for continued global warming and climate change
1126   (Hansen et al., 2011; von Schuckmann et al., 2016; 2020) Hence, we call for an implementation
1127   of the Earth heat inventory into the global stocktake.
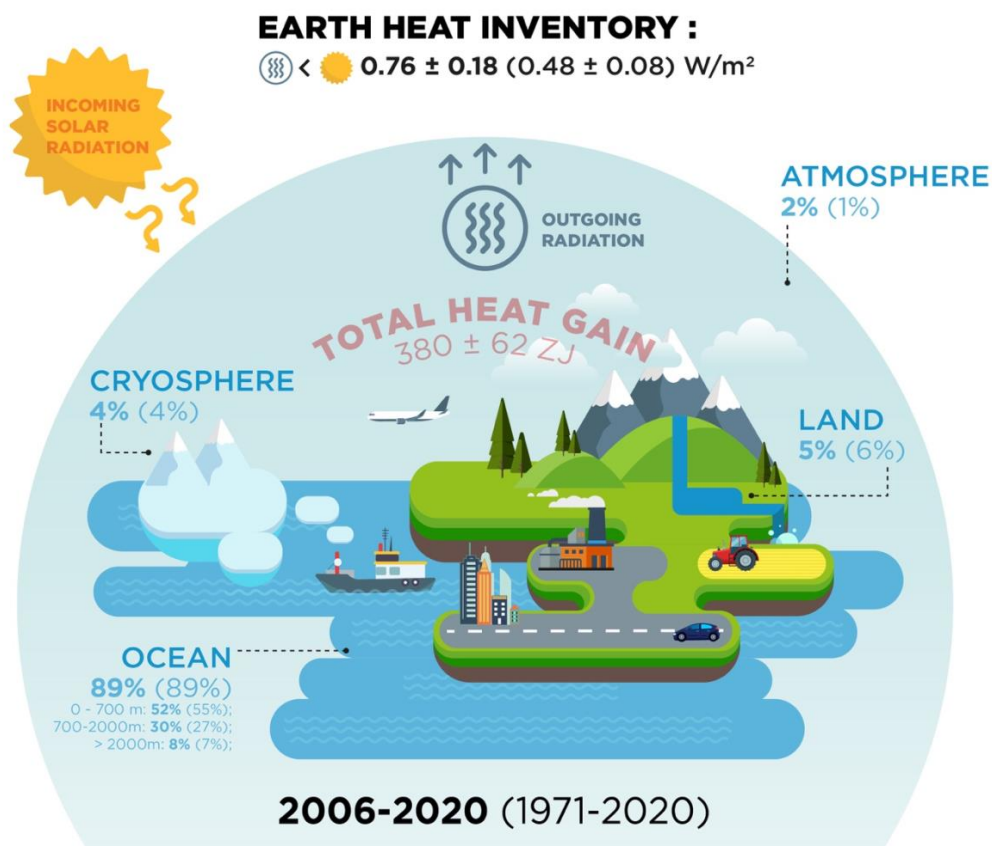1128
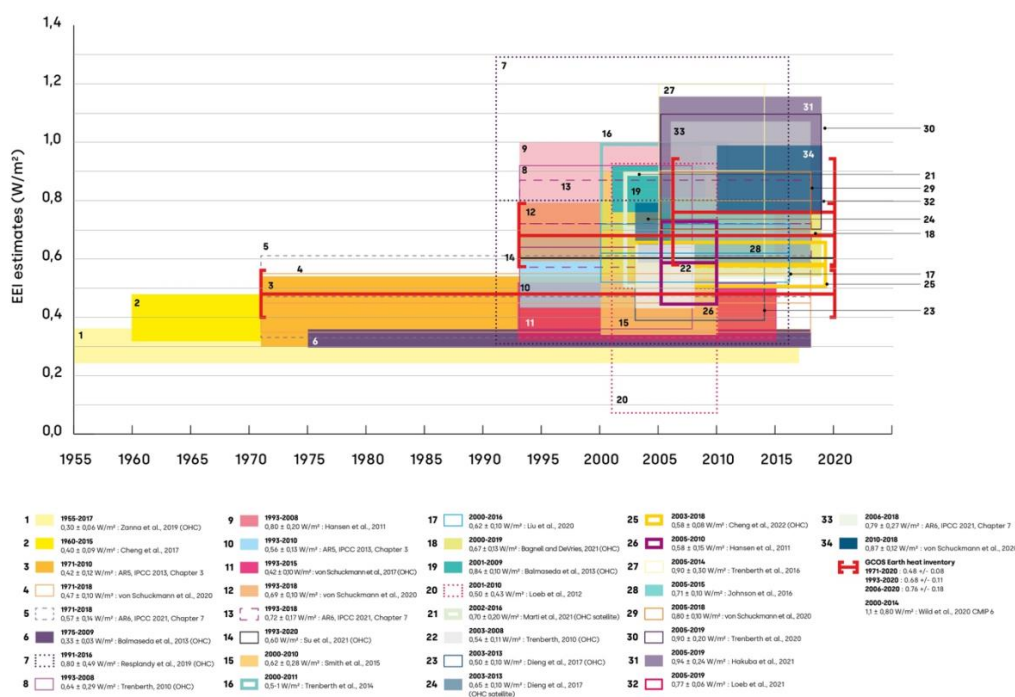
1129
1130   *Figure 10: Overview on EEI and d(OHC)/dt (indicated with (OHC) in the legend) estimates as*
1131   *obtained from previous publications; references are listed in the figure legend. The color bars take*
1132   *into account the uncertainty ranges provided in each publication, respectively. For comparison,*

---

[13]   https://unfccc.int/topics/global-stocktake/global-
stocktake#:~:text=The%20global%20stocktake%20of%20the,term%20goals%20(Article%2014)
.

1133   *the estimates of our Earth heat inventory based on the results of Fig. 8 have been added (red lines)*
1134   *for the periods 1971–2020, 1993–2020 and 2006–2020.*
1135
1136

EARTH HEAT INVENTORY :
$\langle$ < 0.76 ± 0.18 (0.48 ± 0.08) W/m²

INCOMING SOLAR RADIATION

OUTGOING RADIATION

ATMOSPHERE
2% (1%)

TOTAL HEAT GAIN
380 ± 62 ZJ

CRYOSPHERE
4% (4%)

LAND
5% (6%)

OCEAN
89% (89%)
0 - 700 m: **52%** (55%);
700-2000m: **30%** (27%);
> 2000m: **8%** (7%);

2006-2020 (1971-2020)

1137
1138
1139   ***Figure 11:*** *Schematic presentation on the Earth heat inventory for the current anthropogenically*
1140   *driven positive Earth energy imbalance at the top of the atmosphere (TOA). The relative partition*
1141   *(in %) of the Earth heat inventory presented in Fig. 8 for the different components is given for the*
1142   *ocean (upper: 0–700 m, intermediate: 700–2000 m, deep: >2000 m), land, cryosphere (grounded*
1143   *and floating ice) and atmosphere, for the periods 2006–2020 and 1971–2020 (for the latter period*
1144   *values are provided in parentheses), as well as for the EEI. The total heat gain (in red) over the*
1145   *period 1971–2020 is obtained from the Earth heat inventory as presented in Fig. 8.*
1146
1147   The quantifications presented in this study are the result of multidisciplinary global-scale
1148   collaboration and demonstrate the critical importance of concerted international efforts for climate
1149   change monitoring and community-based recommendations for the GCOS. For the GOOS, the
1150   core Argo sampling needs to be sustained – which includes the maintenance of shipboard
1151   collection of reference data for validation - and complemented by remote sensing data. Extensions

1152 such as into the deep ocean layer need to be further fostered, and technical developments for the
1153 measurements under ice and in shallower areas need to be sustained and extended. Moreover,
1154 continued efforts are needed to further advance bias correction methodologies, uncertainty
1155 evaluations, data recovery and processing of the historical dataset.
1156
1157 For the ground heat storage, the estimate had been hampered by a lack of subsurface temperature
1158 profiles in the southern hemisphere, as well as by the fact that most of the profiles were measured
1159 before the 2000s. Subsurface temperature data are direct and independent (not proxy)
1160 measurements of temperature yielding information on the temporal variation of the ground surface
1161 temperature and ground heat flux at the land surface. A larger spatial scale dataset of the thermal
1162 state of the subsurface from the last millennium to the present will aid in the continuing monitoring
1163 of continental heat storage, provide initial conditions for Land Surface Model (LSM) components
1164 of Earth System Models (ESMs) (Cuesta-Valero et al., 2019), and serve as a dataset for validation
1165 of climate models' simulations (Cuesta-Valero et al., 2021; Cuesta-Valero et al., 2016). Progress
1166 in understanding climate variability through the last millennium must lean on additional data
1167 acquisition as the only way to reduce uncertainty in the paleoclimatic record and on changes to the
1168 current state of the continental energy reservoir. Remote sensing data are expected to be very
1169 valuable to retrieve recent past and future changes in ground heat flux at short-time scales with
1170 near global coverage. However, collecting subsurface temperature data is urgent as we must make
1171 a record of the present thermal state of the subsurface before the subsurface climate baseline is
1172 affected by the downward propagating thermal signal from current climate heating. Furthermore,
1173 an international organization should take responsibility to gather and curate all measured
1174 subsurface temperature profiles currently available and those that will be measured in the future,
1175 as the current practices, in which individual researchers are responsible for measuring, storing and
1176 distributing the data, have led to fragmented datasets, restrictions in the use of data, and loss of the
1177 original datasets. Support from GCOS for an international data acquisition and curating efforts
1178 would be extremely important in this context.
1179
1180 For the permafrost estimates, the primary sources of uncertainty arise from lacking information
1181 about the amount and distribution of ground ice in permafrost regions, as well as measurements of
1182 liquid water content (Nitzbon et al., 2022). Permafrost heat storage is defined as the required heat
1183 to change the mass of ground ice at a certain location, thus monitoring changes in ground ice and
1184 water contents would be required to improve estimates of this component of the continental heat
1185 storage. Nevertheless, the current monitoring system for permafrost soils is focused on soil
1186 temperature, and the distribution of stations is still relatively scarce in comparison with the vast
1187 areas that need to be surveyed (Biskaborn et al., 2015). Due to the current limitations in the
1188 observational data, a permafrost model was used to estimate the heat uptake by thawing of ground
1189 ice. This approach retrieves latent heat fluxes in extensive areas and at depths relevant to analyze
1190 the long-term change in ground ice mass, but at the cost of ignoring other relevant processes, such
1191 as ground subsidence, to balance model performance with computational resources. Including
1192 permafrost heat storage in the Tibetan Plateau is a priority for the next iteration of this work, as
1193 well as to explore new methods to evaluate model simulations using the available observations in
1194 permafrost areas.
1195
1196 For inland water heat storage, a better representation of lake and reservoir volume would be
1197 possible by better accounting for lake bathymetry using the GLOBathy (Khazaei et al., 2022)

1198   dataset and results from the upcoming Surface Water and Ocean Topography (SWOT) mission.
1199   These improvements in the representation of lake volume, and an updated lake mask will be
1200   available in the upcoming ISIMIP3 simulation round, next to improved meteorological forcing
1201   data (Golub et al., 2022). In contrast to (Vanderkelen et al., 2020), the heat storage in rivers is not
1202   included in this analysis due to the high uncertainties in simulated river water volume. To reduce
1203   the uncertainty in river heat storage, the estimation of river water storage should be improved,
1204   together with an explicit representation of water temperature in the global hydrological models
1205   (Wanders et al., 2019). These improvements will be incorporated in ISIMIP3 and will lead to
1206   better estimates of inland water heat storage, thus enhancing future estimates of continental heat
1207   storage. In the long run, these model-based estimates could be supplemented or replaced by
1208   observation-based estimates, which would however require a large, global-scale effort to monitor
1209   lake and river temperatures at high spatial resolution and over long time periods.
1210
1211   For the cryosphere, sustained remote sensing for all of the cryosphere components is critical in
1212   quantifying future changes over these vast and inaccessible regions; in situ observations are also
1213   needed for process understanding and in order to properly calibrate and validate them. For sea ice,
1214   observations of the albedo, the area and ice thickness are all essential - the continuation of satellite
1215   altimeter missions with high inclination, polar focused orbits is critical in our ability to monitor
1216   sea ice thickness in particular. Observations of snow thickness with multi-frequency altimeters are
1217   essential for further constraining sea ice thickness estimates. For ice sheets and glaciers, reliable
1218   gravimetric, geodetic, and ice velocity measurements, knowledge of ice thickness and extent,
1219   snow/firn thickness and density, and the continuation of the now three-decade long satellite
1220   altimeter record are essential in understanding changes in the mass balance of grounded and
1221   floating ice. The recent failure of Sentinel-1b, which in tandem with Sentinel-1a could be used to
1222   systematically measure ice speed changes every 6 days, means that images are now being acquired
1223   every 12 days and thus an earlier launch of Sentinel-1c should be encouraged to regain the ability
1224   to monitor ice speed changes over short time-scales. The estimate of glacier heat uptake is
1225   particularly affected by lacking knowledge of ice melt below sea level, and to a lesser degree,
1226   lacking knowledge of firn and ice temperatures. This lack of observations is likely related to most
1227   studies on glaciers focussing on their contribution to sea-level rise or seasonal water availability,
1228   where melt below sea level and warming of ice do not matter much. However, it becomes obvious
1229   here that this gap introduces a systematic bias in the estimate of cryospheric energy uptake, which
1230   is presumably small compared to the other components, but unconstrained. Although the Antarctic
1231   sea ice change and the warming of Greenland and Antarctic firn are poorly constrained or have
1232   not significantly contributed to this assessment, they may become increasingly important over the
1233   coming decades. Similarly, there exists the possibility for rapid change associated with positive
1234   ice dynamical feedbacks at the marine margins of the Antarctic Ice Sheet. Sustained monitoring
1235   of each of these components will, therefore, serve the dual purpose of furthering the understanding
1236   of the dynamics and quantifying the contribution to Earth's energy budget. In addition to data
1237   collection, open access to the data and data synthesis products, as well as coordinated international
1238   efforts, are key to the continued monitoring of the ice loss from the cryosphere and its related
1239   energy uptake.
1240
1241   For the atmosphere, there is a need to sustain and enhance a coherent operational long-term
1242   monitoring system for the provision of climate data records of essential climate variables.
1243   Observations from radiosonde stations within the GCOS reference upper air network (GRUAN)

1244 and from satellite-based GNSS radio occultation deliver thermodynamic profiling observations of
1245 benchmark quality and stability from surface to stratopause. For climate monitoring, it is of critical
1246 importance to ensure continuity of such observations with global coverage over all local times.
1247 This continuity of radio occultation observations in the future is not sufficiently guaranteed as we
1248 are facing an imminent observational gap in mid- to high latitudes for most local times(IROWG,
1249 2021), which is a major concern. Thus, there is an urgent need for satellite missions in high
1250 inclination orbits to provide full global and local time coverage in order to ensure global climate
1251 monitoring. Operational radio occultation missions need to be maintained as backbone for a global
1252 climate observing system and long-term availability and archiving of measurement data, metadata
1253 and processing information needs to be ensured.
1254
1255 In summary, we also call for urgently needed actions for enabling continuity, archiving, rescuing
1256 and calibrating efforts to assure improved and long-term monitoring capacity of the GCOS for the
1257 Earth heat inventory. Particularly, the summarized recommendations include
1258
1259 • Need to sustain, reinforce or even to establish data repositories for historical climate data
1260   (archiving)
1261 • Need to reinforce efforts for recovery projects for historical data and associated meta-data
1262   information (rescuing)
1263 • Need to sustain and reinforce the GCOS for assuring the monitoring of the Earth heat
1264   inventory targets (continuity)
1265 • Need to foster calibration measurements (in situ) for assuring quality and reliability of
1266   large-scale measurement techniques (e.g., remote sensing, autonomous components (eg
1267   argo) (calibrating)
1268
1269 A continuous effort to regularly update the Earth heat inventory is important as this global climate
1270 indicator crosses multidisciplinary boundaries and calls for the inclusion of new science
1271 knowledge from the different disciplines involved, including the evolution of climate observing
1272 systems and associated data products, uncertainty evaluations, and processing tools. The outcomes
1273 have further demonstrated how we are able to evolve our estimates for the Earth heat inventory
1274 while bringing together different expertise and major climate science advancements through a
1275 concerted international effort. All of these component estimates are at the leading edge of climate
1276 science. Their union has provided a new and unique insight on the inventory of heat in the Earth
1277 system, its evolution over time and the absolute values. The data product of this effort is made
1278 available and can be thus used for model validation purposes.
1279
1280 This study has demonstrated the unique value of such a concerted international effort, and we thus
1281 call for a regular evaluation of the Earth heat inventory. This updated attempt presented here has
1282 been focused on the global area average only, and evolving into regional heat storage and
1283 redistribution, the inclusion of various timescales (e.g., seasonal, year to year) and other climate
1284 study tools (e.g., indirect methods, ocean reanalyses) would be an important asset of this much
1285 needed regular international framework for the Earth heat inventory. This would also respond
1286 directly to the request of GCOS to establish the observational requirements needed to further
1287 monitor the Earth's cycles and the global energy budget (GCOS, 2021). The outcome of this study
1288 will therefore directly feed into GCOS' assessments of the status of the global climate observing
1289 system, and the identified observation requirements will guide the development of the next

1290   generation of in situ and satellite global climate observations as specified by GCOS by all national
1291   meteorological services and space agencies and other oceanic and terrestrial networks.
1292
1293

1329
1330
1331

References

1334   Abraham, J. P., Baringer, M., Bindoff, N. L., Boyer, T., Cheng, L. J., Church, J. A., Conroy, J.
1335   L., Domingues, C. M., Fasullo, J. T., Gilson, J., Goni, G., Good, S. A., Gorman, J. M.,
1336   Gouretski, V., Ishii, M., Johnson, G. C., Kizu, S., Lyman, J. M., Macdonald, A. M., …
1337   Willis, J. K. (2013). A review of global ocean temperature observations: Implications for
1338   ocean heat content estimates and climate change. *Reviews of Geophysics*, *51*(3), 450–483.
1339   https://doi.org/10.1002/rog.20022
1340   Abram, N., Gattuso, J.-P., Prakash, A., Cheng, L., Chidichimo, M. P., Crate, S., Enomoto, H.,

1341   Garschagen, M., Gruber, N., Harper, S., Holland, E., Kudela, R. M., Rice, J., Steffen, K., &
1342   von Schuckmann, K. (2019). Framing and Context of the Report. In H. O. Pörtner, D. C.
1343   Roberts, V. Masson-Delmotte, P. Zhai, M. Tignor, E. Poloczanska, K. Mintenbeck, A.
1344   Alegría, M. Nicolai, A. Okem, J. Petzold, B. Rama, & N. M. Weyer (Eds.), *IPCC Special*
1345   *Report on the Ocean and Cryosphere in a Changing Climate* (pp. 73–129). in press.
1346   https://www.ipcc.ch/srocc/
1347   Adusumilli, Susheel; Hendricks, Stefan; Korosov, Anton; Straneo, Fiammetta; Lavergne,
1348   Thomas; Lawrence, Isobel; Marzeion, Ben; Otosaka, Inès; Schweiger, Axel; Shepherd,
1349   Andrew; Slater, Donald; Slater, Thomas; Timmermanns, Mary-Louise; Zemp, Michael
1350   (2022). Heat stored in the Earth system 1960-2020: Where does the energy go?, submitted
1351   to Earth System Science Data. (2022). World Data Center for Climate (WDCC) at DKRZ.
1352   https://www.wdc-climate.de/ui/entry?acronym=GCOS_EHI_1960-2020_CrHC
1353   Adusumilli, S., Fricker, H. A., Medley, B., Padman, L., & Siegfried, M. R. (2020). Interannual
1354   variations in meltwater input to the Southern Ocean from Antarctic ice shelves. *Nature*
1355   *Geoscience*, *13*(9), 616–620. https://doi.org/10.1038/s41561-020-0616-z
1356   Allison, L. C., Roberts, C. D., Palmer, M. D., Hermanson, L., Killick, R. E., Rayner, N. A.,
1357   Smith, D. M., & Andrews, M. B. (2019). Towards quantifying uncertainty in ocean heat
1358   content changes using synthetic profiles. *Environmental Research Letters*, *14*(8), 084037.
1359   https://doi.org/10.1088/1748-9326/ab2b0b
1360   Angerer, B., Ladstädter, F., Scherllin-Pirscher, B., Schwärz, M., Steiner, A. K., Foelsche, U., &
1361   Kirchengast, G. (2017). Quality aspects of the Wegener Center multi-satellite GPS radio
1362   occultation record OPSv5.6. *Atmospheric Measurement Techniques*, *10*(12), 4845–4863.
1363   https://doi.org/10.5194/amt-10-4845-2017
1364   Bell, B., Hersbach, H., Simmons, A., Berrisford, P., Dahlgren, P., Horányi, A., Muñoz-Sabater,
1365   J., Nicolas, J., Radu, R., Schepers, D., Soci, C., Villaume, S., Bidlot, J.-R., Haimberger, L.,
1366   Woollen, J., Buontempo, C., & Thépaut, J.-N. (2021). The ERA5 global reanalysis:
1367   Preliminary extension to 1950. *Quarterly Journal of the Royal Meteorological Society*,
1368   *147*(741), 4186–4227. https://doi.org/https://doi.org/10.1002/qj.4174
1369   Beltrami, H., & Mareschal, J.-C. (1992). Ground temperature histories for central and eastern
1370   Canada from geothermal measurements: Little Ice Age signature. *Geophysical Research*
1371   *Letters*, *19*(7), 689–692. https://doi.org/10.1029/92GL00671
1372   Beltrami, H., Smerdon, J. E., Pollack, H. N., & Huang, S. (2002). Continental heat gain in the
1373   global climate system. *Geophysical Research Letters*, *29*(8), 8-1-8–3.
1374   https://doi.org/10.1029/2001GL014310
1375   Berrisford, P., Kållberg, P., Kobayashi, S., Dee, D., Uppala, S., Simmons, A. J., Poli, P., & Sato,
1376   H. (2011). Atmospheric conservation properties in ERA-Interim. *Quarterly Journal of the*
1377   *Royal Meteorological Society*, *137*(659), 1381–1399. https://doi.org/10.1002/qj.864
1378   Biskaborn, B. K., Lanckman, J.-P., Lantuit, H., Elger, K., Streletskiy, D. A., Cable, W. L., &
1379   Romanovsky, V. E. (2015). The new database of the Global Terrestrial Network for
1380   Permafrost (GTN-P). *Earth Syst. Sci. Data*, *7*(2), 245–259. https://doi.org/10.5194/essd-7-
1381   245-2015
1382   Boyer, T., Domingues, C. M., Good, S. A., Johnson, G. C., Lyman, J. M., Ishii, M., Gouretski,
1383   V., Willis, J. K., Antonov, J., Wijffels, S., Church, J. A., Cowley, R., & Bindoff, N. L.
1384   (2016). Sensitivity of Global Upper-Ocean Heat Content Estimates to Mapping Methods,
1385   XBT Bias Corrections, and Baseline Climatologies. *Journal of Climate*, *29*(13), 4817–4842.
1386   https://doi.org/10.1175/JCLI-D-15-0801.1

1387 Cabanes, C., Grouazel, A., von Schuckmann, K., Hamon, M., Turpin, V., Coatanoan, C., Paris,
1388   F., Guinehut, S., Boone, C., Ferry, N., de Boyer Montégut, C., Carval, T., Reverdin, G.,
1389   Pouliquen, S., & Le Traon, P.-Y. (2013). The CORA dataset: validation and diagnostics of
1390   in-situ ocean temperature and salinity measurements. *Ocean Sci.*, *9*(1), 1–18.
1391   https://doi.org/10.5194/os-9-1-2013
1392 Castelao, G. P. (2020). A Framework to Quality Control Oceanographic Data. Journal of Open
1393   Source Software. *Journal of Open Source Software*, *5*(48), 2063.
1394   https://doi.org/https://doi.org/10.21105/joss.02063
1395 Castelão, G. P. (2021). A machine learning approach to quality control oceanographic data.
1396   *Computers & Geosciences*, *155*, 104803.
1397   https://doi.org/https://doi.org/10.1016/j.cageo.2021.104803
1398 Cheng, L., Abraham, J., Hausfather, Z., & Trenberth, K. E. (2019). How fast are the oceans
1399   warming? *Science*, *363*(6423), 128. https://doi.org/10.1126/science.aav7619
1400 Cheng, L., Foster, G., Hausfather, Z., Trenberth, K. E., & Abraham, J. (2022). Improved
1401   Quantification of the Rate of Ocean Warming. *Journal of Climate*, *35*(14), 4827–4840.
1402   https://doi.org/10.1175/JCLI-D-21-0895.1
1403 Cheng, L., Luo, H., Boyer, T., Cowley, R., Abraham, J., Gouretski, V., Reseghetti, F., & Zhu, J.
1404   (2018). How Well Can We Correct Systematic Errors in Historical XBT Data? *Journal of
1405   Atmospheric and Oceanic Technology*, *35*(5), 1103–1125. https://doi.org/10.1175/JTECH-
1406   D-17-0122.1
1407 Cheng, L., Schuckmann, K. von, Abraham, J., Trenberth, K., Mann, M., Zanna, L., England, M.
1408   H., Zika, J. D., Fasullo, J., Yu1, Y., Pan, Y., Zhu, J., Newsom, E., Bronselaer, B., & Lin, X.
1409   (2022). Past and future ocean warming. *Nature*, *under revi*.
1410 Cheng, L., Trenberth, K. E., Fasullo, J., Boyer, T., Abraham, J., & Zhu, J. (2017). Improved
1411   estimates of ocean heat content from 1960 to 2015. *Science Advances*, *3*(3), e1601545.
1412   https://doi.org/10.1126/sciadv.1601545
1413 Cheng, L., Trenberth, K., Fasullo, J., Abraham, J., Boyer, T., von Schuckmann, K., & Zhu, J.
1414   (2017). Taking the Pulse of the Planet. *Eos*. https://doi.org/10.1029/2017EO081839
1415 Chiodo, G., & Haimberger, L. (2010). Interannual changes in mass consistent energy budgets
1416   from ERA-Interim and satellite data. *Journal of Geophysical Research: Atmospheres*,
1417   *115*(D2). https://doi.org/10.1029/2009JD012049
1418 Church, J. A., White, N. J., Konikow, L. F., Domingues, C. M., Cogley, J. G., Rignot, E.,
1419   Gregory, J. M., van den Broeke, M. R., Monaghan, A. J., & Velicogna, I. (2011). Revisiting
1420   the Earth's sea-level and energy budgets from 1961 to 2008. *Geophysical Research Letters*,
1421   *38*(18). https://doi.org/10.1029/2011GL048794
1422 Ciais, P., Sabine, C., Bala, G., Bopp, L., Brovkin, V., Canadell, J., Chhabra, A., DeFries, R.,
1423   Galloway, J., Heimann, M., Jones, C., Le Quéré, C., Myneni, R. B., Piao, S., & Thornton, P.
1424   (2014). *Carbon and Other Biogeochemical Cycles. In Climate Change 2013 – The Physical
1425   Science Basis: Working Group I Contribution to the Fifth Assessment Report of the
1426   Intergovernmental Panel on Climate Change*. Cambridge University Press.
1427   https://doi.org/https://doi.org/DOI: 10.1017/CBO9781107415324.015
1428 Cleveland, W. S. (1979). Robust Locally Weighted Regression and Smoothing Scatterplots. *J.
1429   Am.Stat.Assoc.*, *74*, 829–836.
1430 Clough, W. J., & Hansen, L. B. (1979). The Ross Ice Shelf Project. *Science*, *203*(4379), 433–
1431   434. https://doi.org/10.1126/science.203.4379.433
1432 Cohen, J., Zhang, X., Francis, J., Jung, T., Kwok, R., Overland, J., Ballinger, T., Bhatt, U. S.,

1433   Chen, H. W., Coumou, D., Feldstein, S., Handorf, D., Henderson, G., Ionita, M.,
1434   Kretschmer, M., Laliberte, F., Lee, S., Linderholm, H. W., Maslowski, W., … Yoon, J.
1435   (2020). Divergent consensuses on Arctic amplification influence on midlatitude severe
1436   winter weather. *Nature Climate Change*, *10*, 20–29. https://doi.org/10.1038/s41558-019-
1437   0662-y
1438   Cook, A. J., & Vaughan, D. G. (2010). Overview of areal changes of the ice shelves on the
1439   Antarctic Peninsula over the past 50 years. *The Cryosphere*, *4*(1), 77–98.
1440   https://doi.org/10.5194/tc-4-77-2010
1441   Cowley, R., Killick, R. E., Boyer, T., Gouretski, V., Reseghetti, F., Kizu, S., Palmer, M. D.,
1442   Cheng, L., Storto, A., Le Menn, M., Simoncelli, S., Macdonald, A. M., & Domingues, C.
1443   M. (2021). International Quality-Controlled Ocean Database (IQuOD) v0.1: The
1444   Temperature Uncertainty Specification   . In *Frontiers in Marine Science*   (Vol. 8).
1445   https://www.frontiersin.org/articles/10.3389/fmars.2021.689695
1446   Crisp, D., Dolman, H., Tanhua, T., McKinley, G. A., Hauck, J., Bastos, A., Sitch, S., Eggleston,
1447   S., & Aich, V. (2022). How Well Do We Understand the Land-Ocean-Atmosphere Carbon
1448   Cycle? *Reviews of Geophysics*, *60*(2), e2021RG000736.
1449   https://doi/https://doi.org/10.1029/2021RG000736
1450   Cuesta-Valero, F. J., Beltrami, H., García-García, A., Krinner, G., Langer, M., MacDougall, A.,
1451   Nitzbon, J., Peng, J., von Schuckmann, K., Seneviratne, S. I., Smith, N., Thiery, W.,
1452   Vanderkelen, I., & Wu, T. (2022). Continental Heat Storage: Contributions from Ground,
1453   Inland Waters, and Permafrost Thawing, submitted. *Earth System Dynamics*, *submitted*.
1454   Cuesta-Valero, F. J., Beltrami, H., Gruber, S., García-García, A., & González-Rouco, J. F.
1455   (2022). A new bootstrap technique to quantify uncertainty in estimates of ground surface
1456   temperature and ground heat flux histories from geothermal data. Submitted. *Geoscientific
1457   Model Development*, *submitted*.
1458   Cuesta-Valero, Francisco; Beltrami, Hugo; García-García, Almudena; Krinner, Gerhard; Langer,
1459   Moritz; MacDougall, Andrew; Nitzbon, Jean; Peng, Jian; von Schuckmann, Karina;
1460   Seneviratne, Sonia; Smith, Noah; Thiery, Wim; Vanderkelen, Inne; Wu, Tonghua (2022).
1461   Continental heat storage: Contributions from the ground, inland waters, and permafrost
1462   thawing, submitted to Earth System Dynamics (2022c). World Data Center for Climate
1463   (WDCC) at DKRZ. https://www.wdc-climate.de/ui/entry?acronym=GCOS_EHI_1960-
1464   2020_CoHC
1465   Cuesta-Valero, F J, García-García, A., Beltrami, H., & Finnis, J. (2021). First assessment of the
1466   earth heat inventory within CMIP5 historical simulations. *Earth Syst. Dynam.*, *12*(2), 581–
1467   600. https://doi.org/10.5194/esd-12-581-2021
1468   Cuesta-Valero, F J, Garcia-Garcia, A., Beltrami, H., González-Rouco, J. F., & Garcia-
1469   Bustamante, E. (2021). Long-Term Global Ground Heat Flux and Continental Heat Storage
1470   from Geothermal Data. *Climate of the Past*, *17*(1), 451–468. https://doi.org/10.5194/cp-17-
1471   451-2021
1472   Cuesta-Valero, F J, García-García, A., Beltrami, H., Zorita, E., & Jaume-Santero, F. (2019).
1473   Long-term Surface Temperature (LoST) database as a complement for GCM preindustrial
1474   simulations. *Clim. Past*, *15*(3), 1099–1111. https://doi.org/10.5194/cp-15-1099-2019
1475   Cuesta-Valero, Francisco José, Beltrami, H., Burke, E., García-García, A., MacDougall, A.,
1476   Peng, J., Schuckmann, K. von, Seneviratne, S. I., Smith, N., Thiery, W., Vanderkelen, I., &
1477   Wu, T. (2022). Continental Heat Storage: Contributions from the Ground, Inland Waters,
1478   and Permafrost Thawing. *Submitted to Earth System Data*.

1479   Cuesta-Valero, Francisco José, García-García, A., Beltrami, H., & Smerdon, J. E. (2016). First
1480   assessment of continental energy storage in CMIP5 simulations. *Geophysical Research*
1481   *Letters*, *43*(10), 5326–5335. https://doi.org/10.1002/2016GL068496
1482   de Vrese, P., Stacke, T., Caves Rugenstein, J., Goodman, J., & Brovkin, V. (2021). Snowfall-
1483   albedo feedbacks could have led to deglaciation of snowball Earth starting from mid-
1484   latitudes. *Communications Earth & Environment*, *2*(1), 91. https://doi.org/10.1038/s43247-
1485   021-00160-4
1486   Demezhko, D. Y., & Gornostaeva, A. A. (2015). Late Pleistocene–Holocene ground surface heat
1487   flux changes reconstructed from borehole temperature data. *Climate of the Past*, *11*(4), 647–
1488   652. https://doi.org/D O I: 10.5194/cp 11-647-2015
1489   Denning, A. S. (2022). Where Has All the Carbon Gone? *Annual Review of Earth and Planetary*
1490   *Sciences*, *50*(1), 55–78. https://doi.org/10.1146/annurev-earth-032320-092010
1491   Desbruyères, D. G., Purkey, S. G., McDonagh, E. L., Johnson, G. C., & King, B. A. (2016).
1492   Deep and abyssal ocean warming from 35 years of repeat hydrography. *Geophysical*
1493   *Research Letters*, *43*(19), 10, 310–356, 365. https://doi.org/10.1002/2016GL070413
1494   Desbruyères, D., McDonagh, E. L., King, B. A., & Thierry, V. (2017). Global and Full-Depth
1495   Ocean Temperature Trends during the Early Twenty-First Century from Argo and Repeat
1496   Hydrography. *Journal of Climate*, *30*(6), 1985–1997. https://doi.org/10.1175/JCLI-D-16-
1497   0396.1
1498   Dieng, H. B., Cazenave, A., Meyssignac, B., & Ablain, M. (2017). New estimate of the current
1499   rate of sea level rise from a sea level budget approach. *Geophysical Research Letters*, *44*(8),
1500   3744–3751. https://doi.org/10.1002/2017GL073308
1501   Domingues, C. M., Church, J. A., White, N. J., Gleckler, P. J., Wijffels, S. E., Barker, P. M., &
1502   Dunn, J. R. (2008). Improved estimates of upper-ocean warming and multi-decadal sea-
1503   level rise. *Nature*, *453*(7198), 1090–1093. https://doi.org/10.1038/nature07080
1504   Dorigo, W., Dietrich, S., Aires, F., Brocca, L., Carter, S., Cretaux, J.-F., Dunkerley, D.,
1505   Enomoto, H., Forsberg, R., Güntner, A., Hegglin, M. I., Hollmann, R., Hurst, D. F.,
1506   Johannessen, J. A., Kummerow, C., Lee, T., Luojus, K., Looser, U., Miralles, D. G., …
1507   Aich, V. (2021). Closing the Water Cycle from Observations across Scales: Where Do We
1508   Stand? *Bulletin of the American Meteorological Society*, *102*(10), E1897–E1935.
1509   https://doi.org/10.1175/BAMS-D-19-0316.1
1510   Eicken, H., Fischer, H., & Lemke, P. (1995). Effects of the snow cover on Antarctic sea ice and
1511   potential modulation of its response to climate change. *Annals of Glaciology*, *21*, 369–376.
1512   https://doi.org/DOI: 10.3189/S0260305500016086
1513   Farinotti, D., Huss, M., Fürst, J. J., Landmann, J., Machguth, H., Maussion, F., & Pandit, A.
1514   (2019). A consensus estimate for the ice thickness distribution of all glaciers on Earth.
1515   *Nature Geoscience*, *12*, 168–173. https://doi.org/10.1038/s41561-019-0300-3
1516   Fischer, E. M., Sippel, S., & Knutti, R. (2021). Increasing probability of record-shattering
1517   climate extremes. *Nature Climate Change*, *11*(8), 689–695. https://doi.org/10.1038/s41558-
1518   021-01092-9
1519   Forster, P., Storelvmo, T., Armour, K., Collins, W., Dufresne, J.-L., Frame, D., Lunt, D. J.,
1520   Mauritsen, T., Palmer, M. D., Watanabe, M., Wild, M., & Zhang, H. (2022). *The Earth's*
1521   *Energy Budget, Climate Feedbacks, and Climate Sensitivity. In Climate Change 2021: The*
1522   *Physical Science Basis. Contribution of Working Group I to the Sixth Assessment Report of*
1523   *the Intergovernmental Panel on Climate Change* (V. Masson-Delmotte, P. Zhai, A. Pirani,
1524   S. L. Connors, C. Péan, S. Berger, N. Caud, Y. Chen, L. Goldfarb, M. I. Gomis, M. Huang,

1525   K. Leitzell, E. Lonnoy, J. B. R. Matthews, T. K. Maycock, T. Waterfield, O. Yelekçi, R.
1526   Yu, & B. Zhou (eds.)). Cambridge University Press, Cambridge, United Kingdom and New
1527   York, NY, USA. https://doi.org/10.1017/9781009157896.009
1528   Friedlingstein, P., Jones, M. W., O'Sullivan, M., Andrew, R. M., Bakker, D. C. E., Hauck, J., Le
1529   Quéré, C., Peters, G. P., Peters, W., Pongratz, J., Sitch, S., Canadell, J. G., Ciais, P.,
1530   Jackson, R. B., Alin, S. R., Anthoni, P., Bates, N. R., Becker, M., Bellouin, N., … Zeng, J.
1531   (2022). Global Carbon Budget 2021. *Earth Syst. Sci. Data*, *14*(4), 1917–2005.
1532   https://doi.org/10.5194/essd-14-1917-2022
1533   Frieler, K., Lange, S., Piontek, F., Reyer, C., Schewe, J., Warszawski, L., Zhao, F., Chini, L.,
1534   Denvil, S., Emanuel, K., Geiger, T., Halladay, K., Hurtt, G., Mengel, M., Murakami, D.,
1535   Ostberg, S., Popp, A., Riva, R., Stevanovic, M., & Yamagata, Y. (2017). Assessing the
1536   impacts of 1.5°C global warming - Simulation protocol of the Inter-Sectoral Impact Model
1537   Intercomparison Project (ISIMIP2b). *Geoscientific Model Development*, *10*, 4321–4345.
1538   https://doi.org/10.5194/gmd-10-4321-2017
1539   Fu, Q., Solomon, S., Pahlavan, H. A., & Lin, P. (2019). Observed changes in Brewer–Dobson
1540   circulation for 1980–2018. *Environmental Research Letters*, *14*(11), 114026.
1541   https://doi.org/10.1088/1748-9326/ab4de7
1542   Gädeke, A., Langer, M., Boike, J., Burke, E. J., Chang, J., Head, M., Reyer, C. P. O., Schaphoff,
1543   S., Thiery, W., & Thonicke, K. (2021). Climate change reduces winter overland travel
1544   across the Pan-Arctic even under low-end global warming scenarios. *Environmental
1545   Research Letters*, *16*(2), 24049. https://doi.org/10.1088/1748-9326/abdcf2
1546   Gaillard, F., Reynaud, T., Thierry, V., Kolodziejczyk, N., & von Schuckmann, K. (2016). In
1547   Situ–Based Reanalysis of the Global Ocean Temperature and Salinity with ISAS:
1548   Variability of the Heat Content and Steric Height. *Journal of Climate*, *29*(4), 1305–1323.
1549   https://doi.org/10.1175/JCLI-D-15-0028.1
1550   GCOS. (2016). *The Global Observing System for Climate: Implementation needs, World
1551   Meteorological Organization, Geneva, Switzerland*.
1552   GCOS. (2021). *The Status of the Global Climate Observing System 2021: Executive Summary.
1553   (GCOS-239)*.
1554   Gelaro, R., McCarty, W., Suárez, M. J., Todling, R., Molod, A., Takacs, L., Randles, C. A.,
1555   Darmenov, A., Bosilovich, M. G., Reichle, R., Wargan, K., Coy, L., Cullather, R., Draper,
1556   C., Akella, S., Buchard, V., Conaty, A., da Silva, A. M., Gu, W., … Zhao, B. (2017). The
1557   Modern-Era Retrospective Analysis for Research and Applications, Version 2 (MERRA-2)
1558   (I200, trans.). *Journal of Climate*, *30*(14), 5419–5454. https://doi.org/10.1175/JCLI-D-16-
1559   0758.1
1560   Golub, M., Thiery, W., Marcé, R., Pierson, D., Vanderkelen, I., Mercado-Bettín, D., Woolway,
1561   R., Grant, L., Jennings, E., Kraemer, B., Schewe, J., Zhao, F., Frieler, K., Mengel, M.,
1562   Bogomolov, V., Bouffard, D., Côté, M., Couture, R.-M., Debolskiy, A., & Zdorovennova,
1563   G. (2022). A framework for ensemble modelling of climate change impacts on lakes
1564   worldwide: the ISIMIP Lake Sector. *Geoscientific Model Development*, *15*, 4597–4623.
1565   https://doi.org/10.5194/gmd-15-4597-2022
1566   Goni, G. J., Sprintall, J., Bringas, F., Cheng, L., Cirano, M., Dong, S., Domingues, R., Goes, M.,
1567   Lopez, H., Morrow, R., Rivero, U., Rossby, T., Todd, R. E., Trinanes, J., Zilberman, N.,
1568   Baringer, M., Boyer, T., Cowley, R., Domingues, C. M., … Volkov, D. (2019). More Than
1569   50 Years of Successful Continuous Temperature Section Measurements by the Global
1570   Expendable Bathythermograph Network, Its Integrability, Societal Benefits, and Future.

1571 *Frontiers in Marine Science*, *6*, 452.
1572 https://www.frontiersin.org/article/10.3389/fmars.2019.00452
1573 Good, S. A. (2017). The impact of observational sampling on time series of global 0–700 m
1574 ocean average temperature: a case study. *International Journal of Climatology*, *37*(5),
1575 2260–2268. https://doi.org/10.1002/joc.4654
1576 Good, S. A., Martin, M. J., & Rayner, N. A. (2013). EN4: Quality controlled ocean temperature
1577 and salinity profiles and monthly objective analyses with uncertainty estimates (I5197,
1578 trans.). *Journal of Geophysical Research: Oceans*, *118*(12), 6704–6716.
1579 https://doi.org/10.1002/2013JC009067
1580 GOOS. (2019). *The Global Ocean Observing System Strategy. GOOS Report No. 239, IOC*
1581 *Brochure 2019-5 (IOC/Bro/2019/5 rev.2)*.
1582 https://www.goosocean.org/index.php?option=com_oe&task=viewDocumentRecord&docI
1583 D=24590
1584 Gorfer, M. (2022). *Monitoring of climate change and variability in atmospheric heat content*
1585 *based on climate records and reanalyses, Sci. Rep. 94-2022*. Wegener Center Verlag.
1586 https://wegcenter.uni-graz.at/wegener-center-verlag/2022
1587 Gould, J., Sloyan, B., & Visbeck, M. (2013). Chapter 3 - In Situ Ocean Observations: A Brief
1588 History, Present Status, and Future Directions. In G. Siedler, S. M. Griffies, J. Gould, & J.
1589 A. Church (Eds.), *Ocean Circulation and Climate* (Vol. 103, pp. 59–81). Academic Press.
1590 https://doi.org/https://doi.org/10.1016/B978-0-12-391851-2.00003-9
1591 Gouretski, V., & Cheng, L. (2020). Correction for Systematic Errors in the Global Dataset of
1592 Temperature Profiles from Mechanical Bathythermographs. *Journal of Atmospheric and*
1593 *Oceanic Technology*, *37*(5), 841–855. https://doi.org/10.1175/JTECH-D-19-0205.1
1594 Grant, L., Vanderkelen, I., Gudmundsson, L., Tan, Z., Perroud, M., Stepanenko, V. M.,
1595 Debolskiy, A. V, Droppers, B., Janssen, A. B. G., Woolway, R. I., Choulga, M., Balsamo,
1596 G., Kirillin, G., Schewe, J., Zhao, F., del Valle, I. V., Golub, M., Pierson, D., Marcé, R., …
1597 Thiery, W. (2021). Attribution of global lake systems change to anthropogenic forcing.
1598 *Nature Geoscience*, *14*(11), 849–854. https://doi.org/10.1038/s41561-021-00833-x
1599 Gregory, J. M., & Andrews, T. (2016). Variation in climate sensitivity and feedback parameters
1600 during the historical period. *Geophysical Research Letters*, *43*(8), 3911–3920.
1601 https://doi.org/10.1002/2016GL068406
1602 Grise, K. M., Davis, S. M., Simpson, I. R., Waugh, D. W., Fu, Q., Allen, R. J., Rosenlof, K. H.,
1603 Ummenhofer, C. C., Karnauskas, K. B., Maycock, A. C., Quan, X. W., Birner, T., & Staten,
1604 P. W. (2019). Recent tropical expansion: Natural variability or forced response? *Journal of*
1605 *Climate*, *32*(5), 1551–1571. https://doi.org/10.1175/JCLI-D-18-0444.1
1606 Guinehut, S., Dhomps, A.-L., Larnicol, G., & Le Traon, P.-Y. (2012). High resolution 3-D
1607 temperature and salinity fields derived from in situ and satellite observations. *Ocean Sci.*,
1608 *8*(5), 845–857. https://doi.org/10.5194/os-8-845-2012
1609 Gulev, S. K., Thorne, P. W., Ahn, J., Dentener, F. J., Domingues, C. M., Gerland, S., Gong, D.,
1610 Kaufman, D. S., Nnamchi, H. C., Quaas, J., Rivera, J. A., Sathyendranath, S., Smith, S. L.,
1611 Trewin, B., Schuckmann, K. von, & Vose, R. S. (2021). *Changing State of the Climate*
1612 *System Supplementary Material. In Climate Change 2021: The Physical Science Basis.*
1613 *Contribution of Working Group I to the Sixth Assessment Report of the Intergovernmental*
1614 *Panel on Climate Change* (V. Masson-Delmotte, P. Zhai, A. Pirani, S. L. Connors, C. Péan,
1615 S. Berger, N. Caud, Y. Chen, L. Goldfarb, M. I. Gomis, M. Huang, K. Leitzell, E. Lonnoy,
1616 J. B. R. Matthews, T. K. Maycock, T. Waterfield, O. Yelekçi, R. Yu, & B. Zhou (eds.)).

1617   Cambridge University Press,. https://doi.org/10.1017/9781009157896.004
1618   Hakuba, M. Z., Frederikse, T., & Landerer, F. W. (2021). Earth's Energy Imbalance From the
1619   Ocean Perspective (2005–2019). *Geophysical Research Letters*, *48*(16), e2021GL093624.
1620   https://doi.org/https://doi.org/10.1029/2021GL093624
1621   Hansen, J, Sato, M., Kharecha, P., & von Schuckmann, K. (2011). Earth's energy imbalance and
1622   implications. *Atmos. Chem. Phys.*, *11*(24), 13421–13449. https://doi.org/10.5194/acp-11-
1623   13421-2011
1624   Hansen, J, Sato, M., Kharecha, P., von Schuckmann, K., Beerling, D. J., Cao, J., Marcott, S.,
1625   Masson-Delmotte, V., Prather, M. J., Rohling, E. J., Shakun, J., Smith, P., Lacis, A.,
1626   Russell, G., & Ruedy, R. (2017). Young people's burden: requirement of negative CO2
1627   emissions. *Earth Syst. Dynam.*, *8*(3), 577–616. https://doi.org/10.5194/esd-8-577-2017
1628   Hansen, James, Nazarenko, L., Ruedy, R., Sato, M., Willis, J., Del Genio, A., Koch, D., Lacis,
1629   A., Lo, K., Menon, S., Novakov, T., Perlwitz, J., Russell, G., Gavin A., S., & Tausnev, N.
1630   (2005). Earth's Energy Imbalance: Confirmation and Implications. *Science*, *308*(5727),
1631   1431–1435. https://doi.org/10.1126/science.1110252
1632   Hartmann, A., & Rath, V. (2005). Uncertainties and shortcomings of ground surface temperature
1633   histories derived from inversion of temperature logs. *Journal of Geophysics and
1634   Engineering*, *2*(4), 299–311. https://doi.org/10.1088/1742-2132/2/4/S02
1635   Hersbach, H., de Rosnay, P., Bell, B., Schepers, D., Simmons, A., Soci, C., Abdalla, S., Alonso-
1636   Balmaseda, M., Balsamo, G., Bechtold, P., Berrisford, P., Bidlot, J.-R., de Boisséson, E.,
1637   Bonavita, M., Browne, P., Buizza, R., Dahlgren, P., Dee, D., Dragani, R., … Zuo, H.
1638   (2018). *Operational global reanalysis: progress, future directions and synergies with NWP*.
1639   https://www.ecmwf.int/node/18765
1640   Hersbach, Hans, Bell, B., Berrisford, P., Hirahara, S., Horányi, A., Muñoz-Sabater, J., Nicolas,
1641   J., Peubey, C., Radu, R., Schepers, D., Simmons, A., Soci, C., Abdalla, S., Abellan, X.,
1642   Balsamo, G., Bechtold, P., Biavati, G., Bidlot, J., Bonavita, M., … Thépaut, J. N. (2020).
1643   The ERA5 global reanalysis. *Quarterly Journal of the Royal Meteorological Society*, *146*,
1644   1999–2049. https://doi.org/10.1002/qj.3803
1645   Hopcroft, P. O., Gallagher, K., & Pain, C. C. (2007). Inference of past climate from borehole
1646   temperature data using Bayesian Reversible Jump Markov chain Monte Carlo. *Geophysical
1647   Journal International*, *171*(3), 1430–1439. https://doi.org/10.1111/j.1365-
1648   246X.2007.03596.x
1649   Hosoda, S., Ohira, T., & Nakamura, T. (2008). *A monthly mean dataset of global oceanic
1650   temperature and salinity derived from Argo float observations*.
1651   http://www.jamstec.go.jp/ARGO/argo_web/ancient/MapQ/Hosoda_etal_MOAA_GPV.pdf
1652   IPCC. (2019). *IPCC Special Report on the Ocean and Cryosphere in a Changing Climate* (H.-O.
1653   Pörtner, D. C. Roberts, V. Masson-Delmotte, P. Zhai, M. Tignor, E. Poloczanska, K.
1654   Mintenbeck, A. Alegría, M. Nicolai, A. Okem, J. Petzold, B. Rama, & N. M. Weyer (eds.)).
1655   Cambridge University Press. https://doi.org/https://doi.org/10.1017/9781009157964
1656   IPCC. (2021). *Summary for Policymakers. In: Climate Change 2021: The Physical Science
1657   Basis. Contribution of Working Group I to the Sixth Assessment Report of the
1658   Intergovernmental Panel on Climate Change* (V. Masson-Delmotte, P. Zhai, A. Pirani, S. L.
1659   Connors, C. Péan, S. Berger, N. Caud, Y. Chen, L. Goldfarb, M. I. Gomis, M.Huang, K.
1660   Leitzell, E. Lonnoy, J. B. R. Matthews, T. K. Maycock, T. Waterfield, O. Yelekçi, R. Yu, &
1661   B. Zhou (eds.)). Cambridge University Press. https://doi.org/10.1017/9781009157896.001
1662   IPCC. (2022a). *Climate Change 2022: Impacts, Adaptation, and Vulnerability. Contribution of*

1663   *Working Group II to the Sixth Assessment Report of the Intergovernmental Panel on*
1664   *Climate Change* (H.-O. Pörtner, D. C. Roberts, M. Tignor, E. S. Poloczanska, K.
1665   Mintenbeck, A. Alegría, M. Craig, S. Langsdorf, S. Löschke, V. Möller, A. Okem, & B.
1666   Rama (eds.)). Cambridge University Press, Cambridge, UK and New York, NY, USA.
1667   https://doi.org/in press
1668   IPCC. (2022b). *Climate Change 2022: Mitigation of Climate Change. Contribution of Working*
1669   *Group III to the Sixth Assessment Report of the Intergovernmental Panel on Climate*
1670   *Change* (P. R. Shukla, J. Skea, R. Slade, A. Al Khourdajie, R. van Diemen, D. McCollum,
1671   M. Pathak, S. Some, P. Vyas, R. Fradera, M. Belkacemi, A. Hasija, G. Lisboa, S. Luz, & J.
1672   Malley (eds.)). Cambridge University Press, Cambridge, UK and New York, NY, USA.
1673   https://doi.org/10.1017/9781009157926
1674   IPCC. (2022c). *Summary for Policymakers, In: Climate Change 2022: Impacts, Adaptation, and*
1675   *Vulnerability. Contribution of Working Group II to the Sixth Assessment Report of the*
1676   *Intergovernmental Panel on Climate Change* (H.-O. Pörtner, D. C. Roberts, M. Tignor, E.
1677   S. Poloczanska, K. Mintenbeck, A. Alegría, M. Craig, S. Langsdorf, S. Löschke, V. Möller,
1678   A. Okem, & B. Rama (eds.)). Cambridge University Press. https://doi.org/in press
1679   IROWG. (2021). *Report of IROWG activities: Outcome and recommendations from the IROWG-*
1680   *8 Workshop, CGMS-49 IROWG-WP-01 V3, 28 April 2021, International Radio Occultation*
1681   *Working Group*. https://irowg.org/wpcms/wp-content/uploads/2021/07/CGMS-49-IROWG-
1682   WP-01.pdf
1683   Ishii, M., Fukuda, Y., Hirahara, S., Yasui, S., Suzuki, T., & Sato, K. (2017). Accuracy of Global
1684   Upper Ocean Heat Content Estimation Expected from Present Observational Data Sets.
1685   *SOLA*, *13*, 163–167. https://doi.org/10.2151/sola.2017-030
1686   Jan, A., & Painter, S. L. (2020). Permafrost thermal conditions are sensitive to shifts in snow
1687   timing. *Environmental Research Letters*, *15*(8), 084026. https://doi.org/10.1088/1748-
1688   9326/ab8ec4
1689   Jaume-Santero, F., Pickler, C., Beltrami, H., & Mareschal, J.-C. (2016). North American
1690   regional climate reconstruction from ground surface temperature histories. *Clim. Past*,
1691   *12*(12), 2181–2194. https://doi.org/10.5194/cp-12-2181-2016
1692   Johnson, G. C., Lyman, J. M., & Loeb, N. G. (2016). Improving estimates of Earth's energy
1693   imbalance. *Nature Climate Change*, *6*(7), 639–640. https://doi.org/10.1038/nclimate3043
1694   Johnson, G. C., Purkey, S. G., Zilberman, N. V, & Roemmich, D. (2019). Deep Argo Quantifies
1695   Bottom Water Warming Rates in the Southwest Pacific Basin. *Geophysical Research*
1696   *Letters*, *46*(5), 2662–2669. https://doi.org/10.1029/2018GL081685
1697   Kashiwase, H., Ohshima, K. I., Nihashi, S., & Eicken, H. (2017). Evidence for ice-ocean albedo
1698   feedback in the Arctic Ocean shifting to a seasonal ice zone. *Scientific Reports*, *7*(1), 8170.
1699   https://doi.org/10.1038/s41598-017-08467-z
1700   Khazaei, B., Read, L. K., Casali, M., Sampson, K. M., & Yates, D. N. (2022). GLOBathy, the
1701   global lakes bathymetry dataset. *Scientific Data*, *9*(1), 36. https://doi.org/10.1038/s41597-
1702   022-01132-9
1703   King, B. A., Firing, E., & Joyce, T. (2001). Chapter 3.1 Shipboard observations during WOCE.
1704   *Int. Geophys.*, *77*, 99–122. https://doi.org/https://doi.org/10.1016/S0074-6142(01)80114-5
1705   Kirchengast, Gottfried; Gorfer, Maximilian; Haimberger, Leopold; Mayer, Michael; Steiner,
1706   Andrea; Allan, Richard (2022). Heat stored in the Earth system 1960-2020: Where does the
1707   energy go?, submitted to Earth System Science Data. (2022). World Data Center for
1708   Climate (WDCC) at DKRZ. https://www.wdc-

1709   climate.de/ui/entry?acronym=GCOS_EHI_1960-2020_AHC
1710   Kobayashi, S., Ota, Y., Harada, Y., Ebita, A., Moriya, M., Onoda, H., Onogi, K., Kamahori, H.,
1711   Kobayashi, C., Endo, H., MiyaokaI, K., & Takahashi, K. (2015). The JRA-55 Reanalysis:
1712   General Specifications and Basic Characteristics. *Journal of the Meteorological Society of*
1713   *Japan. Ser. II*, *93*(1), 5–48. https://doi.org/10.2151/jmsj.2015-001
1714   Kramer, R. J., He, H., Soden, B. J., Oreopoulos, L., Myhre, G., Forster, P. M., & Smith, C. J.
1715   (2021). Observational Evidence of Increasing Global Radiative Forcing. *Geophysical*
1716   *Research Letters*, *48*(7), e2020GL091585.
1717   https://doi.org/https://doi.org/10.1029/2020GL091585
1718   Kuhlbrodt, T., & Gregory, J. M. (2012). Ocean heat uptake and its consequences for the
1719   magnitude of sea level rise and climate change. *Geophysical Research Letters*, *39*(18).
1720   https://doi.org/10.1029/2012GL052952
1721   Kuusela, M., & Giglio, D. (2022). *Global Ocean Heat Content Anomalies based on Argo data.*
1722   https://doi.org/10.5281/ZENODO.6131625
1723   Labe, Z., Magnusdottir, G., & Stern, H. (2018). Variability of Arctic Sea Ice Thickness Using
1724   PIOMAS and the CESM Large Ensemble. *Journal of Climate*, *31*(8), 3233–3247.
1725   https://doi.org/10.1175/JCLI-D-17-0436.1
1726   Ladstädter, F., Steiner, A. K., Schwärz, M., & Kirchengast, G. (2015). Climate intercomparison
1727   of GPS radio occultation, RS90/92 radiosondes and GRUAN from 2002 to 2013.
1728   *Atmospheric Measurement Techniques*, *8*(4), 1819–1834. https://doi.org/10.5194/amt-8-
1729   1819-2015
1730   Lane, A. C. (1923). Geotherms of Lake Superior Copper Country. *GSA Bulletin*, *34*(4), 703–720.
1731   https://doi.org/10.1130/GSAB-34-703
1732   Lavergne, T., Macdonald Sørensen, A., Kern, S., Tonboe, R., Notz, D., Aaboe, S., Bell, L.,
1733   Dybkjær, G., Eastwood, S., Gabarro, C., Heygster, G., Anne Killie, M., Brandt Kreiner, M.,
1734   Lavelle, J., Saldo, R., Sandven, S., & Pedersen, L. T. (2019). Version 2 of the EUMETSAT
1735   OSI SAF and ESA CCI sea-ice concentration climate data records. *Cryosphere*, *13*(1), 49–
1736   78. https://doi.org/10.5194/tc-13-49-2019
1737   Laxon, S. W., Giles, K. A., Ridout, A. L., Wingham, D. J., Willatt, R., Cullen, R., Kwok, R.,
1738   Schweiger, A., Zhang, J., Haas, C., Hendricks, S., Krishfield, R., Kurtz, N., Farrell, S., &
1739   Davidson, M. (2013). CryoSat-2 estimates of Arctic sea ice thickness and volume (I326,
1740   trans.). *Geophysical Research Letters*. https://doi.org/10.1002/grl.50193
1741   Leahy, T. P., Llopis, F. P., Palmer, M. D., & Robinson, N. H. (2018). Using Neural Networks to
1742   Correct Historical Climate Observations (I6042, trans.). *Journal of Atmospheric and*
1743   *Oceanic Technology*, *35*(10), 2053–2059. https://doi.org/10.1175/JTECH-D-18-0012.1
1744   Levitus, S., Antonov, J. I., Boyer, T. P., Baranova, O. K., Garcia, H. E., Locarnini, R. A.,
1745   Mishonov, A. V, Reagan, J. R., Seidov, D., Yarosh, E. S., & Zweng, M. M. (2012). World
1746   ocean heat content and thermosteric sea level change (0–2000 m), 1955–2010. *Geophysical*
1747   *Research Letters*, *39*(10). https://doi.org/10.1029/2012GL051106
1748   Li, H., Xu, F., Zhou, W., Wang, D., Wright, J. S., Liu, Z., & Lin, Y. (2017). Development of a
1749   global gridded Argo data set with Barnes successive corrections. *Journal of Geophysical*
1750   *Research: Oceans*, *122*(2), 866–889. https://doi.org/https://doi.org/10.1002/2016JC012285
1751   Liao, S., Luo, H., Wang, J., Shi, Q., Zhang, J., & Yang, Q. (2022). An evaluation of Antarctic
1752   sea-ice thickness from the Global Ice-Ocean Modeling and Assimilation System based on in
1753   situ and satellite observations. *The Cryosphere*, *16*(5), 1807–1819.
1754   https://doi.org/10.5194/tc-16-1807-2022

1755   Ligtenberg, S. R. M., Kuipers Munneke, P., Noël, B. P. Y., & van den Broeke, M. R. (2018).
1756   Brief communication: Improved simulation of the present-day Greenland firn layer (1960–
1757   2016). *The Cryosphere*, *12*(5), 1643–1649. https://doi.org/10.5194/tc-12-1643-2018
1758   Liu, C., Allan, R. P., Mayer, M., Hyder, P., Desbruyères, D., Cheng, L., Xu, J., Xu, F., & Zhang,
1759   Y. (2020). Variability in the global energy budget and transports 1985–2017. *Climate
1760   Dynamics*, *55*(11), 3381–3396. https://doi.org/10.1007/s00382-020-05451-8
1761   Llovel, W., Willis, J. K., Landerer, F. W., & Fukumori, I. (2014). Deep-ocean contribution to sea
1762   level and energy budget not detectable over the past decade. *Nature Climate Change*, *4*(11),
1763   1031–1035. https://doi.org/10.1038/nclimate2387
1764   Loeb, N. G., Johnson, G. C., Thorsen, T. J., Lyman, J. M., Rose, F. G., & Kato, S. (2021).
1765   Satellite and Ocean Data Reveal Marked Increase in Earth's Heating Rate. *Geophysical
1766   Research Letters*, *48*(13), e2021GL093047.
1767   https://doi.org/https://doi.org/10.1029/2021GL093047
1768   Loeb, N. G., Lyman, J. M., Johnson, G. C., Allan, R. P., Doelling, D. R., Wong, T., Soden, B. J.,
1769   & Stephens, G. L. (2012). Observed changes in top-of-the-atmosphere radiation and upper-
1770   ocean heating consistent within uncertainty. *Nature Geoscience*, *5*(2), 110–113.
1771   https://doi.org/10.1038/ngeo1375
1772   Loeb, N. G., Mayer, M., Kato, S., Fasullo, J. T., Zuo, H., Senan, R., Lyman, J. M., Johnson, G.
1773   C., & Balmaseda, M. (2022). Evaluating Twenty-Year Trends in Earth's Energy Flows
1774   From Observations and Reanalyses. *Journal of Geophysical Research: Atmospheres*,
1775   *127*(12), e2022JD036686. https://doi.org/https://doi.org/10.1029/2022JD036686
1776   Lyman, J. M., & Johnson, G. C. (2014). Estimating Global Ocean Heat Content Changes in the
1777   Upper 1800 m since 1950 and the Influence of Climatology Choice. *Journal of Climate*,
1778   *27*(5), 1945–1957. https://doi.org/10.1175/JCLI-D-12-00752.1
1779   MacIntosh, C. R., Merchant, C. J., & von Schuckmann, K. (2017). Uncertainties in Steric Sea
1780   Level Change Estimation During the Satellite Altimeter Era: Concepts and Practices.
1781   *Surveys in Geophysics*, *38*(1), 59–87. https://doi.org/10.1007/s10712-016-9387-x
1782   Mankoff, K. D., Colgan, W., Solgaard, A., Karlsson, N. B., Ahlstrøm, A. P., van As, D., Box, J.
1783   E., Khan, S. A., Kjeldsen, K. K., Mouginot, J., & Fausto, R. S. (2019). Greenland Ice Sheet
1784   solid ice discharge from 1986 through 2017. *Earth Syst. Sci. Data*, *11*(2), 769–786.
1785   https://doi.org/10.5194/essd-11-769-2019
1786   Marti, F., Blazquez, A., Meyssignac, B., Ablain, M., Barnoud, A., Fraudeau, R., Jugier, R.,
1787   Chenal, J., Larnicol, G., Pfeffer, J., Restano, M., & Benveniste, J. (2022). Monitoring the
1788   ocean heat content change and the Earth energy imbalance from space altimetry and space
1789   gravimetry. *Earth Syst. Sci. Data*, *14*(1), 229–249. https://doi.org/10.5194/essd-14-229-
1790   2022
1791   Matthews, T., Byrne, M., Horton, R., Murphy, C., Pielke Sr, R., Raymond, C., Thorne, P., &
1792   Wilby, R. L. (2022). Latent heat must be visible in climate communications. *WIREs Climate
1793   Change*, *13*(4), e779. https://doi.org/https://doi.org/10.1002/wcc.779
1794   Mayer, J., Mayer, M., & Haimberger, L. (2021). Consistency and Homogeneity of Atmospheric
1795   Energy, Moisture, and Mass Budgets in ERA5. *Journal of Climate*, *34*(10), 3955–3974.
1796   https://doi.org/10.1175/JCLI-D-20-0676.1
1797   Mayer, M., Lien, V. S., Mork, K. A., von Schuckmann, K., Monier, M., & Greiner, E. (2021).
1798   Ocean heat content in the High North, in Copernicus Marine Service Ocean State Report,
1799   Issue 5. *Journal of Operational Oceanography*, *14:sup1*, 17–23.
1800   https://doi.org/10.1080/1755876X.2021.1946240

1801   Mayer, Michael, Haimberger, L., Edwards, J. M., & Hyder, P. (2017). Toward Consistent
1802   Diagnostics of the Coupled Atmosphere and Ocean Energy Budgets. *Journal of Climate*,
1803   *30*(22), 9225–9246. https://doi.org/10.1175/JCLI-D-17-0137.1
1804   Meng, L., Liu, J., Tarasick, D. W., Randel, W. J., Steiner, A. K., Wilhelmsen, H., Wang, L., &
1805   Haimberger, L. (2022). Continuous rise of the tropopause in the Northern Hemisphere over
1806   1980–2020. *Science Advances*, *7*(45), eabi8065. https://doi.org/10.1126/sciadv.abi8065
1807   Meyssignac, B., Boyer, T., Zhao, Z., Hakuba, M. Z., Landerer, F. W., Stammer, D., Köhl, A.,
1808   Kato, S., L'Ecuyer, T., Ablain, M., Abraham, J. P., Blazquez, A., Cazenave, A., Church, J.
1809   A., Cowley, R., Cheng, L., Domingues, C. M., Giglio, D., Gouretski, V., … Zilberman, N.
1810   (2019). Measuring Global Ocean Heat Content to Estimate the Earth Energy Imbalance.
1811   *Frontiers in Marine Science*, *6*, 432.
1812   https://www.frontiersin.org/article/10.3389/fmars.2019.00432
1813   Mieruch, S., Demirel, S., Simoncelli, S., Schlitzer, R., & Seitz, S. (2021). SalaciaML: A Deep
1814   Learning Approach for Supporting Ocean Data Quality Control . In *Frontiers in Marine
1815   Science* (Vol. 8). https://www.frontiersin.org/articles/10.3389/fmars.2021.611742
1816   Millan, R., Mouginot, J., Rabatel, A., & Morlighem, M. (2022). Ice velocity and thickness of the
1817   world's glaciers. *Nature Geoscience*, *15*(2), 124–129. https://doi.org/10.1038/s41561-021-
1818   00885-z
1819   Moltmann, T., Turton, J., Zhang, H.-M., Nolan, G., Gouldman, C., Griesbauer, L., Willis, Z.,
1820   Piniella, Á. M., Barrell, S., Andersson, E., Gallage, C., Charpentier, E., Belbeoch, M., Poli,
1821   P., Rea, A., Burger, E. F., Legler, D. M., Lumpkin, R., Meinig, C., … Zhang, Y. (2019). A
1822   Global Ocean Observing System (GOOS), Delivered Through Enhanced Collaboration
1823   Across Regions, Communities, and New Technologies . In *Frontiers in Marine Science*
1824   (Vol. 6, p. 291). https://www.frontiersin.org/article/10.3389/fmars.2019.00291
1825   Moon, T., & Joughin, I. (2008). Changes in ice front position on Greenland's outlet glaciers from
1826   1992 to 2007. *Journal of Geophysical Research: Earth Surface*, *113*(F2).
1827   https://doi.org/https://doi.org/10.1029/2007JF000927
1828   Moore, G. W. K., Våge, K., Renfrew, I. A., & Pickart, R. S. (2022). Sea-ice retreat suggests re-
1829   organization of water mass transformation in the Nordic and Barents Seas. *Nature
1830   Communications*, *13*(1), 67. https://doi.org/10.1038/s41467-021-27641-6
1831   Motyka, R. J., Truffer, M., Fahnestock, M., Mortensen, J., Rysgaard, S., & Howat, I. (2011).
1832   Submarine melting of the 1985 Jakobshavn Isbræ floating tongue and the triggering of the
1833   current retreat. *Journal of Geophysical Research: Earth Surface*, *116*(F1).
1834   https://doi.org/https://doi.org/10.1029/2009JF001632
1835   Mouginot, J., Rignot, E., Bjørk, A., van den Broeke, M., Millan, R., Morlighem, M., Noël, B.,
1836   Scheuchl, B., & Wood, M. (2019). Forty-six years of Greenland Ice Sheet mass balance
1837   from 1972 to 2018. *Proceedings of the National Academy of Sciences*, *116*(19), 9239–9244.
1838   https://doi.org/10.1073/pnas.1904242116
1839   Mouginot, J., Rignot, E., Scheuchl, B., Fenty, I., Khazendar, A., Morlighem, M., Buzzi, A., &
1840   Paden, J. (2015). Fast retreat of Zachariæ Isstrøm, northeast Greenland. *Science*, *350*(6266),
1841   1357–1361. https://doi.org/10.1126/science.aac7111
1842   Münchow, A., Padman, L., & Fricker, H. A. (2014). Interannual changes of the floating ice shelf
1843   of Petermann Gletscher, North Greenland, from 2000 to 2012. *Journal of Glaciology*,
1844   *60*(221), 489–499. https://doi.org/DOI: 10.3189/2014JoG13J135
1845   Nauels, A., Meinshausen, M., Mengel, M., Lorbacher, K., & Wigley, T. M. L. (2017).
1846   Synthesizing long-term sea level rise projections – the MAGICC sea level model v2.0.

1847   *Geosci. Model Dev.*, *10*(6), 2495–2524. https://doi.org/10.5194/gmd-10-2495-2017

1848 Nicolaus, M., Hoppmann, M., Arndt, S., Hendricks, S., Katlein, C., Nicolaus, A., Rossmann, L.,
1849   Schiller, M., & Schwegmann, S. (2021). Snow Depth and Air Temperature Seasonality on
1850   Sea Ice Derived From Snow Buoy Measurements . In *Frontiers in Marine Science* (Vol.
1851   8). https://www.frontiersin.org/article/10.3389/fmars.2021.655446

1852 Nitzbon, J., Krinner, G., Schneider von Deimling, T., Werner, M., & Langer, M. (2022).
1853   Quantifying the Permafrost Heat Sink in Earth's Climate System. Submitted. *Geophysical*
1854   *Research Letters*.

1855 Nitzbon, Jean; Krinner, Gerhard; Langer, Moritz (2022b). Quantifying the Permafrost Heat Sink
1856   in Earth's Climate System, doi:/10.1002/essoar.10511600.1, submitted to Geophysical
1857   Research Letters (2022). World Data Center for Climate (WDCC) at DKRZ.
1858   https://www.wdc-climate.de/ui/entry?acronym=GCOS_EHI_1960-2020_PHC

1859 Palmer, M D, & McNeall, D. J. (2014). Internal variability of Earth's energy budget simulated
1860   by CMIP5 climate models. *Environmental Research Letters*, *9*(3), 034016.
1861   https://doi.org/10.1088/1748-9326/9/3/034016

1862 Palmer, M D, Roberts, C. D., Balmaseda, M., Chang, Y.-S., Chepurin, G., Ferry, N., Fujii, Y.,
1863   Good, S. A., Guinehut, S., Haines, K., Hernandez, F., Köhl, A., Lee, T., Martin, M. J.,
1864   Masina, S., Masuda, S., Peterson, K. A., Storto, A., Toyoda, T., … Xue, Y. (2017). Ocean
1865   heat content variability and change in an ensemble of ocean reanalyses. *Climate Dynamics*,
1866   *49*(3), 909–930. https://doi.org/10.1007/s00382-015-2801-0

1867 Palmer, Matthew D, Boyer, T., Cowley, R., Kizu, S., Reseghetti, F., Suzuki, T., & Thresher, A.
1868   (2018). An Algorithm for Classifying Unknown Expendable Bathythermograph (XBT)
1869   Instruments Based on Existing Metadata. *Journal of Atmospheric and Oceanic Technology*,
1870   *35*(3), 429–440. https://doi.org/10.1175/JTECH-D-17-0129.1

1871 Palmer, Matthew D, Domingues, C. M., Slangen, A. B. A., & Boeira Dias, F. (2021). An
1872   ensemble approach to quantify global mean sea-level rise over the 20th century from tide
1873   gauge reconstructions (I3507, trans.). *Environmental Research Letters*, *16*(4), 044043.
1874   https://doi.org/10.1088/1748-9326/abdaec

1875 Park, H., Fedorov, A. N., Zheleznyak, M. N., Konstantinov, P. Y., & Walsh, J. E. (2015). Effect
1876   of snow cover on pan-Arctic permafrost thermal regimes. *Climate Dynamics*, *44*(9), 2873–
1877   2895. https://doi.org/10.1007/s00382-014-2356-5

1878 Perovich, D., Polashenski, C., Arntsen, A., & Stwertka, C. (2017). Anatomy of a late spring
1879   snowfall on sea ice. *Geophysical Research Letters*, *44*(6), 2802–2809.
1880   https://doi.org/https://doi.org/10.1002/2016GL071470

1881 Pickler, C., Beltrami, H., & Mareschal, jean-claude. (2016). Laurentide Ice Sheet basal
1882   temperatures during the last glacial cycle as inferred from borehole data. *Climate of the*
1883   *Past*, *12*, 115–127. https://doi.org/10.5194/cp-12-115-2016

1884 Pisoft, P., Sacha, P., Polvani, L. M., Añel, J. A., de la Torre, L., Eichinger, R., Foelsche, U.,
1885   Huszar, P., Jacobi, C., Karlicky, J., Kuchar, A., Miksovsky, J., Zak, M., & Rieder, H. E.
1886   (2021). Stratospheric contraction caused by increasing greenhouse gases. *Environmental*
1887   *Research Letters*, *16*(6), 64038. https://doi.org/10.1088/1748-9326/abfe2b

1888 Purkey, S. G., & Johnson, G. C. (2010). Warming of Global Abyssal and Deep Southern Ocean
1889   Waters between the 1990s and 2000s: Contributions to Global Heat and Sea Level Rise
1890   Budgets. *Journal of Climate*, *23*(23), 6336–6351. https://doi.org/10.1175/2010JCLI3682.1

1891 Qu, X., & Hall, A. (2007). What Controls the Strength of Snow-Albedo Feedback? *Journal of*
1892   *Climate*, *20*(15), 3971–3981. https://doi.org/10.1175/JCLI4186.1

1893 Rhein, M., RintoulS., Aoki, S., Campos, E., Chambers, D., `, Feely, R., Gulev, S., Johnson, G.,
1894   Josey, S., Kostianoy, A., Mauritzen, C., Roemmich, D., Talley, L., & Wang, F. (2013).
1895   *Chapter 3: Observations: Ocean. In: Climate Change 2013: The Physical Science Basis.*
1896   *Contribution of Working Group I to the Fifth Assessment Report of the Intergovernmental*
1897   *Panel on Climate Change.* (T. Stocker, D. Qin, G.-K. Plattner, M. Tignor, S. Allen, J.
1898   Boschung, A. Nauels, Y. Xia, V. Bex, & P. Midgley (eds.)). Cambridge University Press.
1899 Rignot, E., Mouginot, J., Scheuchl, B., van den Broeke, M., van Wessem, M. J., & Morlighem,
1900   M. (2019). Four decades of Antarctic Ice Sheet mass balance from 1979–2017. *Proceedings*
1901   *of the National Academy of Sciences*, *116*(4), 1095.
1902   https://doi.org/10.1073/pnas.1812883116
1903 Riser, S. C., Freeland, H. J., Roemmich, D., Wijffels, S., Troisi, A., Belbéoch, M., Gilbert, D.,
1904   Xu, J., Pouliquen, S., Thresher, A., Le Traon, P.-Y., Maze, G., Klein, B., Ravichandran, M.,
1905   Grant, F., Poulain, P.-M., Suga, T., Lim, B., Sterl, A., … Jayne, S. R. (2016). Fifteen years
1906   of ocean observations with the global Argo array. *Nature Climate Change*, *6*(2), 145–153.
1907   https://doi.org/10.1038/nclimate2872
1908 Roemmich, D., Alford, M. H., Claustre, H., Johnson, K., King, B., Moum, J., Oke, P., Owens,
1909   W. B., Pouliquen, S., Purkey, S., Scanderbeg, M., Suga, T., Wijffels, S., Zilberman, N.,
1910   Bakker, D., Baringer, M., Belbeoch, M., Bittig, H. C., Boss, E., … Yasuda, I. (2019). On
1911   the Future of Argo: A Global, Full-Depth, Multi-Disciplinary Array   . In *Frontiers in*
1912   *Marine Science*   (Vol. 6, p. 439).
1913   https://www.frontiersin.org/article/10.3389/fmars.2019.00439
1914 Roemmich, D., Church, J., Gilson, J., Monselesan, D., Sutton, P., & Wijffels, S. (2015).
1915   Unabated planetary warming and its ocean structure since 2006 (I3631, trans.). *Nature*
1916   *Climate Change*, *5*, 240. https://doi.org/10.1038/nclimate2513
1917 Roemmich, D., & Gilson, J. (2009). The 2004–2008 mean and annual cycle of temperature,
1918   salinity, and steric height in the global ocean from the Argo Program. *Progress in*
1919   *Oceanography*, *82*(2), 81–100. https://doi.org/https://doi.org/10.1016/j.pocean.2009.03.004
1920 Santer, B D, Wigley, T. M. L., Doutriaux, C., Boyle, J. S., Hansen, J. E., Jones, P. D., Meehl, G.
1921   A., Roeckner, E., Sengupta, S., & Taylor, K. E. (2001). Accounting for the effects of
1922   volcanoes and ENSO in comparisons of modeled and observed temperature trends. *Journal*
1923   *of Geophysical Research: Atmospheres*, *106*(D22), 28033–28059.
1924   https://doi.org/https://doi.org/10.1029/2000JD000189
1925 Santer, Benjamin D, Po-Chedley, S., Feldl, N., Fyfe, J. C., Fu, Q., Solomon, S., England, M.,
1926   Rodgers, K. B., Stuecker, M. F., Mears, C., Zou, C.-Z., Bonfils, C. J. W., Pallotta, G.,
1927   Zelinka, M. D., Rosenbloom, N., & Edwards, J. (2022). Robust anthropogenic signal
1928   identified in the seasonal cycle of tropospheric temperature. *Journal of Climate*, 1–51.
1929   https://doi.org/10.1175/JCLI-D-21-0766.1
1930 Santer, Benjamin D, Po-Chedley, S., Mears, C., Fyfe, J. C., Gillett, N., Fu, Q., Painter, J. F.,
1931   Solomon, S., Steiner, A. K., Wentz, F. J., Zelinka, M. D., & Zou, C.-Z. (2021). Using
1932   Climate Model Simulations to Constrain Observations. *Journal of Climate*, *34*(15), 6281–
1933   6301. https://doi.org/10.1175/JCLI-D-20-0768.1
1934 Savita, A., Domingues, C. M., Boyer, T., Gouretski, V., Ishii, M., Johnson, G. C., Lyman, J. M.,
1935   Willis, J. K., Marsland, S. J., Hobbs, W., Church, J. A., Monselesan, D. P., Dobrohotoff, P.,
1936   Cowley, R., & Wijffels, S. E. (2022). Quantifying Spread in Spatiotemporal Changes of
1937   Upper-Ocean Heat Content Estimates: An Internationally Coordinated Comparison. *Journal*
1938   *of Climate*, *35*(2), 851–875. https://doi.org/10.1175/JCLI-D-20-0603.1

Schweiger, A. J., Wood, K. R., & Zhang, J. (2019). Arctic Sea Ice Volume Variability over
    1901–2010: A Model-Based Reconstruction. *Journal of Climate*, *32*(15), 4731–4752.
    https://doi.org/10.1175/JCLI-D-19-0008.1
Schweiger, A., Lindsay, R., Zhang, J., Steele, M., Stern, H., & Kwok, R. (2011). Uncertainty in
    modeled Arctic sea ice volume. *Journal of Geophysical Research: Oceans*, *116*(C8).
    https://doi.org/10.1029/2011JC007084
Shen, P. Y., Wang, K., Beltrami, H., & Mareschal, J.-C. (1992). A comparative study of inverse
    methods for estimating climatic history from borehole temperature data. *Palaeogeography,
    Palaeoclimatology, Palaeoecology*, *98*(2), 113–127.
    https://doi.org/https://doi.org/10.1016/0031-0182(92)90192-8
Shen, X., Ke, C.-Q., & Li, H. (2022). Snow depth product over Antarctic sea ice from 2002 to
    2020 using multisource passive microwave radiometers. *Earth Syst. Sci. Data*, *14*(2), 619–
    636. https://doi.org/10.5194/essd-14-619-2022
Shepherd, A., Fricker, H. A., & Farrell, S. L. (2018). Trends and connections across the
    Antarctic cryosphere. *Nature*, *558*(7709), 223–232. https://doi.org/10.1038/s41586-018-
    0171-6
Shepherd, A., Ivins, E., Rignot, E., Smith, B., van den Broeke, M., Velicogna, I., Whitehouse, P.,
    Briggs, K., Joughin, I., Krinner, G., Nowicki, S., Payne, T., Scambos, T., Schlegel, N.,
    Geruo, A., Agosta, C., Ahlström, A., Babonis, G., Barletta, V. R., … Team, T. I. (2019).
    Mass balance of the Greenland Ice Sheet from 1992 to 2018. *Nature*.
    https://doi.org/10.1038/s41586-019-1855-2
Slater, T., Lawrence, I. R., Otosaka, I. N., Shepherd, A., Gourmelen, N., Jakob, L., Tepes, P.,
    Gilbert, L., & Nienow, P. (2021). Review article: Earth's ice imbalance. *The Cryosphere*,
    15(1), 233–246. https://doi.org/10.5194/tc-15-233-2021
Smith, B., Fricker, A. H., Gardner, S. A., Medley, B., Nilsson, J., Paolo, S. F., Holschuh, N.,
    Adusumilli, S., Brunt, K., Csatho, B., Harbeck, K., Markus, T., Neumann, T., Siegfried, M.,
    & Zwally, J. H. (2020). Pervasive ice sheet mass loss reflects competing ocean and
    atmosphere processes. *Science*, *368*(6496), 1239–1242.
    https://doi.org/10.1126/science.aaz5845
Smith, D. M., Allan, R. P., Coward, A. C., Eade, R., Hyder, P., Liu, C., Loeb, N. G., Palmer, M.
    D., Roberts, C. D., & Scaife, A. A. (2015). Earth's energy imbalance since 1960 in
    observations and CMIP5 models. *Geophysical Research Letters*, *42*(4), 1205–1213.
    https://doi.org/10.1002/2014GL062669
Staten, P. W., Grise, K. M., Davis, S. M., Karnauskas, K. B., Waugh, D. W., Maycock, A. C.,
    Fu, Q., Cook, K., Adam, O., Simpson, I. R., Allen, R. J., Rosenlof, K., Chen, G.,
    Ummenhofer, C. C., Quan, X.-W., Kossin, J. P., Davis, N. A., & Son, S.-W. (2020).
    Tropical Widening: From Global Variations to Regional Impacts. *Bulletin of the American
    Meteorological Society*, *101*(6), E897–E904. https://doi.org/10.1175/bams-d-19-0047.1
Steiner, A K, Ladstädter, F., Ao, C. O., Gleisner, H., Ho, S.-P., Hunt, D., Schmidt, T., Foelsche,
    U., Kirchengast, G., Kuo, Y.-H., Lauritsen, K. B., Mannucci, A. J., Nielsen, J. K.,
    Schreiner, W., Schwärz, M., Sokolovskiy, S., Syndergaard, S., & Wickert, J. (2020).
    Consistency and structural uncertainty of multi-mission GPS radio occultation records
    (I1695, trans.). *Atmospheric Measurement Techniques*, *13*(5), 2547–2575.
    https://doi.org/10.5194/amt-13-2547-2020
Steiner, Andrea K., Ladstädter, F., Randel, W. J., Maycock, A. C., Fu, Q., Claud, C., Gleisner,
    H., Haimberger, L., Ho, S.-P., Keckhut, P., Leblanc, T., Mears, C., Polvani, L. M., Santer,

B. D., Schmidt, T., Sofieva, V., Wing, R., & Zou, C.-Z. (2020). Observed Temperature Changes in the Troposphere and Stratosphere from 1979 to 2018 (I3342, trans.). *Journal of Climate*, *33*(19), 8165–8194. https://doi.org/10.1175/JCLI-D-19-0998.1

Storto, A., Alvera-Azcárate, A., Balmaseda, M. A., Barth, A., Chevallier, M., Counillon, F., Domingues, C. M., Drevillon, M., Drillet, Y., Forget, G., Garric, G., Haines, K., Hernandez, F., Iovino, D., Jackson, L. C., Lellouche, J.-M., Masina, S., Mayer, M., Oke, P. R., … Zuo, H. (2019). Ocean Reanalyses: Recent Advances and Unsolved Challenges. *Frontiers in Marine Science*, *6*, 418. https://doi.org/10.3389/fmars.2019.00418

Storto, A., Masina, S., Simoncelli, S., Iovino, D., Cipollone, A., Drevillon, M., Drillet, Y., Schuckman, K., Parent, L., Garric, G., Greiner, E., Desportes, C., Zuo, H., Balmaseda, M., & Peterson, K. (2018). The added value of the multi-system spread information for ocean heat content and steric sea level investigations in the CMEMS GREP ensemble reanalysis product. *Climate Dynamics*. https://doi.org/10.1007/s00382-018-4585-5

Tilling, R. L., Ridout, A., & Shepherd, A. (2018). Estimating Arctic sea ice thickness and volume using CryoSat-2 radar altimeter data. *Advances in Space Research*, *62*(6), 1203–1225. https://doi.org/https://doi.org/10.1016/j.asr.2017.10.051

Trenberth, K. E., & Fasullo, J. T. (2010). Tracking Earth's Energy. *Science*, *328*(5976), 316. https://doi.org/10.1126/science.1187272

Trenberth, K. E., Fasullo, J. T., von Schuckmann, K., & Cheng, L. (2016). Insights into Earth's Energy Imbalance from Multiple Sources. *Journal of Climate*, *29*(20), 7495–7505. https://doi.org/10.1175/JCLI-D-16-0339.1

Vanderkelen, Inne; Thiery, Wim (2022). Global Heat Uptake by Inland Waters. Geophysical Research Letters, 47(12). e2020GL087867. D O I: https://doi.org/10.1029/2020GL087867. (2020). World Data Center for Climate (WDCC) at DKRZ. https://www.wdc-climate.de/ui/entry?acronym=GCOS_EHI_1960-2020_IWHC

Vanderkelen, I., van Lipzig, N. P. M., Lawrence, D. M., Droppers, B., Golub, M., Gosling, S. N., Janssen, A. B. G., Marcé, R., Schmied, H. M., Perroud, M., Pierson, D., Pokhrel, Y., Satoh, Y., Schewe, J., Seneviratne, S. I., Stepanenko, V. M., Tan, Z., Woolway, R. I., & Thiery, W. (2020). Global Heat Uptake by Inland Waters. *Geophysical Research Letters*, *47*(12), e2020GL087867. https://doi.org/https://doi.org/10.1029/2020GL087867

Verver, G., Fujiwara, M., Dolmans, P., Becker, C., Fortuin, P., & Miloshevich, L. (2006). Performance of the Vaisala RS80A/H and RS90 Humicap Sensors and the Meteolabor "Snow White" Chilled-Mirror Hygrometer in Paramaribo, Suriname. *Journal of Atmospheric and Oceanic Technology*, *23*(11), 1506–1518. https://doi.org/10.1175/JTECH1941.1

Vömel, H., Selkirk, H., Miloshevich, L., Valverde-Canossa, J., Valdés, J., Kyrö, E., Kivi, R., Stolz, W., Peng, G., & Diaz, J. A. (2007). Radiation Dry Bias of the Vaisala RS92 Humidity Sensor. *Journal of Atmospheric and Oceanic Technology*, *24*(6), 953–963. https://doi.org/10.1175/JTECH2019.1

von Schuckmann, Karina; Minière, Audrey; Gues, Flora; Cuesta-Valero, Francisco; Kirchengast, Gottfried; Adusumilli, Susheel; Straneo, Fiammetta; Allan, Richard; Barker, Paul M.; Beltrami, Hugo; Boyer, Tim; Cheng, Lijing; Church, John; Desbruyeres, Damien; Dolman, Han; Domingues, Catia; García-García, Almudena; Gilson, John; Gorfer, Maximilian; Haimberger, Leopold; Hendricks, Stefan; Hosoda, Shigeki; Johnson, Gregory; Killick, Rachel; King, Brian; Kolodziejczyk, Nicolas; Korosov, Anton; Krinner, Gerhard; Kuusela, Mikael; Langer, Moritz; Lavergne, Thomas; Lawrence, Isobel; Li, Yuehua; Lyman, John;

Open Access Earth System Science Data Discussions

2031 Marzeion, Ben; Mayer, Michael; MacDougall, Andrew; McDougall, Trevor; Monselesan,
2032 Didier; Nitzbon, Jean; Otosaka, Inès; Peng, Jian; Purkey, Sarah; Roemmich, Dean; Sato,
2033 Kanako; Sato, Katsunari; Savita, Abhishek; Schweiger, Axel; Shepherd, Andrew;
2034 Seneviratne, Sonia; Slater, Donald; Slater, Thomas; Smith, Noah; Steiner, Andrea; Szekely,
2035 Tanguy; Suga, Toshio; Thiery, Wim; Timmermanns, Mary-Louise; Vanderkelen, Inne;
2036 Wijffels, Susan; Wu, Tonghua; Zemp, Michael; Simons, Leon (2022). Heat stored in the
2037 Earth system 1960-2020: Where does the energy go?. World Data Center for Climate
2038 (WDCC) at DKRZ. https://www.wdc-climate.de/ui/entry?acronym=GCOS_EHI_1960-
2039 2020_OHC
2040 von Schuckmann, K., Palmer, M. D., Trenberth, K. E., Cazenave, A., Chambers, D.,
2041 Champollion, N., Hansen, J., Josey, S. A., Loeb, N., Mathieu, P.-P., Meyssignac, B., &
2042 Wild, M. (2016). An imperative to monitor Earth's energy imbalance. *Nature Climate
2043 Change*, *6*(2), 138–144. https://doi.org/10.1038/nclimate2876
2044 von Schuckmann, K, Cheng, L., Palmer, M. D., Hansen, J., Tassone, C., Aich, V., Adusumilli,
2045 S., Beltrami, H., Boyer, T., Cuesta-Valero, F. J., Desbruyères, D., Domingues, C., García-
2046 García, A., Gentine, P., Gilson, J., Gorfer, M., Haimberger, L., Ishii, M., Johnson, G. C., …
2047 Wijffels, S. E. (2020). Heat stored in the Earth system: where does the energy go? *Earth
2048 Syst. Sci. Data*, *12*(3), 2013–2041. https://doi.org/10.5194/essd-12-2013-2020
2049 von Schuckmann, K, & Le Traon, P.-Y. (2011). How well can we derive Global Ocean
2050 Indicators from Argo data? *Ocean Sci.*, *7*(6), 783–791. https://doi.org/10.5194/os-7-783-
2051 2011
2052 von Schuckmann, Karina, Le Traon, P.-Y., Smith, N., Pascual, A., Brasseur, P., Fennel, K.,
2053 Djavidnia, S., Aaboe, S., Fanjul, E. A., Autret, E., Axell, L., Aznar, R., Benincasa, M.,
2054 Bentamy, A., Boberg, F., Bourdallé-Badie, R., Nardelli, B. B., Brando, V. E., Bricaud, C.,
2055 … Zuo, H. (2018). Copernicus Marine Service Ocean State Report. *Journal of Operational
2056 Oceanography*, *11*(sup1), S1–S142. https://doi.org/10.1080/1755876X.2018.1489208
2057 Wanders, N., Thober, S., Kumar, R., Pan, M., Sheffield, J., Samaniego, L., & Wood, E. F.
2058 (2019). Development and Evaluation of a Pan-European Multimodel Seasonal Hydrological
2059 Forecasting System. *Journal of Hydrometeorology*, *20*(1), 99–115.
2060 https://doi.org/10.1175/JHM-D-18-0040.1
2061 Wang, X., Key, J., Kwok, R., & Zhang, J. (2016). Comparison of Arctic Sea Ice Thickness from
2062 Satellites, Aircraft, and PIOMAS Data. In *Remote Sensing* (Vol. 8, Issue 9).
2063 https://doi.org/10.3390/rs8090713
2064 WCRP Global Sea Level Budget Group. (2018). Global sea-level budget 1993–present. *Earth
2065 Syst. Sci. Data*, *10*(3), 1551–1590. https://doi.org/10.5194/essd-10-1551-2018
2066 Webster, M. A., DuVivier, A. K., Holland, M. M., & Bailey, D. A. (2021). Snow on Arctic Sea
2067 Ice in a Warming Climate as Simulated in CESM. *Journal of Geophysical Research:
2068 Oceans*, *126*(1), e2020JC016308. https://doi.org/https://doi.org/10.1029/2020JC016308
2069 Weihs, P., Laimighofer, J., Formayer, H., & Olefs, M. (2021). Influence of snow making on
2070 albedo and local radiative forcing in an alpine area. *Atmospheric Research*, *255*, 105448.
2071 https://doi.org/https://doi.org/10.1016/j.atmosres.2020.105448
2072 WGMS. (2021). *Fluctuations of Glaciers Database. World Glacier Monitoring Service, Zurich,
2073 Switzerland.* https://doi.org/DOI:10.5904/wgms-fog-2021-05
2074 Wijffels, S., Roemmich, D., Monselesan, D., Church, J., & Gilson, J. (2016). Ocean temperatures
2075 chronicle the ongoing warming of Earth. *Nature Climate Change*, *6*(2), 116–118.
2076 https://doi.org/10.1038/nclimate2924

2077 Willis, J. K., Roemmich, D., & Cornuelle, B. (2004). Interannual variability in upper ocean heat
2078   content, temperature, and thermosteric expansion on global scales. *Journal of Geophysical*
2079   *Research: Oceans*, *109*(C12). https://doi.org/10.1029/2003JC002260
2080 Wilson, N., Straneo, F., & Heimbach, P. (2017). Satellite-derived submarine melt rates and mass
2081   balance (2011–2015) for Greenland's largest remaining ice tongues. *The Cryosphere*, *11*,
2082   2773–2782. https://doi.org/10.5194/tc-11-2773-2017
2083 WMO. (2022). *The State of the Global Climate 2021*.
2084   https://library.wmo.int/index.php?lvl=notice_display&id=22080
2085 Wunsch, C. (2020). Is the Ocean Speeding Up? Ocean Surface Energy Trends. *Journal of*
2086   *Physical Oceanography*, *50*, 3205–3217. https://doi.org/10.1175/JPO-D-20-0082.1
2087 Zanna, L., Khatiwala, S., Gregory, J. M., Ison, J., & Heimbach, P. (2019). Global reconstruction
2088   of historical ocean heat storage and transport. *Proceedings of the National Academy of*
2089   *Sciences*, *116*(4), 1126. https://doi.org/10.1073/pnas.1808838115
2090 Zemp, M., Huss, M., Thibert, E., Eckert, N., McNabb, R., Huber, J., Barandun, M., Machguth,
2091   H., Nussbaumer, S. U., Gärtner-Roer, I., Thomson, L., Paul, F., Maussion, F., Kutuzov, S.,
2092   & Cogley, J. G. (2019). *Global and regional glacier mass changes from 1961 to 2016*.
2093   https://doi.org/10.5281/ZENODO.3557199
2094 Zemp, Michael, Huss, M., Eckert, N., Thibert, E., Paul, F., Nussbaumer, U. S., & Gärtner-Roer,
2095   I. (2020). Brief communication: Ad hoc estimation of glacier contributions to sea-level rise
2096   from the latest glaciological observations (I5946, trans.). *Cryosphere*, *14*(3).
2097   https://doi.org/10.5194/tc-14-1043-2020
2098 Zhang, J., & Rothrock, D. A. (2003). Modeling Global Sea Ice with a Thickness and Enthalpy
2099   Distribution Model in Generalized Curvilinear Coordinates. *Monthly Weather Review*,
2100   *131*(5), 845–861. https://doi.org/10.1175/1520-0493(2003)131<0845:MGSIWA>2.0.CO;2
2101 Zhang, R., Wang, H., Fu, Q., Rasch, J. P., & Wang, X. (2019). Unraveling driving forces
2102   explaining significant reduction in satellite-inferred Arctic surface albedo since the 1980s.
2103   *Proceedings of the National Academy of Sciences*, *116*(48), 23947–23953.
2104   https://doi.org/10.1073/pnas.1915258116
2105 Zou, C.-Z., Xu, H., Hao, X., & Fu, Q. (2021). Post-Millennium Atmospheric Temperature
2106   Trends Observed From Satellites in Stable Orbits. *Geophysical Research Letters*, *48*(13),
2107   e2021GL093291. https://doi.org/https://doi.org/10.1029/2021GL093291
2108